REPORT DOCUMENTATION PAGE

Form Approved
OMB No. 0704-0188

1. REPORT DATE *(DD-MM-YYYY)*	**2. REPORT TYPE**	**3. DATES COVERED** *(From - To)*
May 2012	Briefing Charts	Jan 2012 – May 2012

4. TITLE AND SUBTITLE
Mixing in Shear Coaxial Jets with and without Acoustics (Briefing Slides)

5a. CONTRACT NUMBER

5b. GRANT NUMBER

5c. PROGRAM ELEMENT NUMBER

6. AUTHOR(S)
Ivett Leyva, Sophonias Teshome, Juan Rodriguez, Jeffrey Graham,
Doug Talley, Ann Karagozian

5d. PROJECT NUMBER

5e. TASK NUMBER

5f. WORK UNIT NUMBER
Q0AY

7. PERFORMING ORGANIZATION NAME(S) AND ADDRESS(ES)

Air Force Research Laboratory (AFMC)
AFRL/RQRC
10 E. Saturn Blvd
Edwards AFB, CA 93524

8. PERFORMING ORGANIZATION REPORT NO.

9. SPONSORING / MONITORING AGENCY NAME(S) AND ADDRESS(ES)

Air Force Research Laboratory (AFMC)
AFRL/RQR
5 Pollux Drive
Edwards AFB, CA 93524

10. SPONSOR/MONITOR'S ACRONYM(S)

11. SPONSOR/MONITOR'S REPORT NUMBER(S)
AFRL-RZ-ED-VG-2012-171

12. DISTRIBUTION / AVAILABILITY STATEMENT
Approved for public release; distribution unlimited

13. SUPPLEMENTARY NOTES
Presented at Caltech Seminar, Pasadena, CA, 21 May 2012
PA Case Number: 12415; Clearance Date: 7 Jun 2012.

14. ABSTRACT

Briefing Slides

15. SUBJECT TERMS

16. SECURITY CLASSIFICATION OF:			**17. LIMITATION OF ABSTRACT**	**18. NUMBER OF PAGES**	**19a. NAME OF RESPONSIBLE PERSON**
					Douglas Talley
a. REPORT	**b. ABSTRACT**	**c. THIS PAGE**	SAR		**19b. TELEPHONE NO** *(include area code)*
Unclassified	**Unclassified**	**Unclassified**			661 275-6174

Standard Form 298 (Rev. 8-98)
Prescribed by ANSI Std. 239.18

Mixing in Shear Coaxial Jets with and without Acoustics

Ivett A Leyva

Current and former students and staff researchers:

Sophonias Teshome, Juan Rodriguez, Jeff Graham

Sr. Advisors:

Doug Talley, Ann Karagozian

Caltech

21 May 2012

Motivation

- Combustion instability is an ***unsustainable growth of pressure and heat transfer fluctuations in a rocket engine***
  - Irreparable damage can occur in <1s
- Combustion Instability caused a 4-yr delay in the development of the F-1 engine used in the Apollo program
  - More than $400M for the propellants alone at 2010 prices
  - More than 2000 full scale test

Damaged engine injector faceplate caused by combustion instabilities

"Combustion instabilities have been observed in almost every engine development effort, including even the most recent development programs" – current JANNAF Stability Panel Draft

Motivation (cont'd)

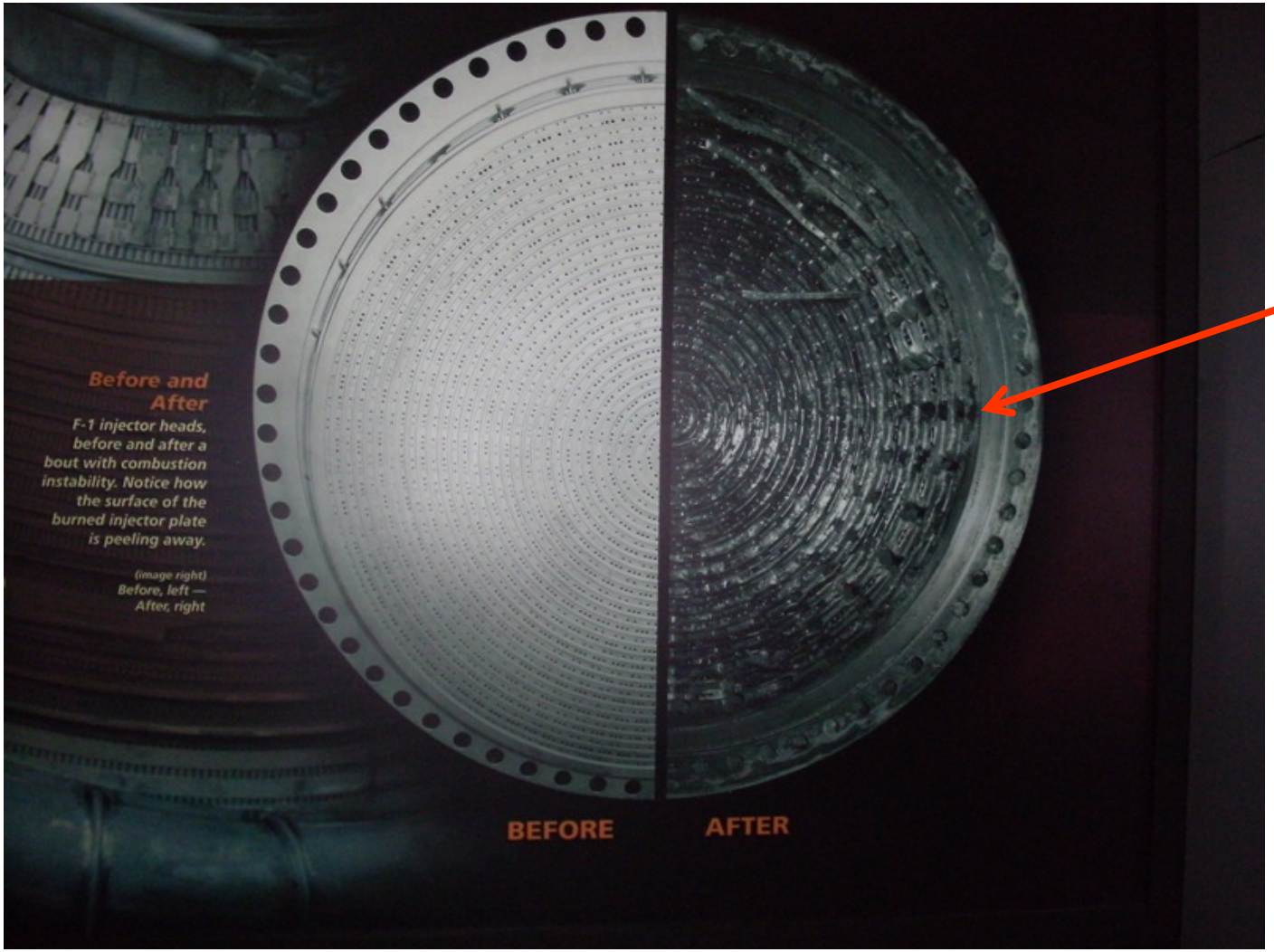

Injector head molten after a combustion instability event

Courtesy: U.S. Rocket and Space Center, Huntsville, AL

Statement of need

- Modern rockets operate at supercritical pressures with respect to the propellants
  - Need to understand mixing and combustion beyond liquid, gas states
- Shear coaxial injectors are a common choice for cryogenic liquid rocket engines
- Interactions of transverse acoustics with injector's own modes and mixing needs to be understood for combustion instability
  - Need to understand differences in response to pressure and velocity nodes
- Understand what non-dimensional numbers capture the mixing of typical injectors
- Characterize how geometry affects mixing

Highlights from previous work on jet instabilities 1/2

- Michalke, 1964
  - Linear stability theory for inviscid instability of a hyperbolic tangent velocity profile
- Crow and Champagne, 1971
  - Single jet preferred mode, $St_d=fd/U\sim0.3$
- Ko et al,1976-1989
  - Some of earliest detailed description of near field mixing for coaxial jets
- Boldman et al, 1975
  - Experimental and theoretical analysis for mixing of two air streams with different velocities – points out different vortex interactions, $St_l\sim0.2$ (U_{ave})
- Gutmark and Ho, 1983
  - Collects previous results on jet preferred mode, St_d has a range from ~0.24-0.64
- Wicker and Eaton, 1994
  - Forces air inner and outer jets independently – observes vortex growth
- Dahm et al, 1992
  - Seminal pictures of different instabilities plus effect of absolute velocity and R

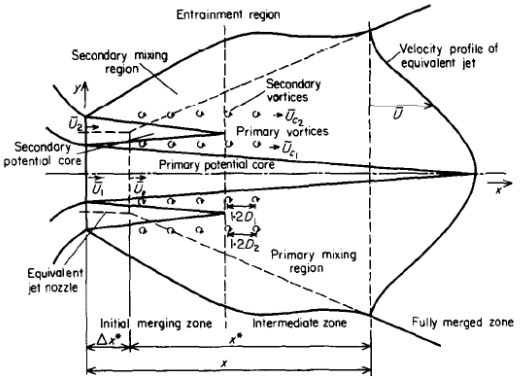

Kwan and Ko, J. Sound and Vibration, 48 (2), 1976

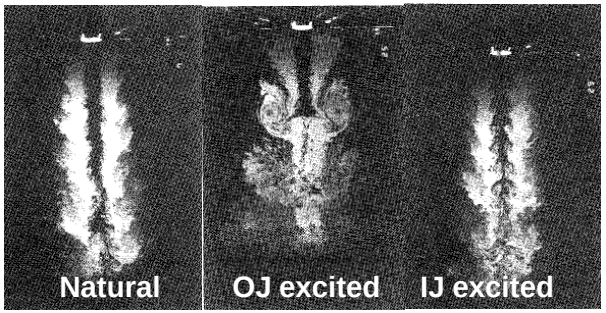

Wicker and Eaton, AIAA J, (32) No.3,1994

Highlights from previous work 2/2

- Balarac, da Silva, Metais et al (2003, 2007)
  - DNS analysis of coaxial jets - same density, top-hat profiles
  - Consider two shear layers, study effect of R
  - Consider axisymmetric and azimuthal excitation
- Buresti, Talamelli, Petagna (1994, 1998)
  - Air jets, same density, top-hat profile, $St_{do}=fd_o/U_{oj}$~0.3 to 1, function of x/D_i
- Segalini, Talamelli, et al (2006, 2011)
  - Air jets, same density, top-hat profile, $St_{b(lip)}=fb(lip)/U_{average}$
- Birbaud, Ducruix, Durox, Candel (2006-2007)
  - Single air jets, low Re, laminar, top-hat profile, subjected to acoustic modulation
  - Systematic study of effect of modulation in terms of St_d, St_θ
- Tshohas, Canino, Heister (2004, 2009)
  - 2D unsteady CFD for LOX/H2 elements but non-reacting
  - Unforced behavior, found $St_{lip}=fd_{lox}/U_{lox}$~0.10-0.25
- Richecoeur, Scouflaire, Ducruix, Candel (2006)
  - Forced transverse acoustic excitation of flames

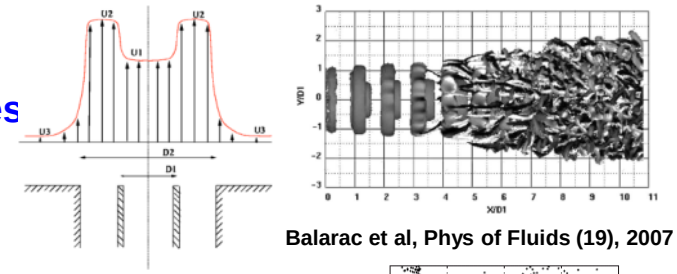

Balarac et al, Phys of Fluids (19), 2007

Segalini et al, Phys of Fluids (23), 2011

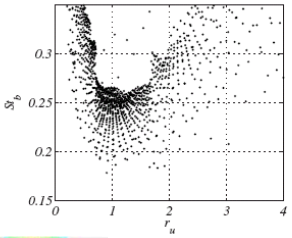

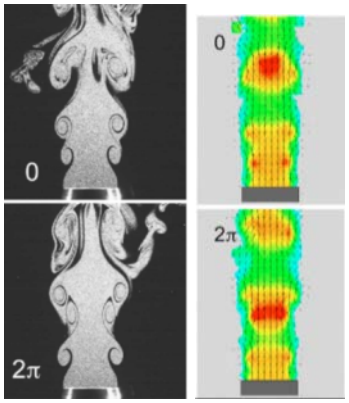

Birbaud et al, Phys of Fluids (19), 2007

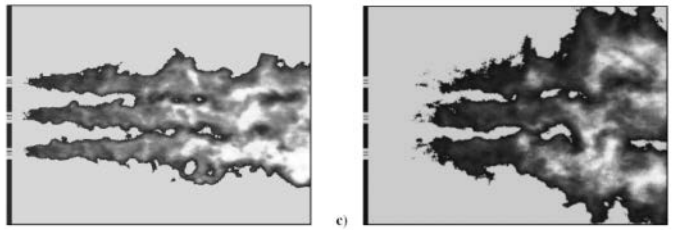

Richecoeur et al, JPP (22) No 4, 2006

Thermodynamic States of N2

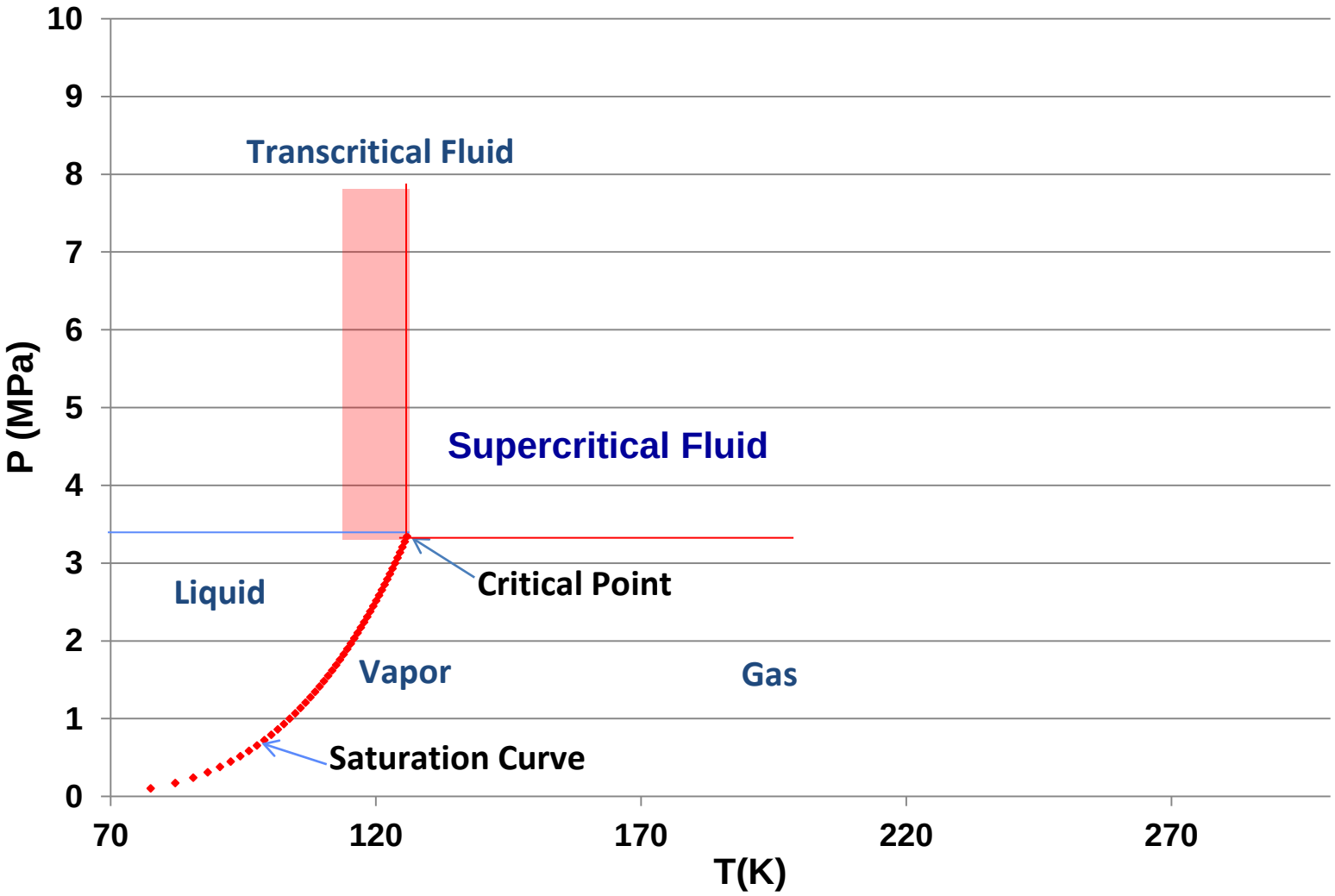

Property gradients around critical point

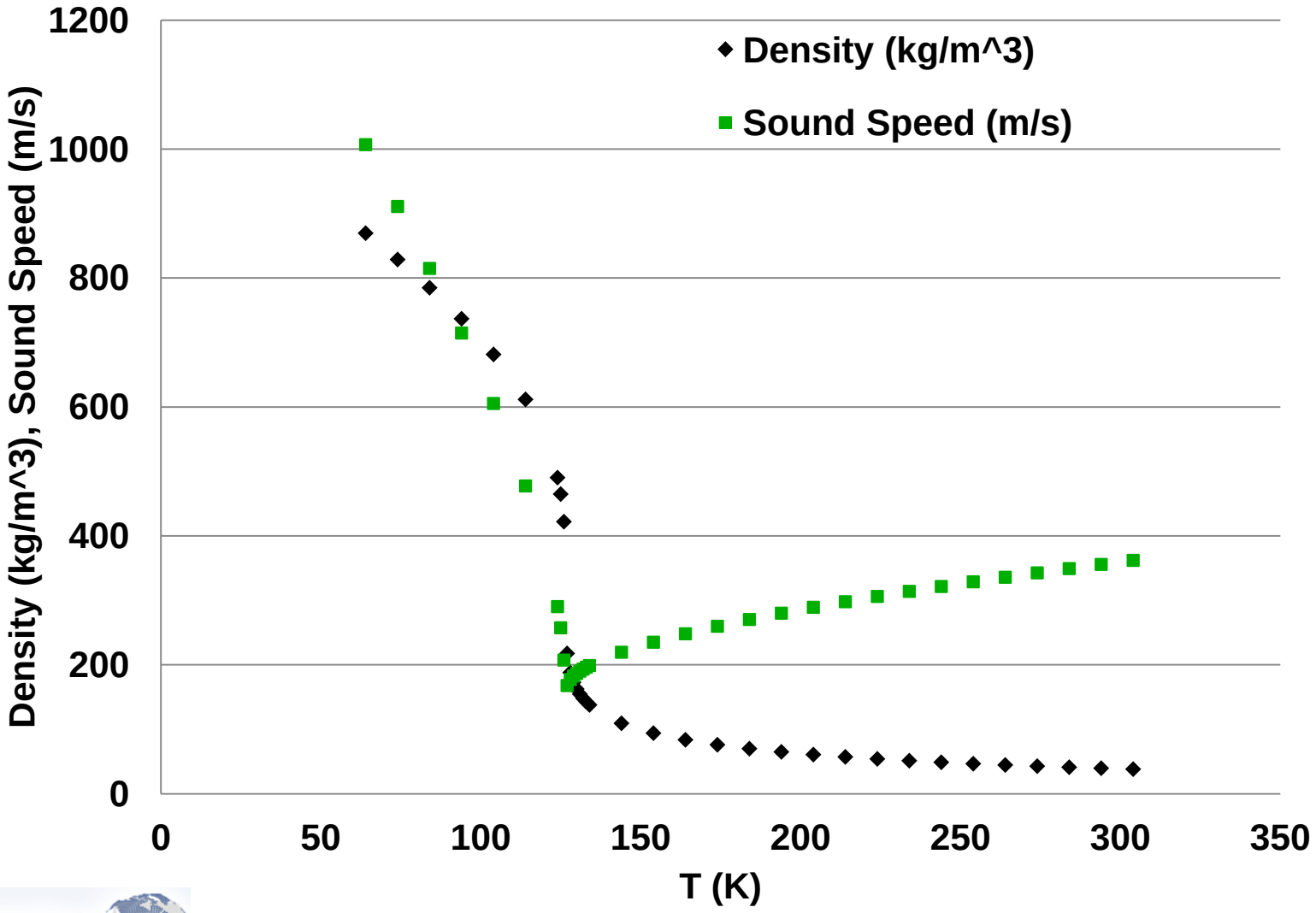

Geometric Configurations

LAR-thin

LAR-thick

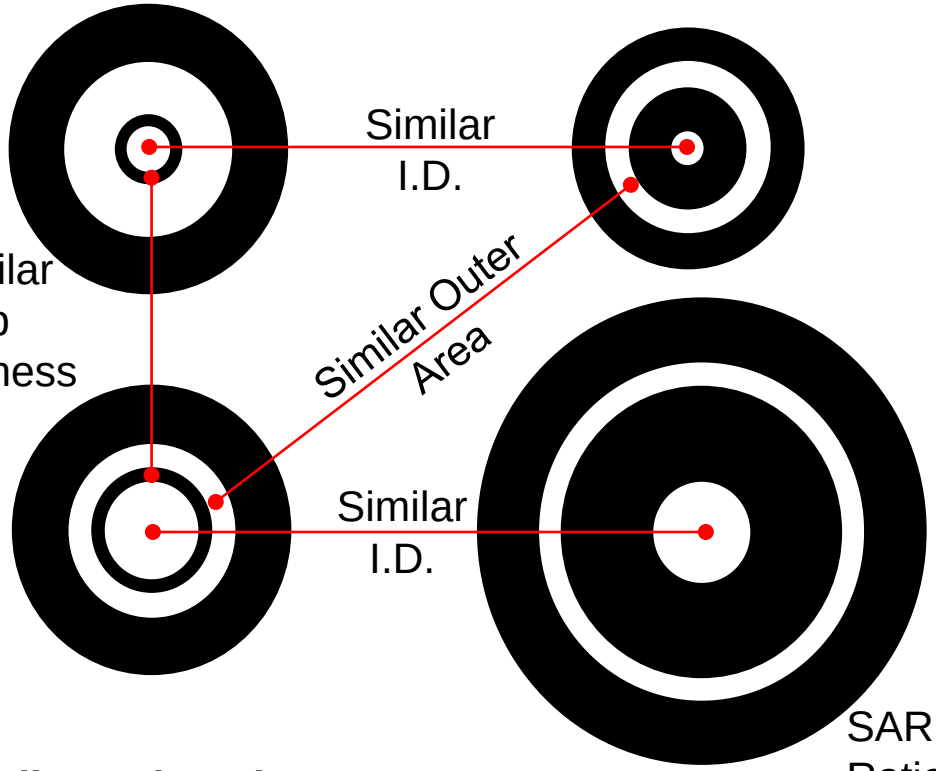

SAR-thin

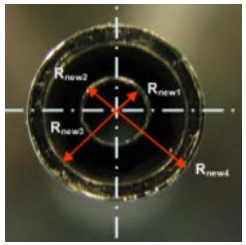

SAR-thick

SAR, LAR → Small, Large Area Ratio

Thick, Thin → Post lip thickness

All dimensions in mm

Injector	D_1	D_2	D_3	D_4	t/D_1	A_o/A_i
LAR-thick	0.51	1.59	2.42	3.18	1.05	12.9
SAR-thin	1.40	1.65	2.44	3.94	0.09	1.6
SAR-thick	1.47	3.96	4.70	6.35	0.84	2.9
LAR-thin	0.70	0.89	2.44	3.94	0.13	10.6

Davis, Rodriguez, Leyva *et al.* (0.5 D_1 recess)

Rodriguez (0.5 D_1 recess), Graham *et al.* (no recess)

Teshhome

Relevant variables for cold-flow studies

Geometry	Acoustics	Recess	Phase	VR	J	Coupling
Single Jet	On/Off	N/A	v' max	N/A		No
LAR_thickLip (injector 1)	Off P' max U'max	1/2D1	2-phase P<Pc P>Pc T>Tc T<Tc	0.1-20 0.1-20		No
SAR_thinLip (injector 2)		1/2D1 D1 0				Yes& No
SAR_thickLip (injector 3)		-0.2				
LAR_thinLip (injector 4)		-0.2				

Experimental setup – EC-4

Piezo-Siren

Waveguide

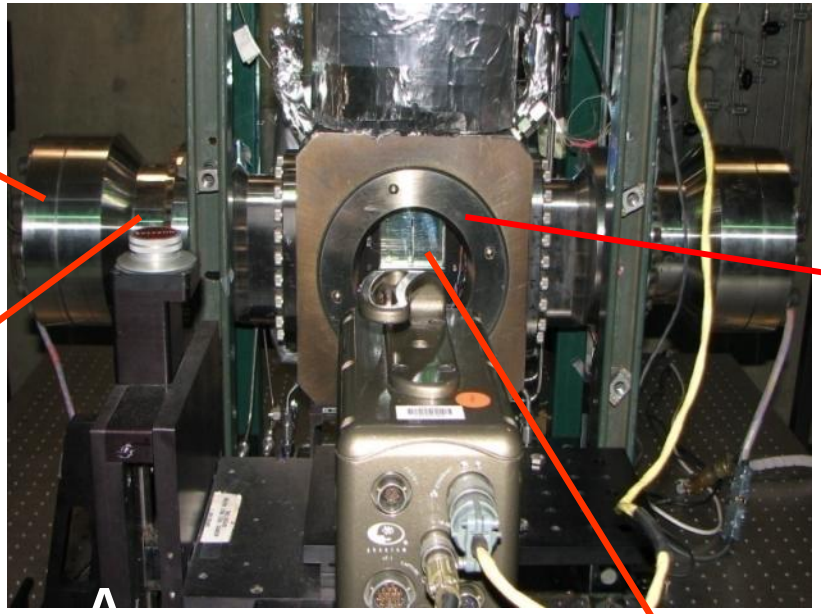

Coaxial Injector

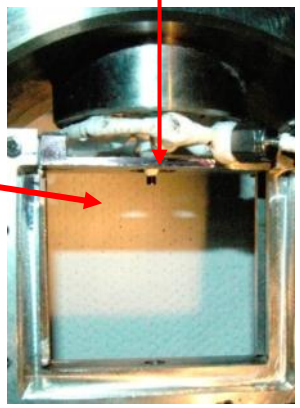

Inner Chamber

f=~3kHz

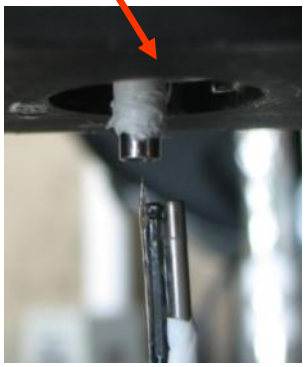

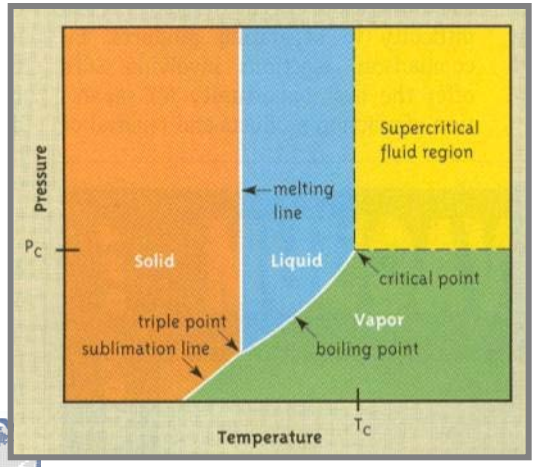

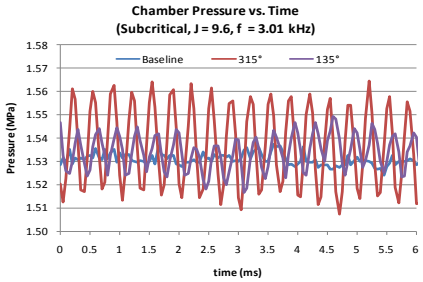

Thermocouple and P transducer

Dark-Core Length Measurement

- First raw grayscale images were converted to binary images
- A contour was drawn around the “dark-column” in the binary image
- Axial length of the dark-column measured and defined as the Dark-Core Length, *L*

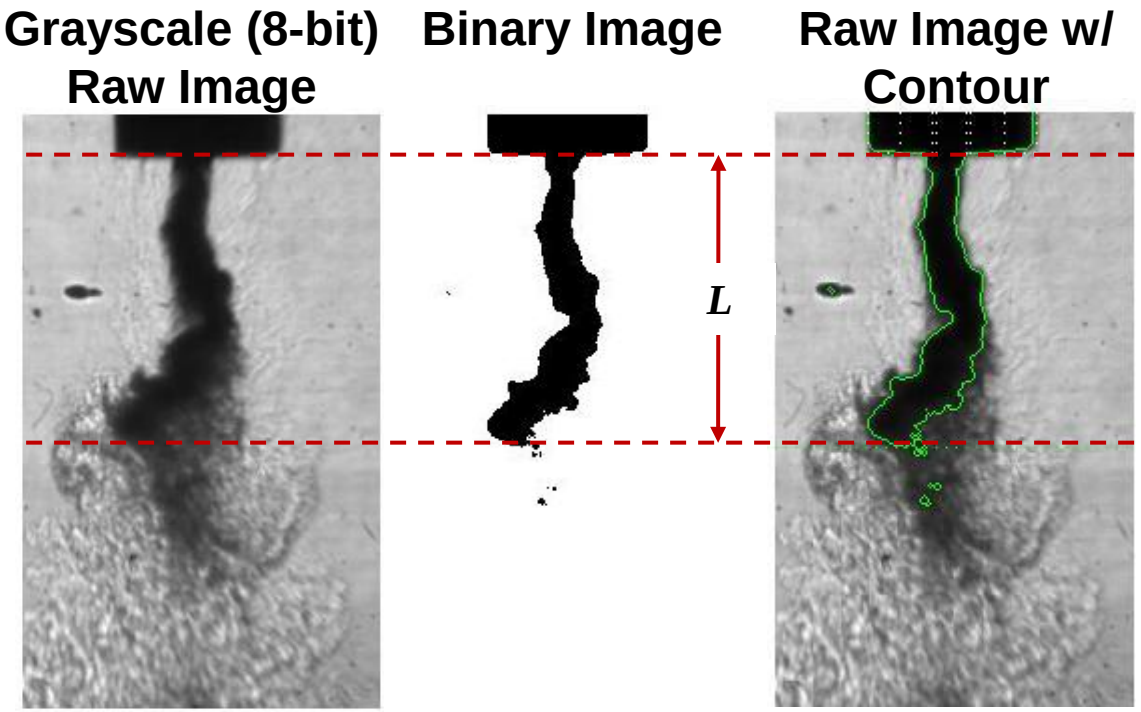

State of the art for mixing in shear coaxial jets - 2007

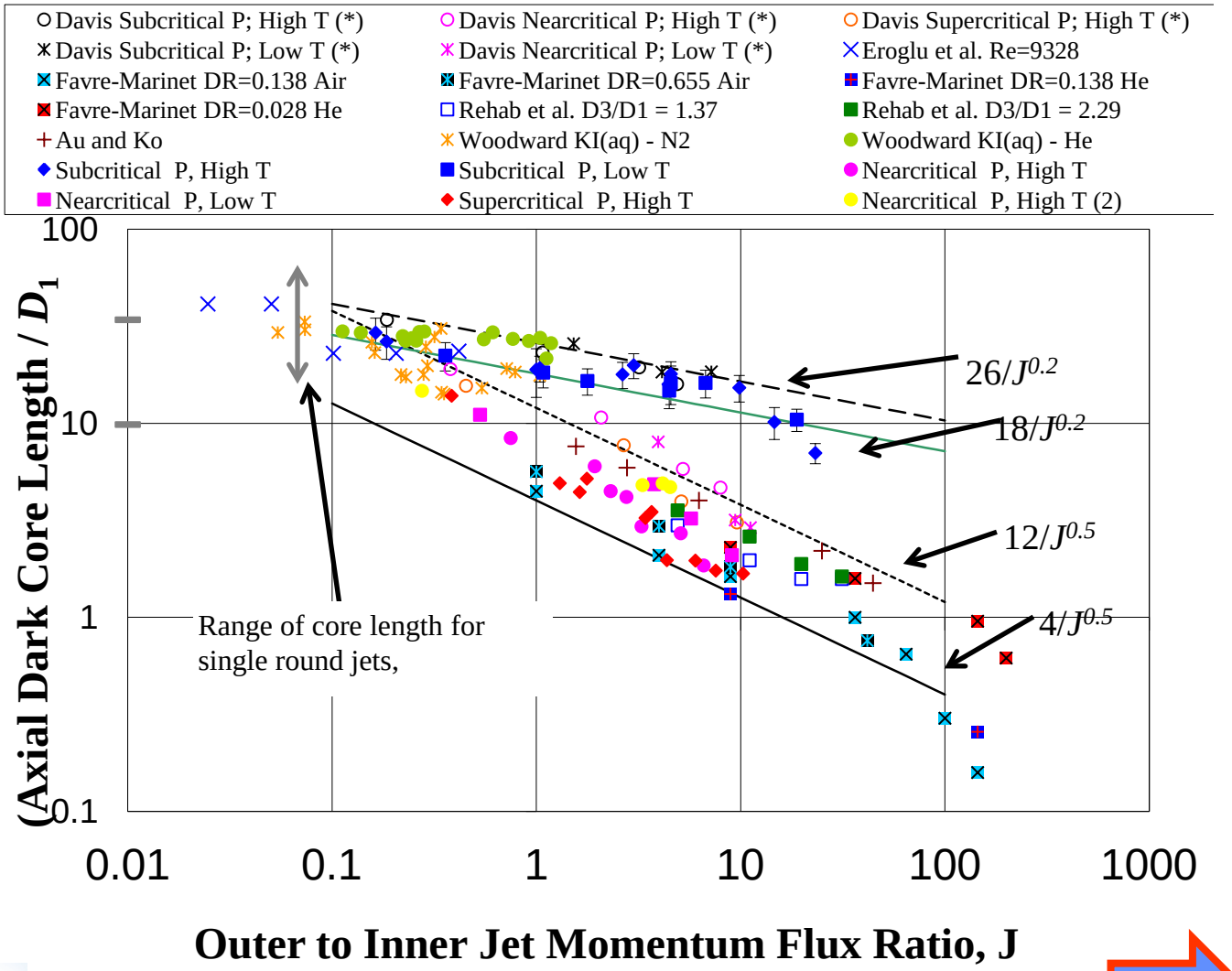

Dark Core Length – SAR-thick – All data

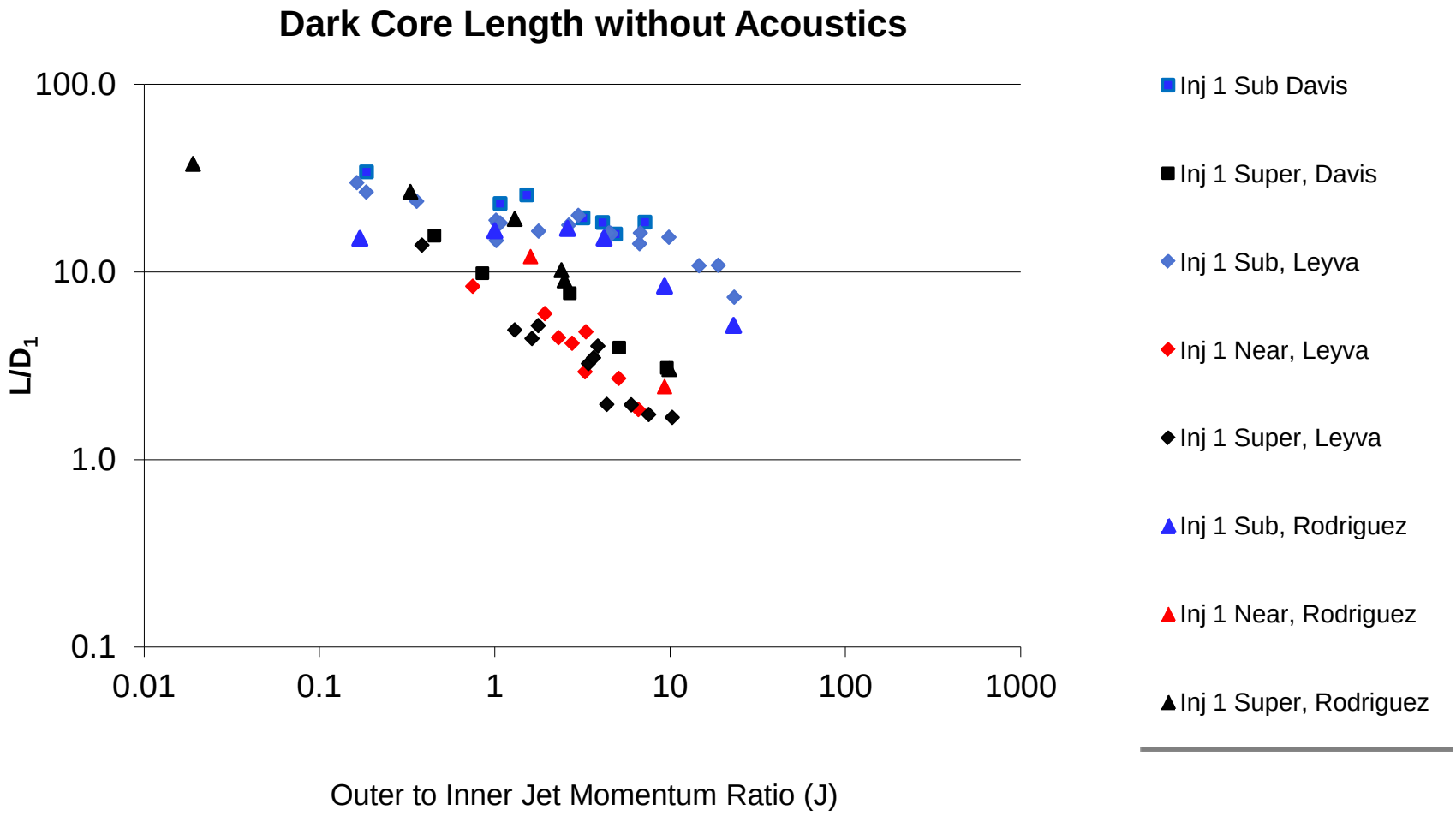

Dark Core Length – SAR-thick – All data

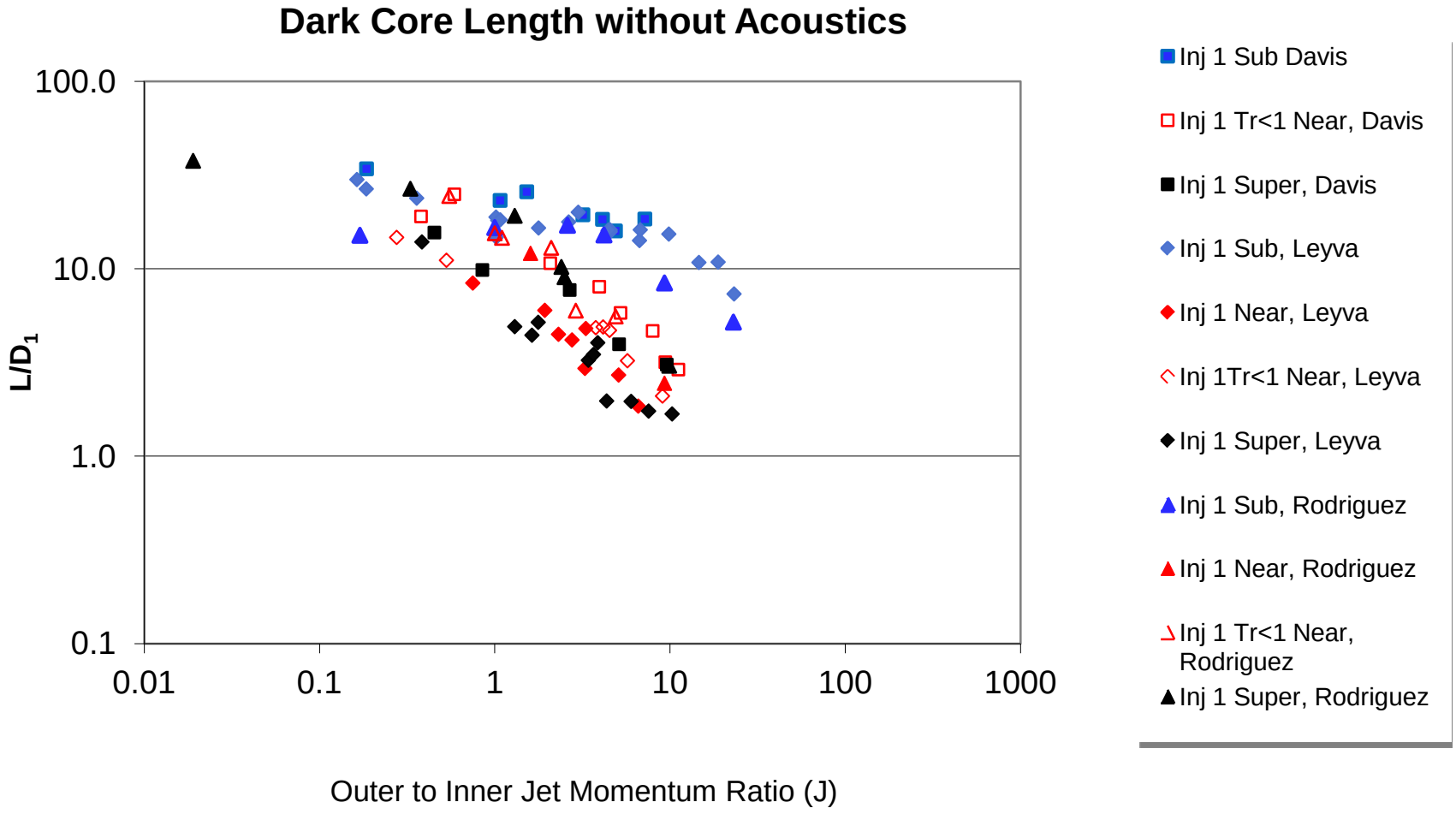

Dark Core Length – SAR thick – supercritical pressure

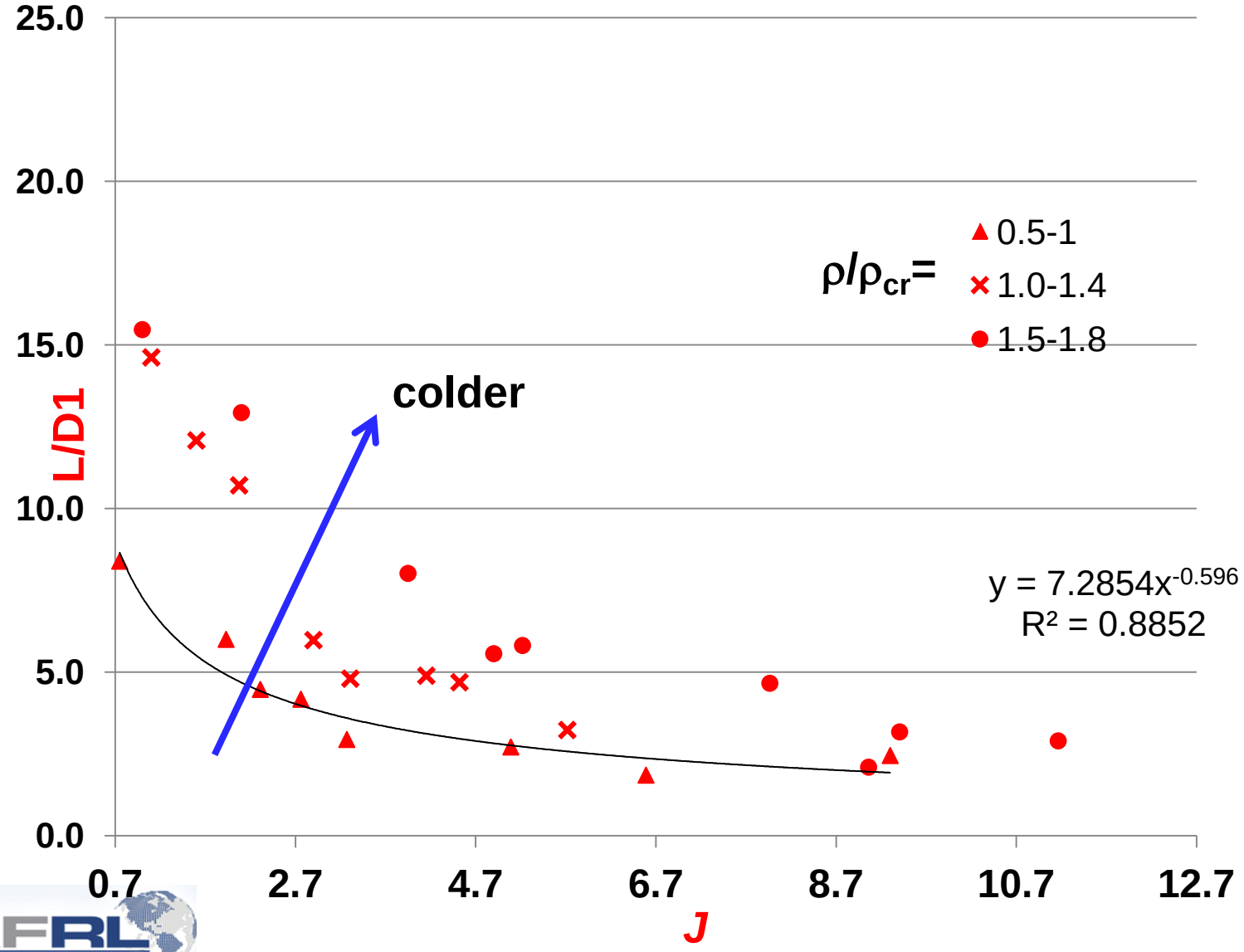

Dark Core Length – SAR thick – supercritical pressure

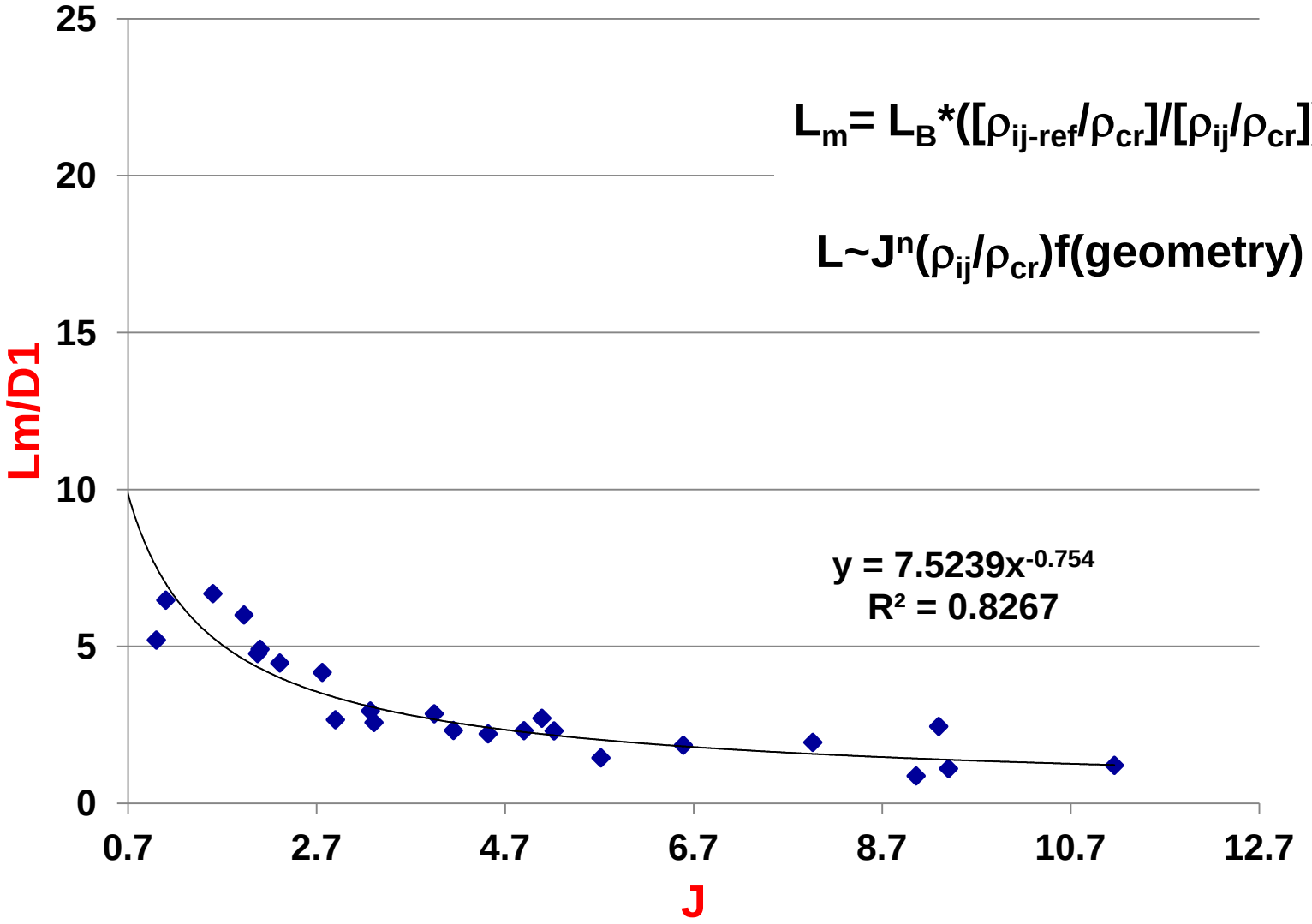

Geometric Configurations

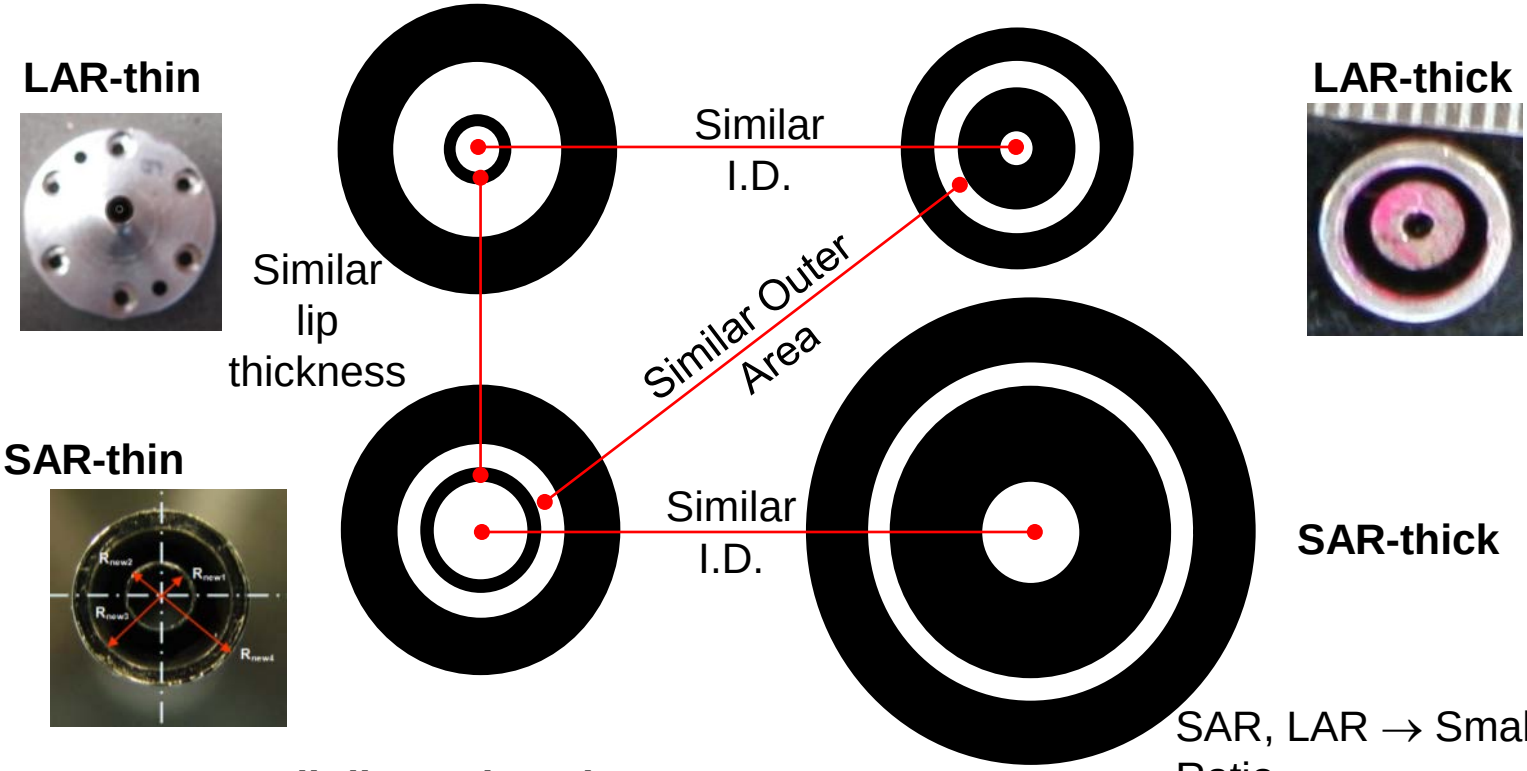

All dimensions in mm

Injector	D_1	D_2	D_3	D_4	t/D_1	A_o/A_i
LAR-thick	0.51	1.59	2.42	3.18	1.05	12.9
SAR-thin	1.40	1.65	2.44	3.94	0.09	1.6
SAR-thick	1.47	3.96	4.70	6.35	0.84	2.9
LAR-thin	0.70	0.89	2.44	3.94	0.13	10.6

SAR, LAR → Small, Large Area Ratio

Thick, Thin → Post lip thickness

Davis, Rodriguez, Leyva *et al.* (0.5 D_1 recess)

Rodriguez (0.5 D_1 recess), Graham *et al.* (no recess)

Teshhome

Baseline Flows: LAR-thin Injector

P_r = 0.44

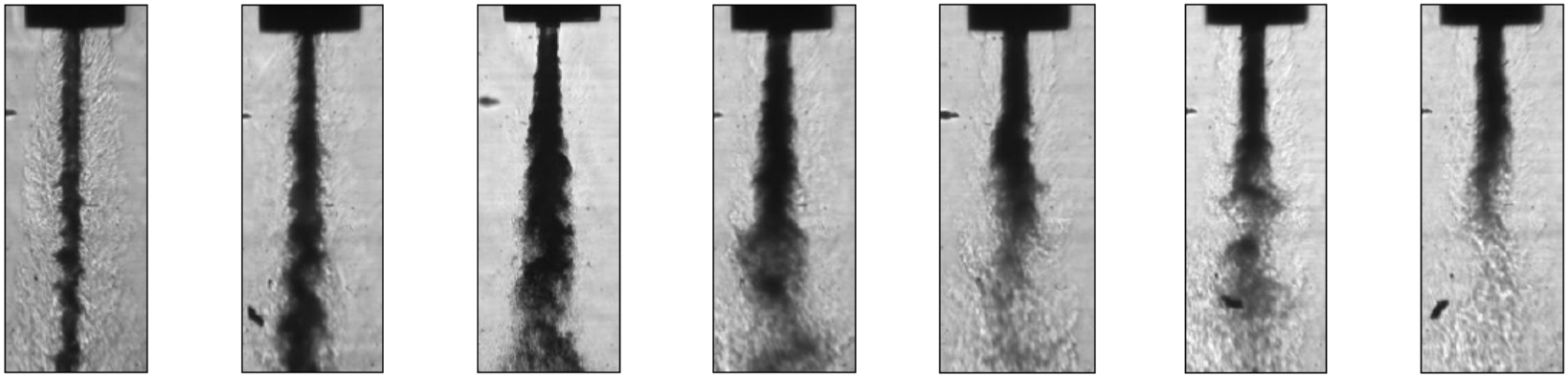

J = 0.1 | 0.5 | 2.1 | 5.2 | 11 | 14 | 20

P_r = 1.05

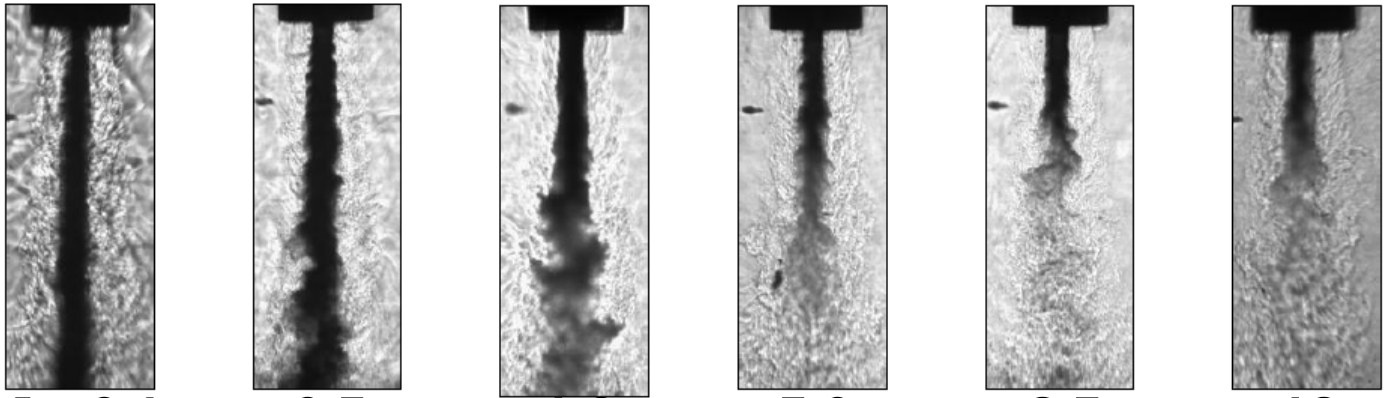

J = 0.1 | 0.5 | 1.9 | 5.0 | 8.5 | 12

Baseline Flows: SAR-thick Injector

$P_r = 0.44$

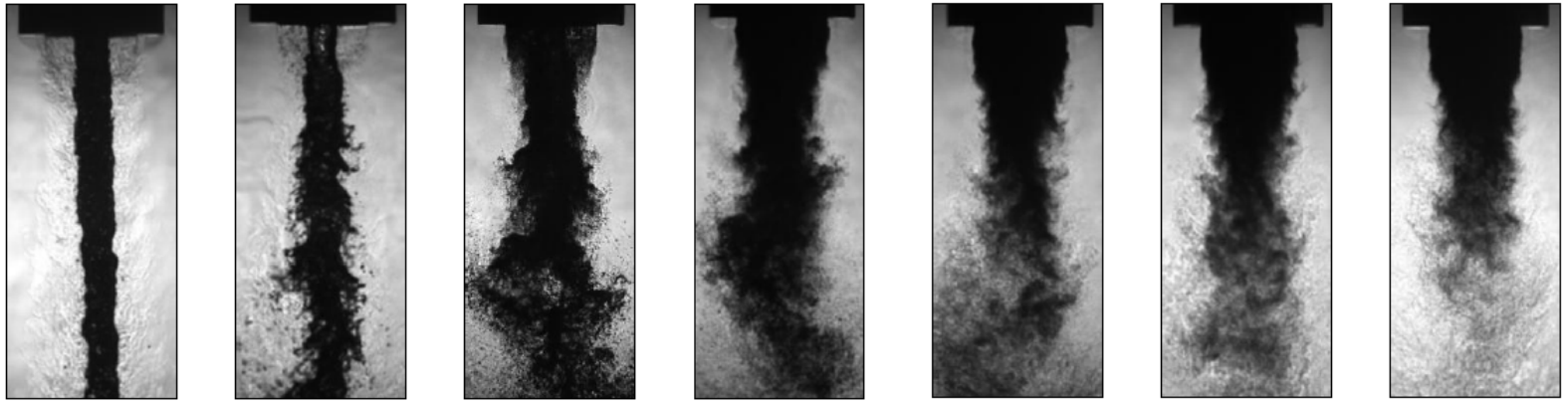

$J = 0.1$ 0.5 2.1 5.7 10 15 21

$P_r = 1.05$

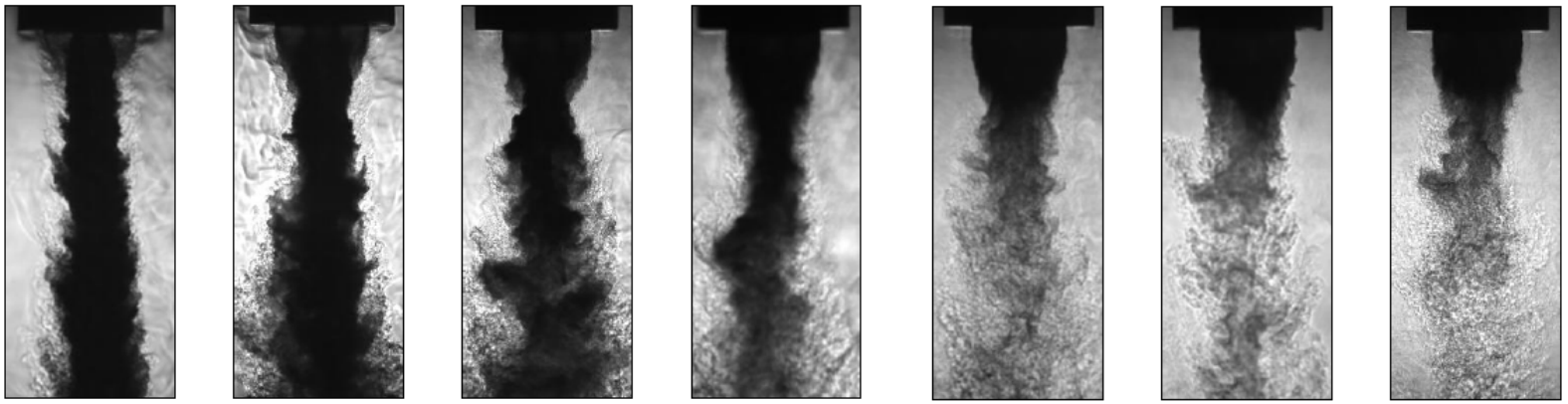

$J = 0.1$ 0.5 2.1 5.2 9.2 14 21

Sub and Nearcritical Baseline Dark Core Lengths for 4 Geometries

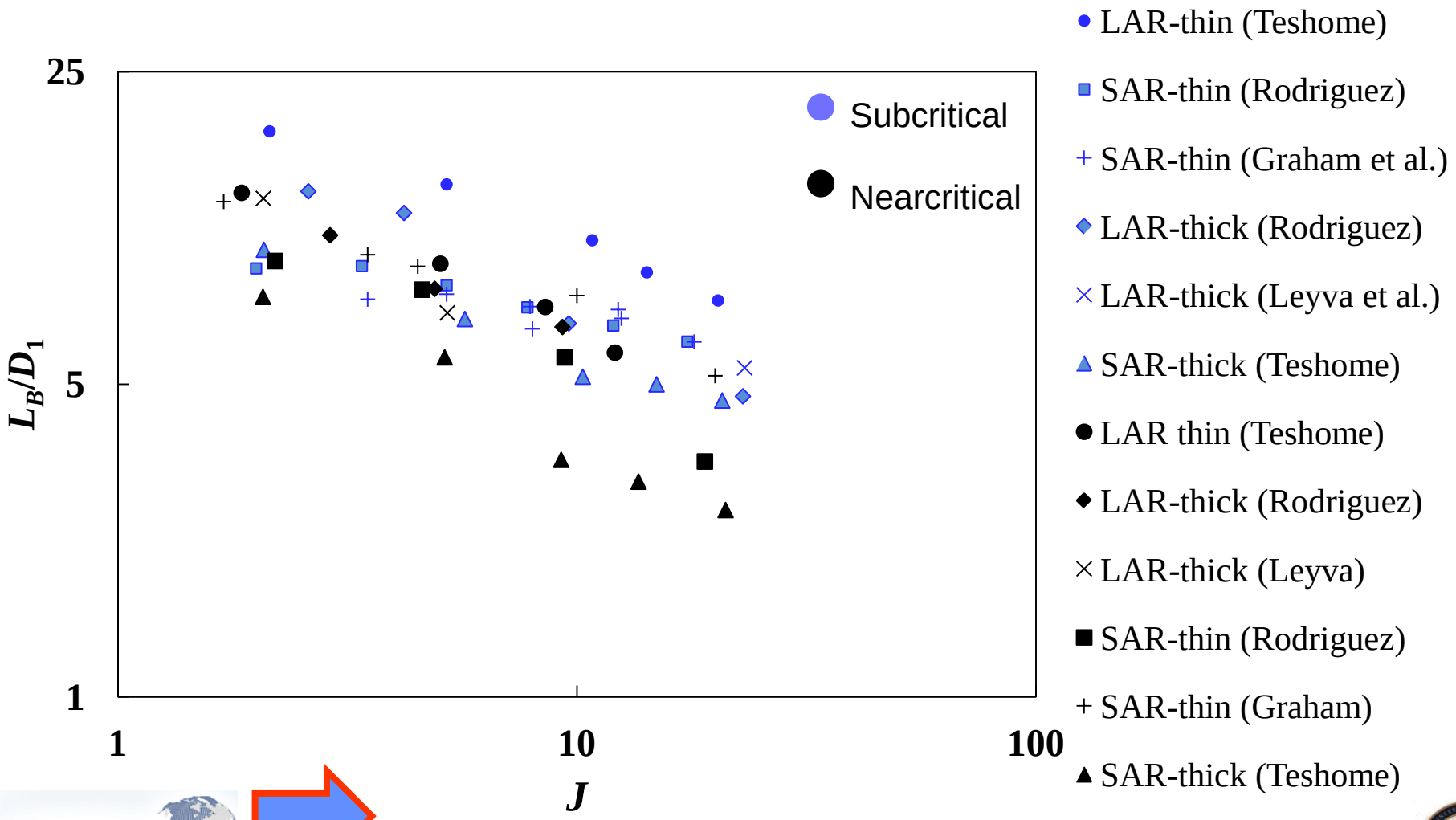

Baseline Normalized DCL, L_B/D_1 – $P_r = 0.44$

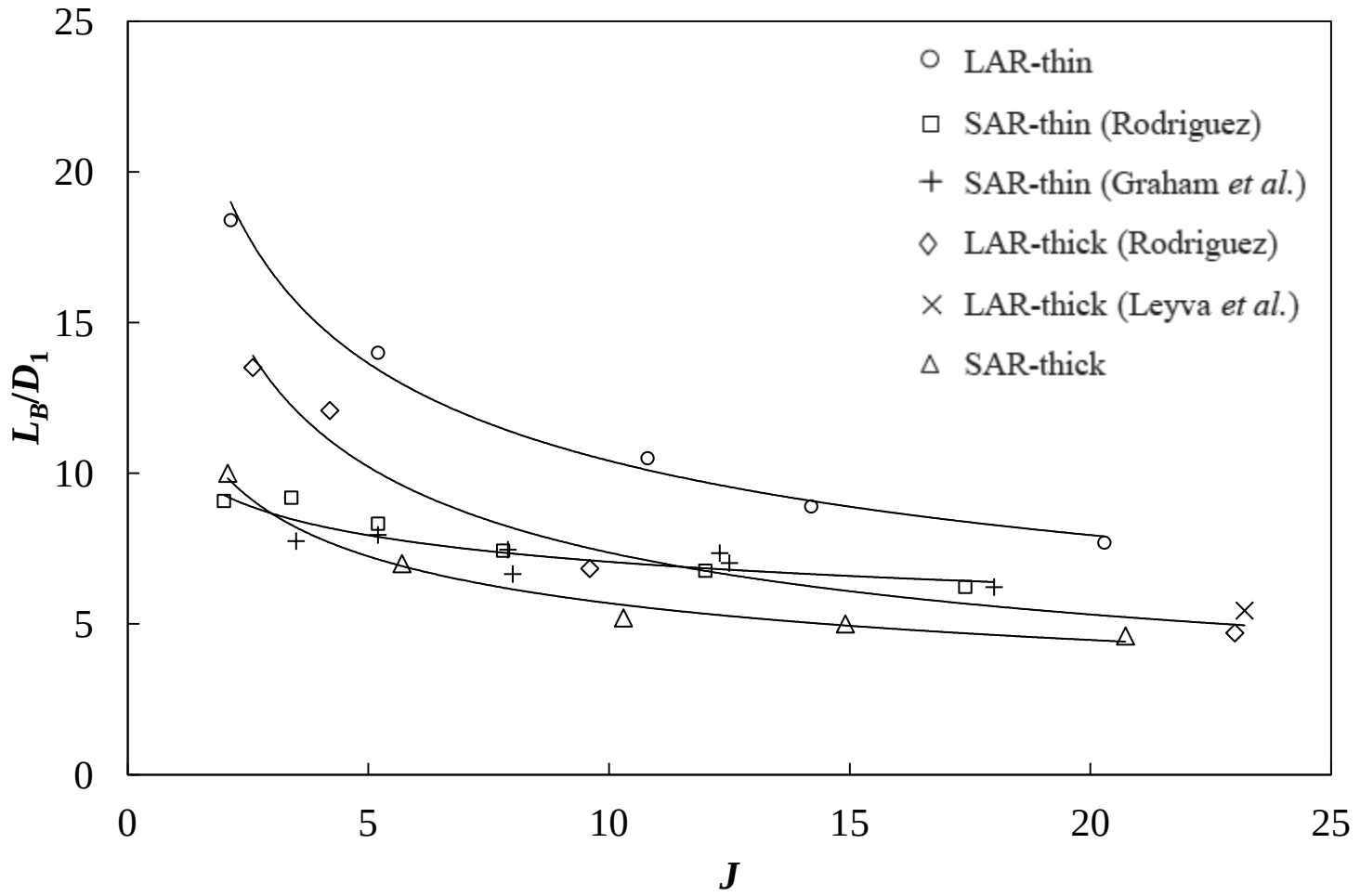

Baseline Normalized DCL, L_B/D_1 – $P_r = 1.05$

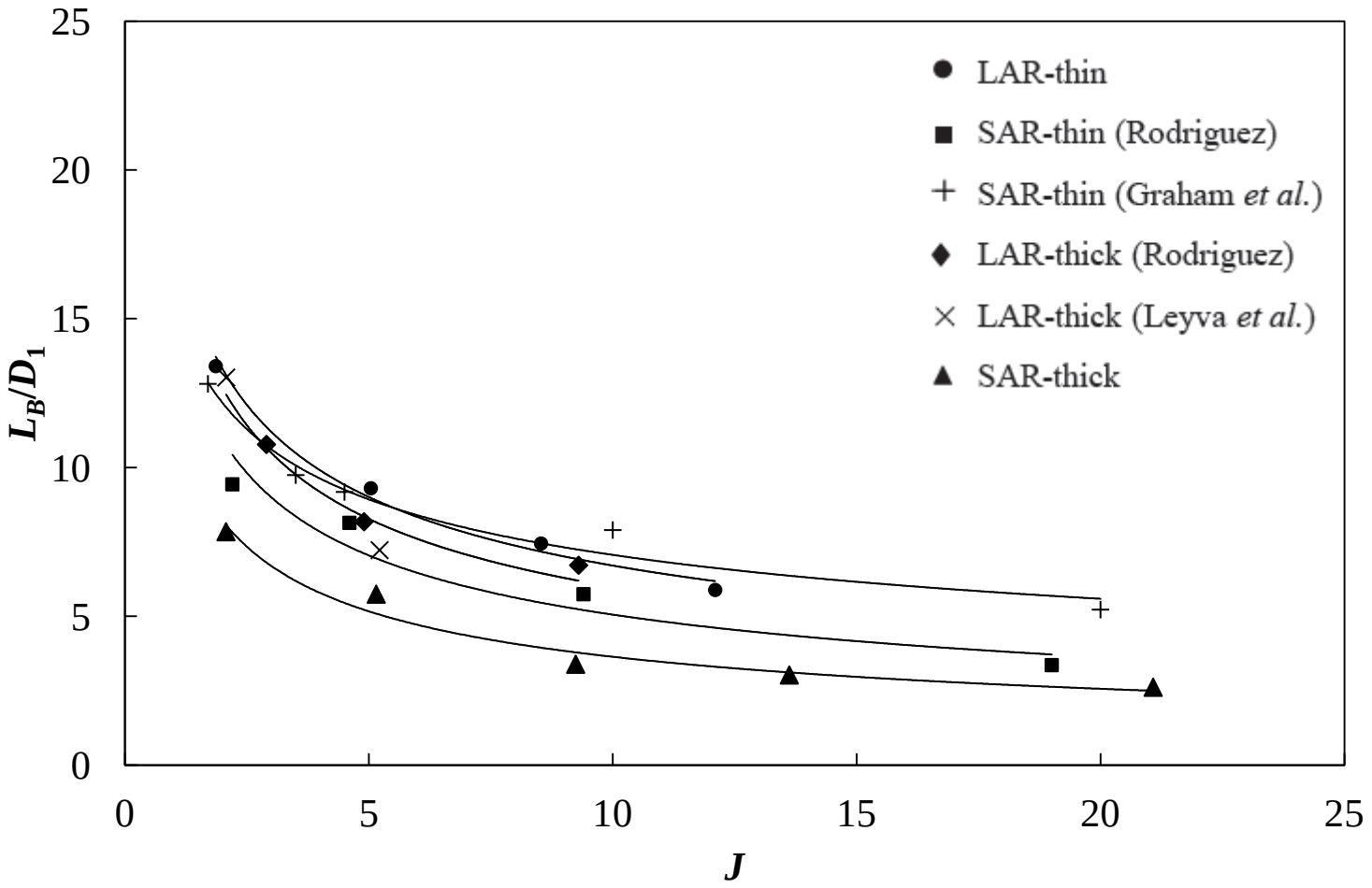

Baseline Normalized DCL, L_B/D_1 Collapse

- Non-linear regression of L_B/D_1 data from all four injectors at each P_r

$$\left(\frac{L_B}{D_1}\right) = c_1 J^{c_2} \left(\frac{t}{D_1}\right)^{c_3} \left(\frac{A_o}{A_i}\right)^{c_4}$$

P_r = 0.44

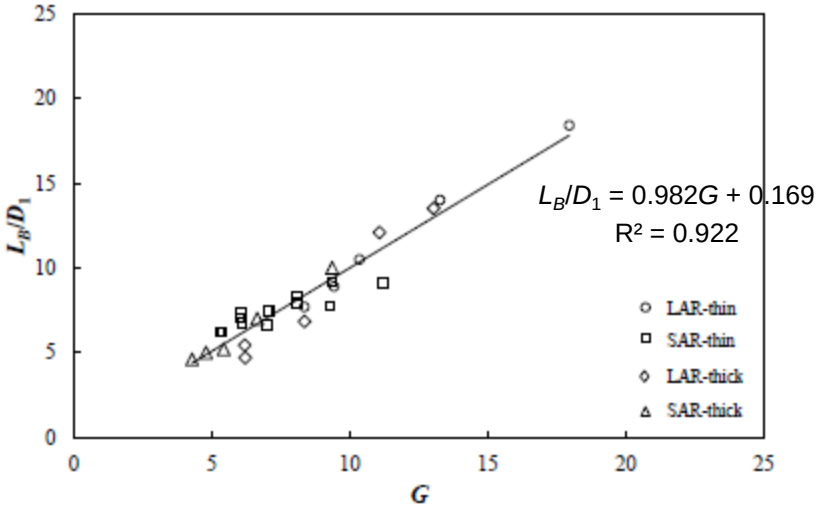

P_r = 1.05

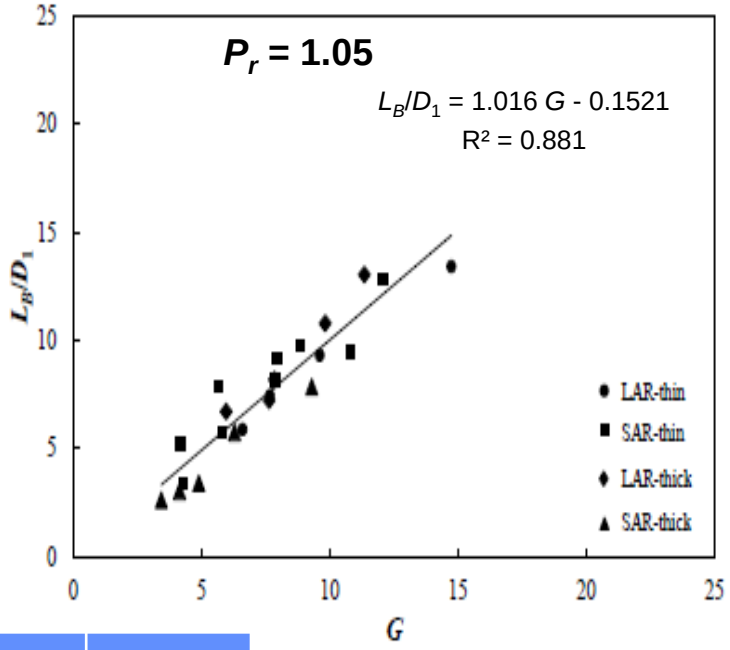

P_r	c_1	c_2	c_3	c_4
0.44	9	-0.34	-0.15	0.30
1.05	11	-0.43	-0.12	0.15

ACOUSTIC EXCITATION ANALYSIS

Acoustic Field Set-Up: Pressure Antinode

- Pressure antinode (PAN) – condition of maximum pressure perturbation in the acoustic field
- Piezo-sirens forced in-phase
- Superposition of quasi-1D acoustic waves traveling in opposite directions ⇒ PAN at the jet location (geometric center of test section)

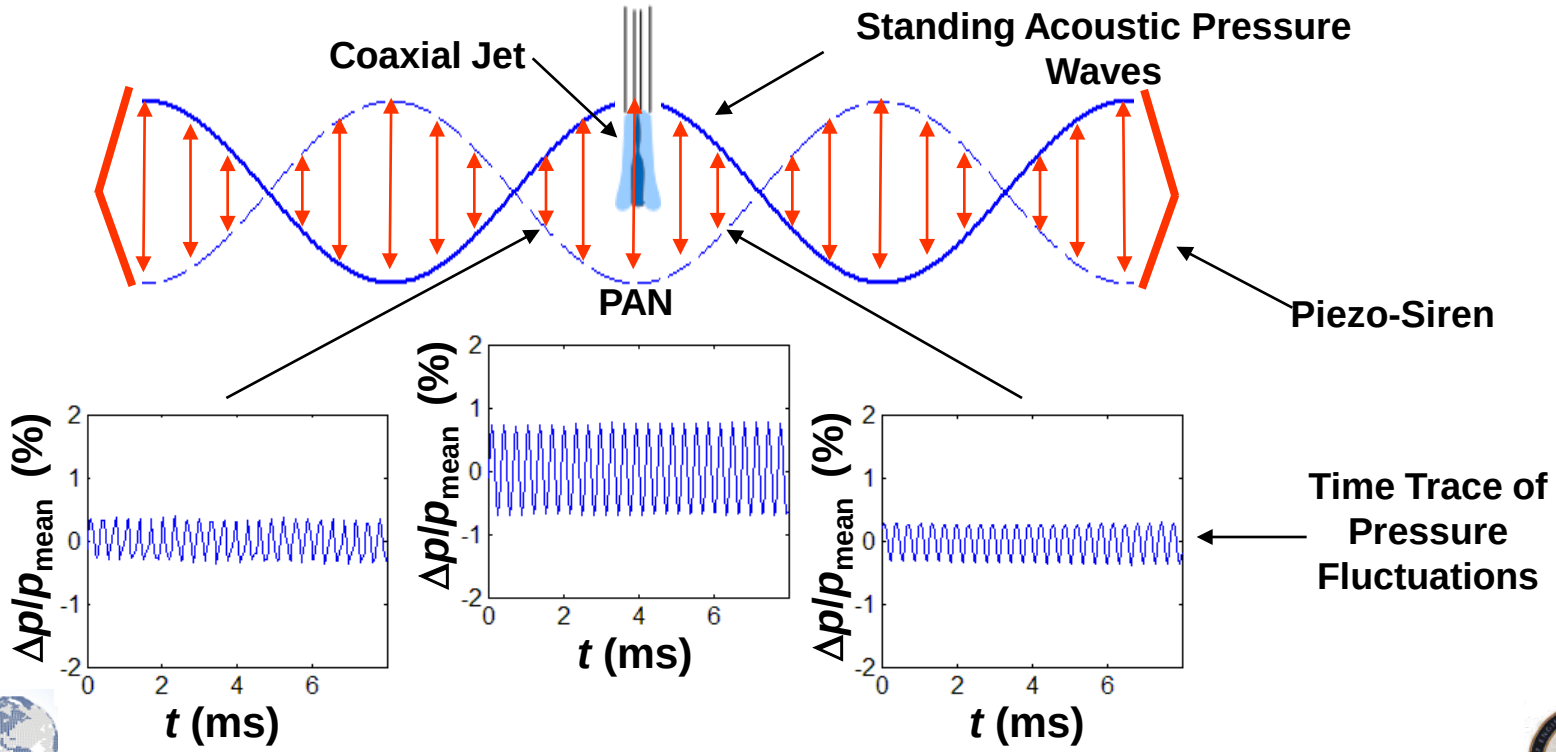

Image interpretation key

Baseline:
Acoustics
off

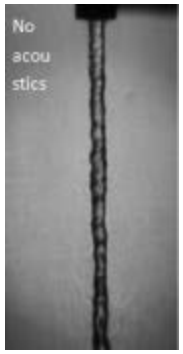

0^{o}
Acoustics on
PAN, VN
"Pressure coupled"

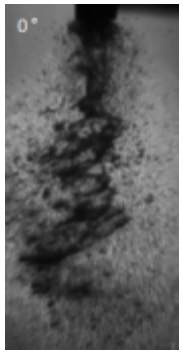

180^{o}
PN, VAN
Largest difference
expected from 0^{o}
"Velocity coupled"

pressure = fixed

$J\ (\rho_o u_o^2/\rho_i u_i^2)$ = fixed

PN – pressure node - Min
PAN – pressure antinode - Max
VN – velocity node
VAN – velocity antinode

Sub-Critical Pressure: Two Geometries

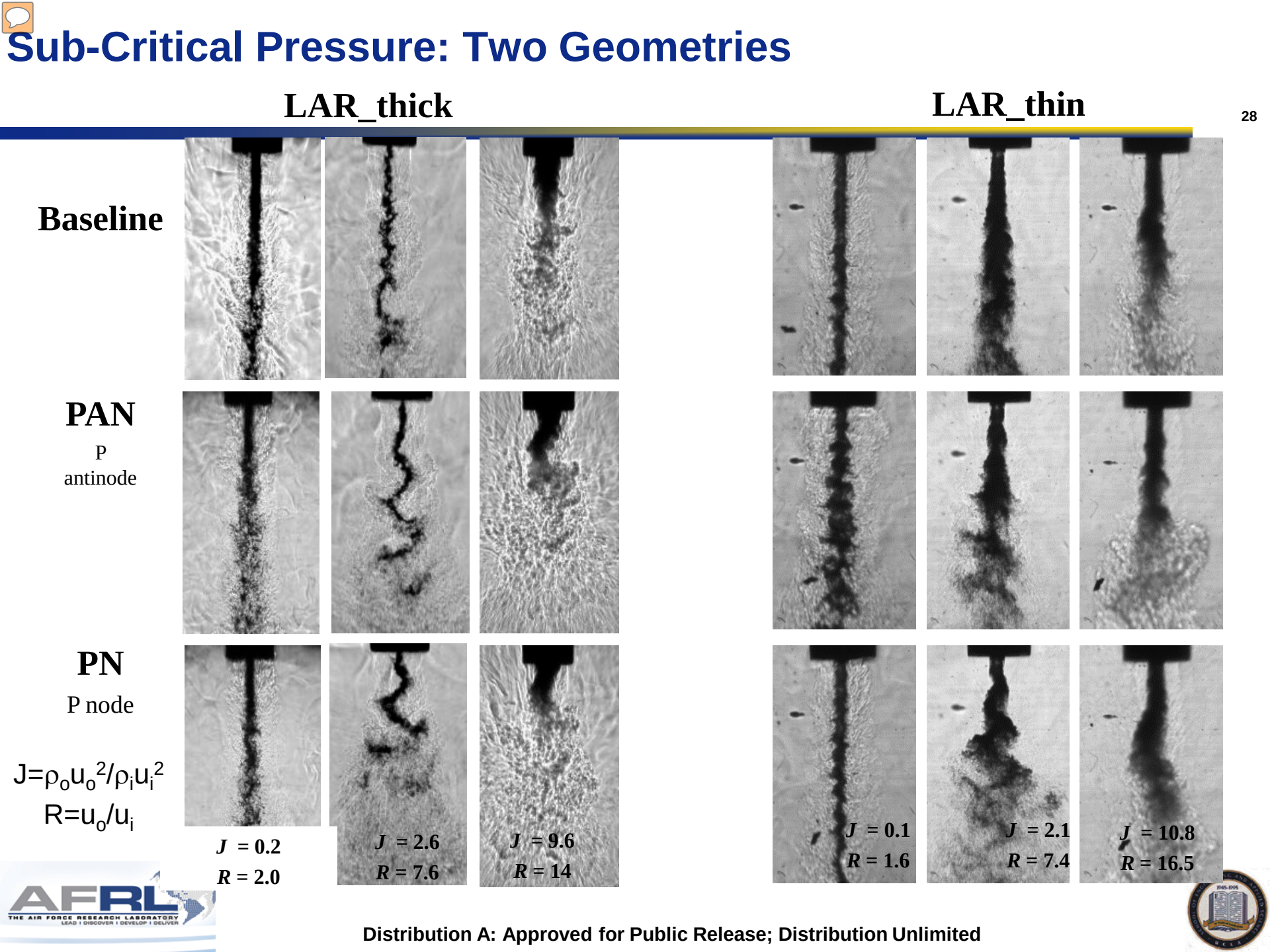

Near-Critical Pressure: Two geometries

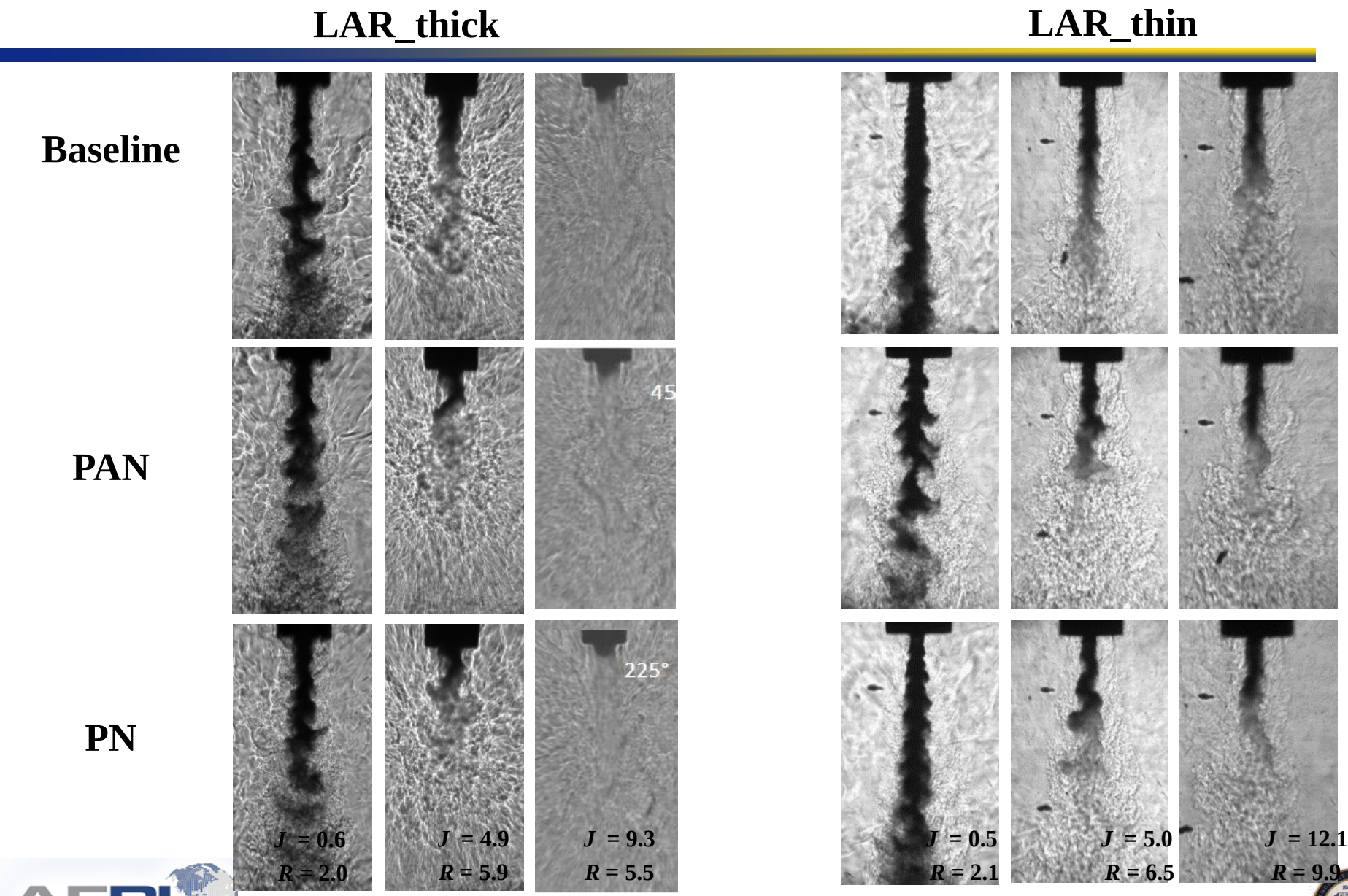

SAR_thinLip

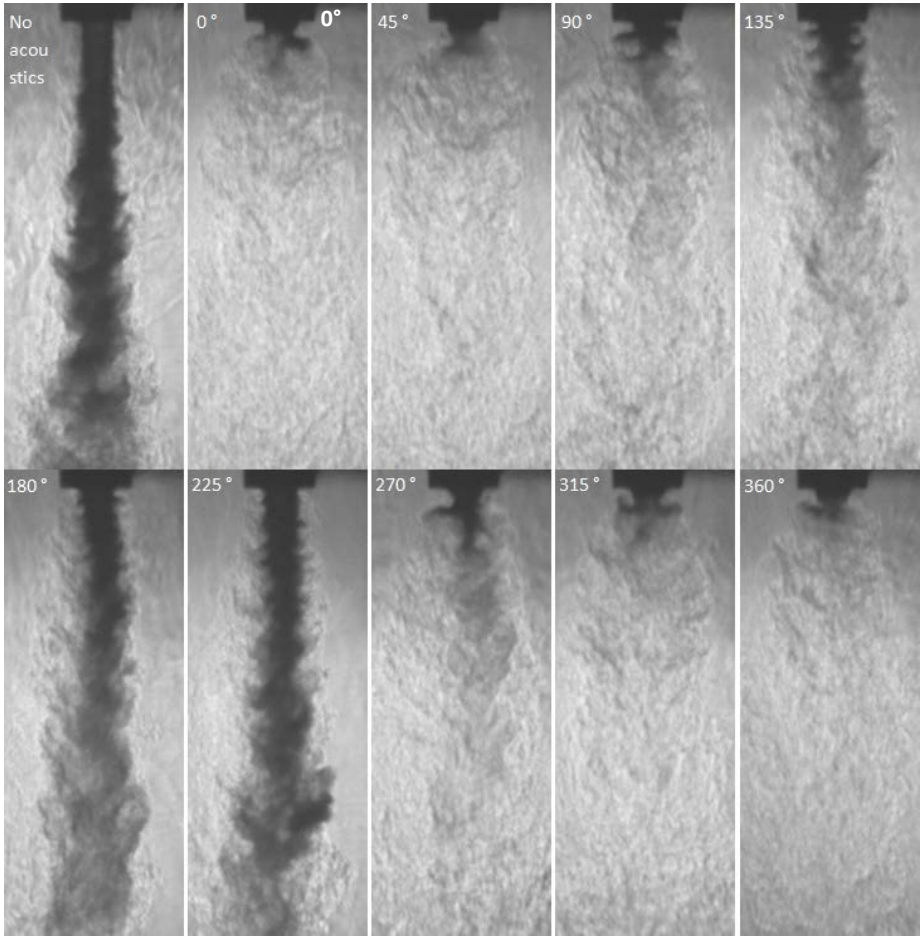

Pr=1.05, J=1.7, p´/p=0.32%

Coupled to Outer Jet Acoustic Mode

- Nearcritical conditions
  - No jet bending observed
  - large vortical structures generated when coupled to injector mode
  - Reduction of dark core can be as large as 90%
  - More clear response of jet to pressure antinode
- Subcritical conditions
  - Same mode – vortical structures
  - Not as dramatic reduction as with nearcritical cases

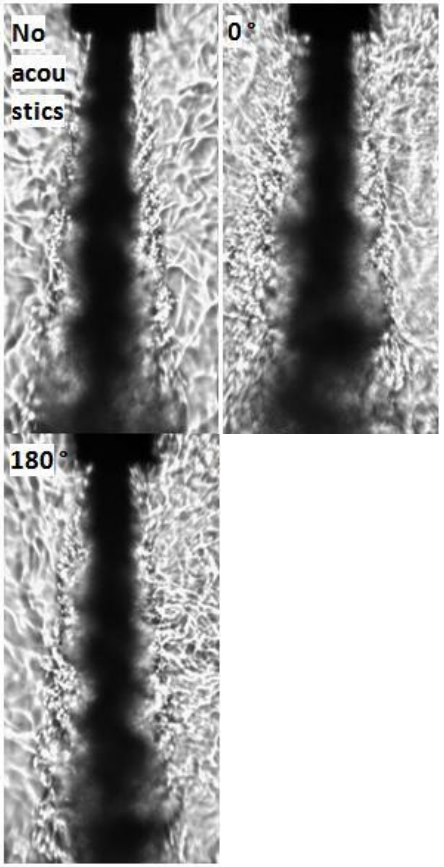

Pr=1.05, J=2.2, p´/p=0.25%

Non Coupled

New analysis: synchronized p' and images taken with microscopic lens

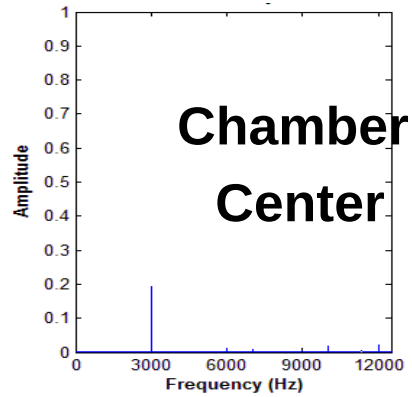

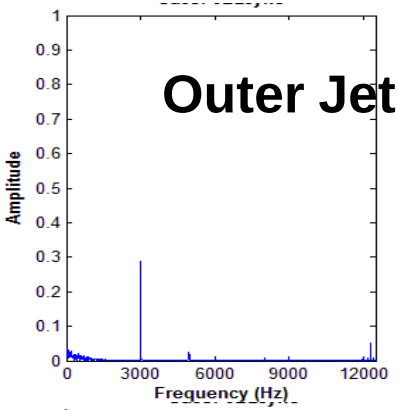

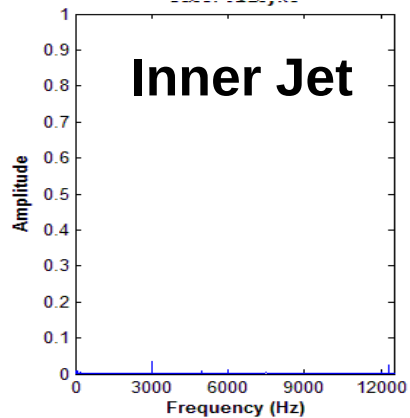

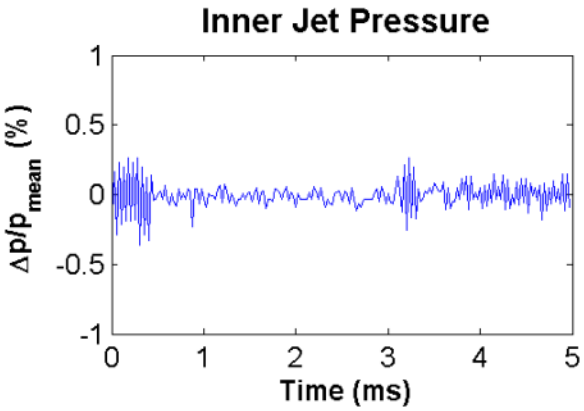

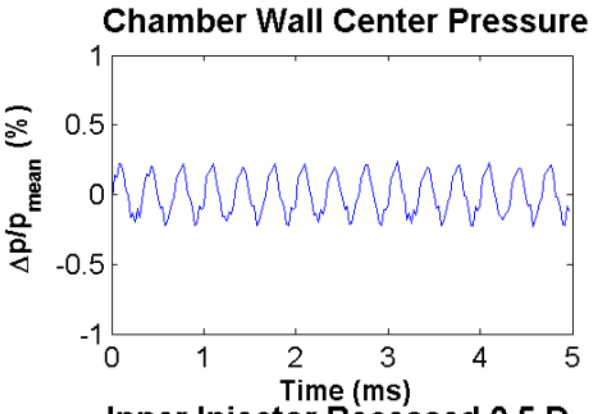

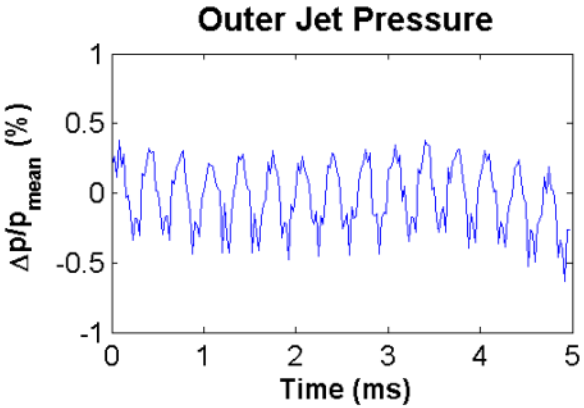

Inner Injector Recessed 0.5 D_i

Pr = 1.03, J = 5.1, VR = 5.9

Forcing Condition: 3000 Hz, Maximum Δp

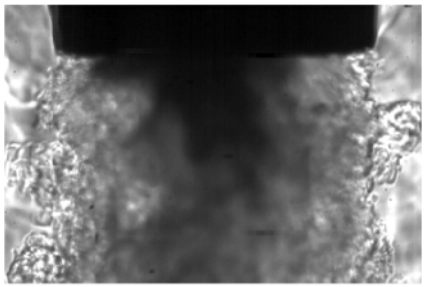

Uo=6. 25 m/s, Ui=1.06 m/s, To=165K , Ti=118 K

Results – Baseline Low *J* Flow at P_r = 0.44

- **LAR-thin , *Pr* = 0.44, *J* = 0.5**

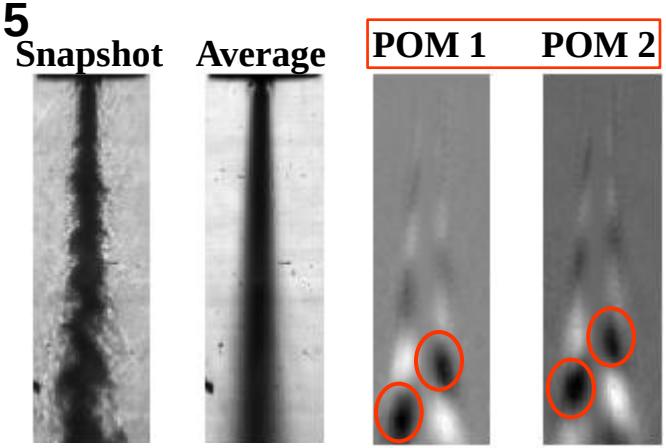

Amplitude information contained in singular values

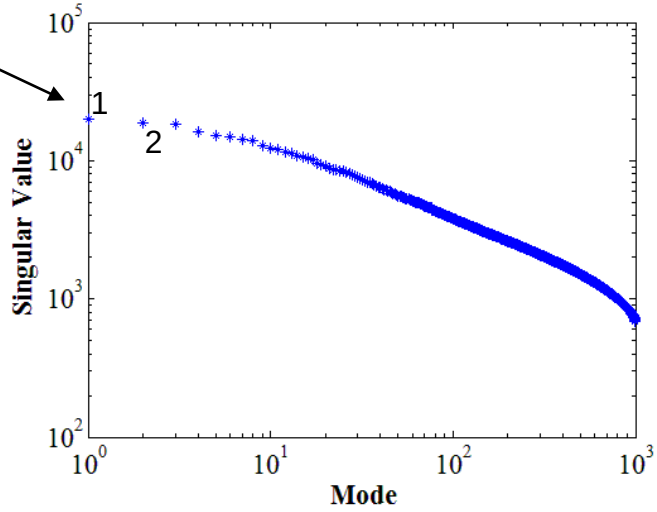

Antisymmetric Structures Identified with Characteristic Frequencies

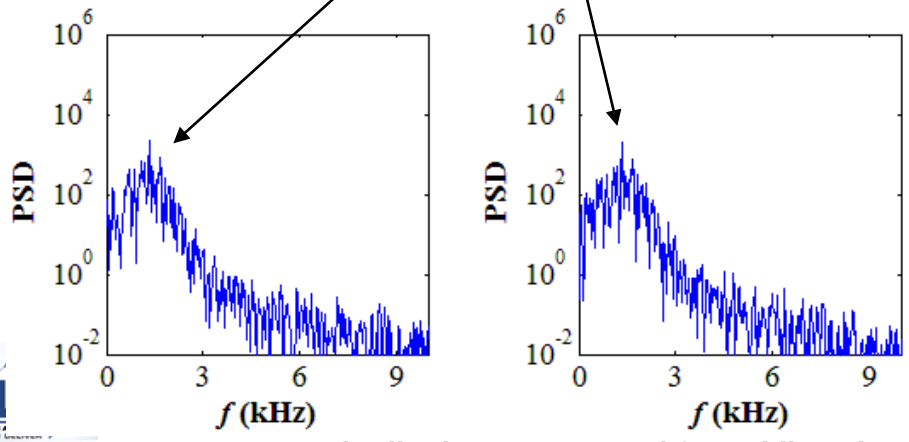

Power Spectral Densities (PSD) of Temporal Coefficients of POMs 1 and 2

Sample Animation – PAN (f_F = 3.14 kHz)

- **LAR thin *Pr* = 0.44, *J* = 0.5**

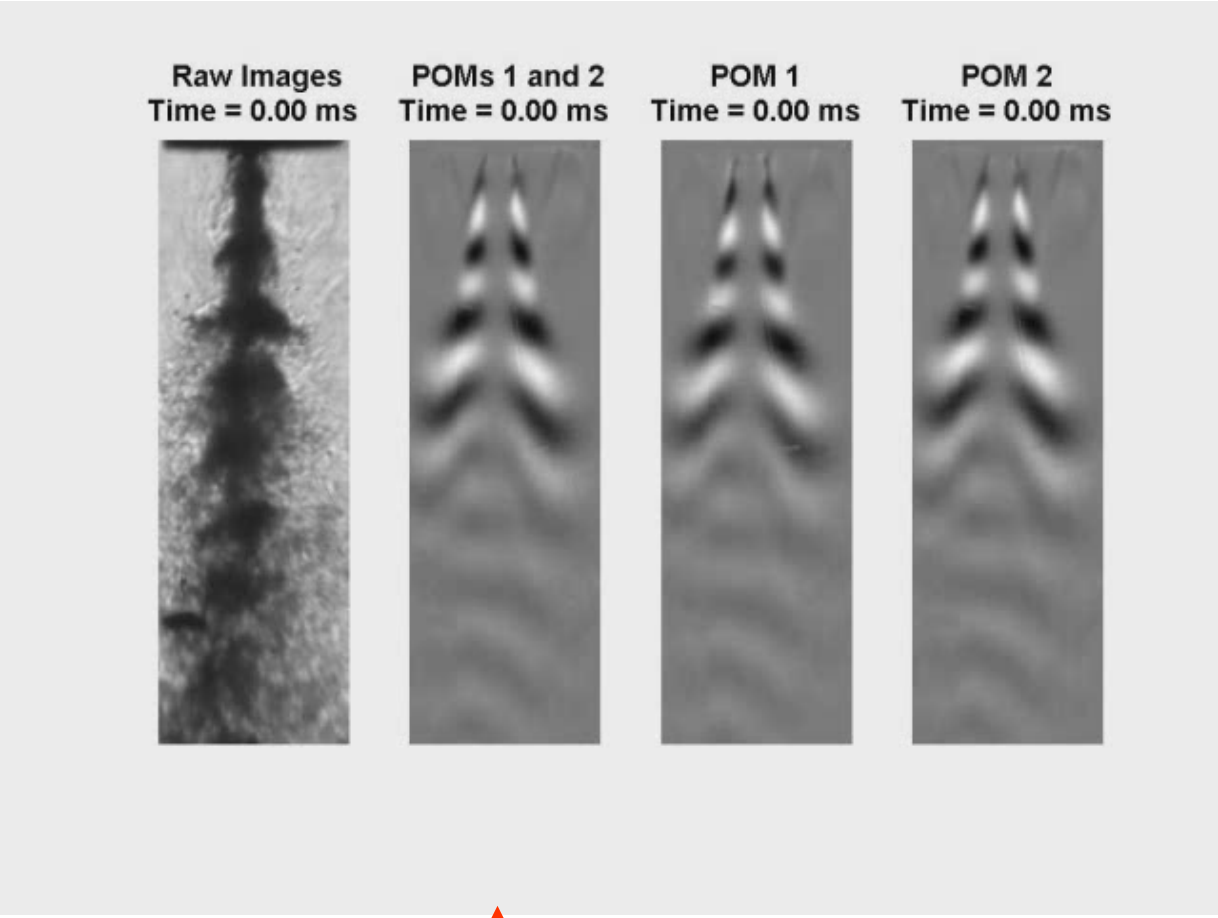

Superposition of POMs 1 and 2 Resulted in Downstream Propagating Structures

Results – LAR-thin, *Pr* = 0.44, Baseline

- **Antisymmetric flow structures indicated helical type flow instabilities for all *J***

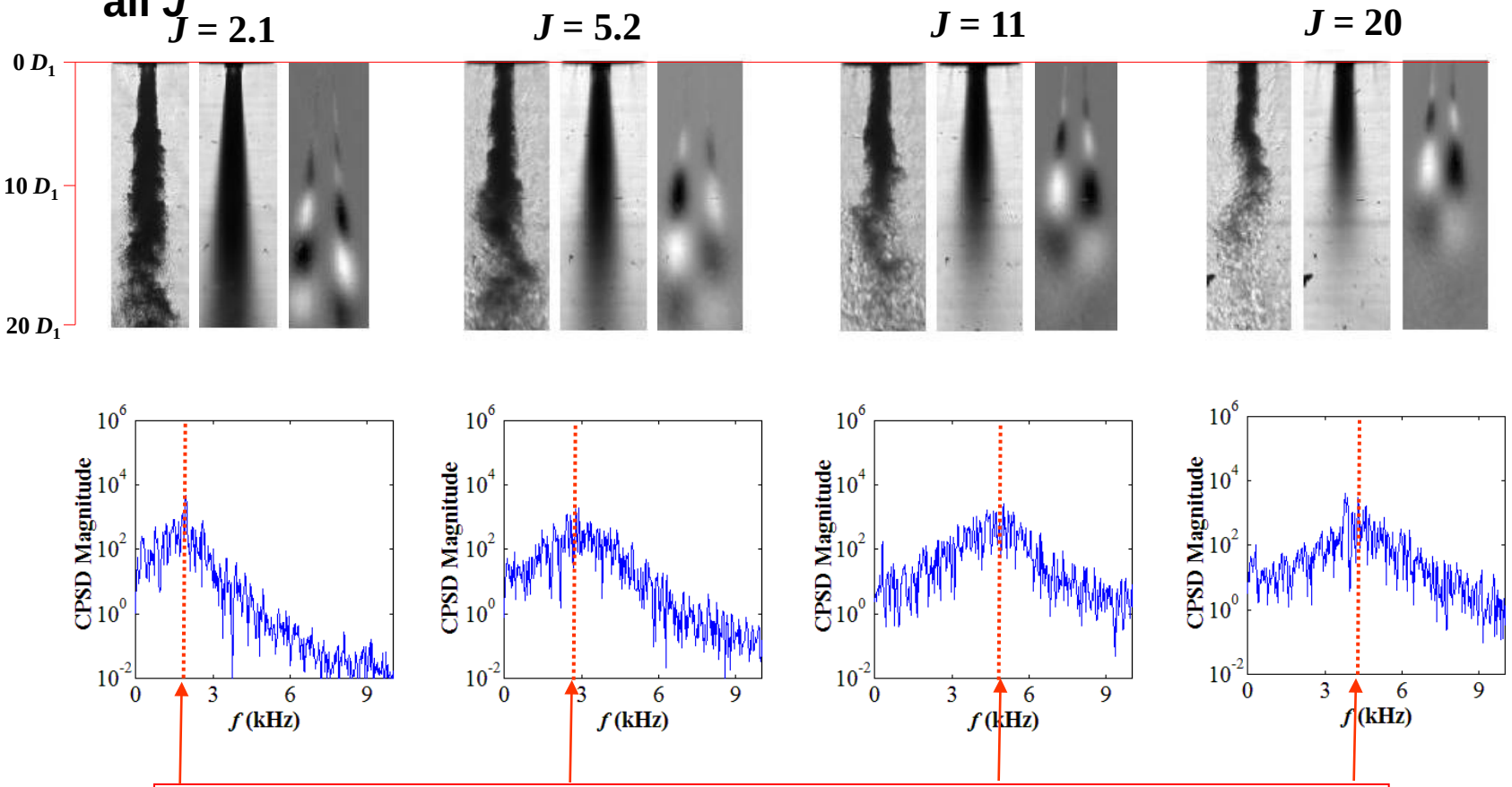

Characteristic peaks broadened and shifted to higher frequencies with increasing outer jet velocity

Results – LAR-thin, *Pr* = 0.44, PAN

- Gradual shift from symmetric to antisymmetric flow structures with increasing *J*
- Response at forcing frequency, f_F, dominant at lower *J*

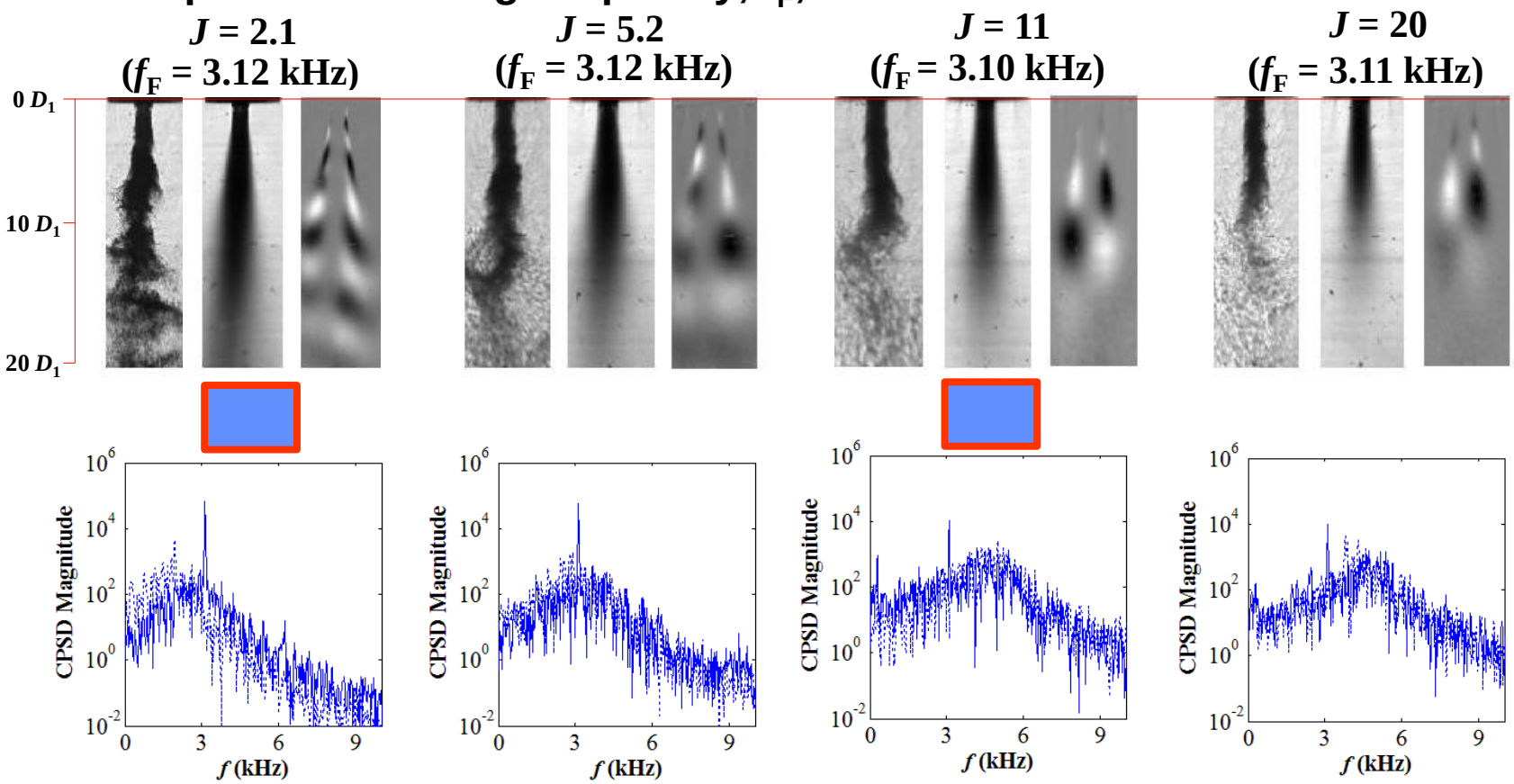

Results – SAR-thin, *Pr* = 0.44, Baseline

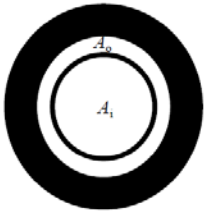

- **Helical type flow instabilities became more well-defined with increasing *J***

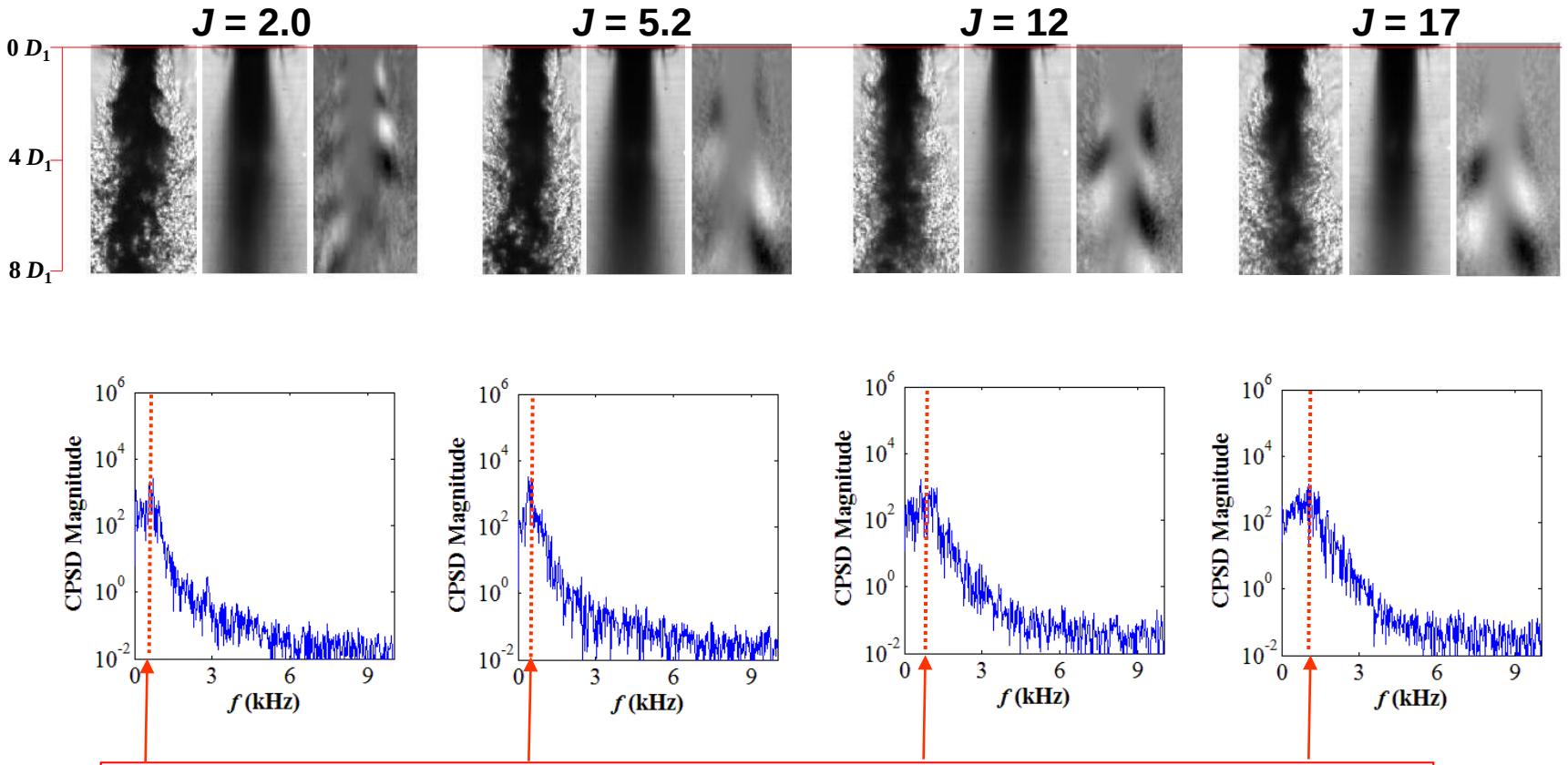

Unlike LAR flows, characteristic peaks showed minimal variation in frequency with outer jet velocity

Results – SAR-thin, *Pr* = 0.44, PAN

- Symmetric structures persist despite increasing *J*
- Response seen for all *J*

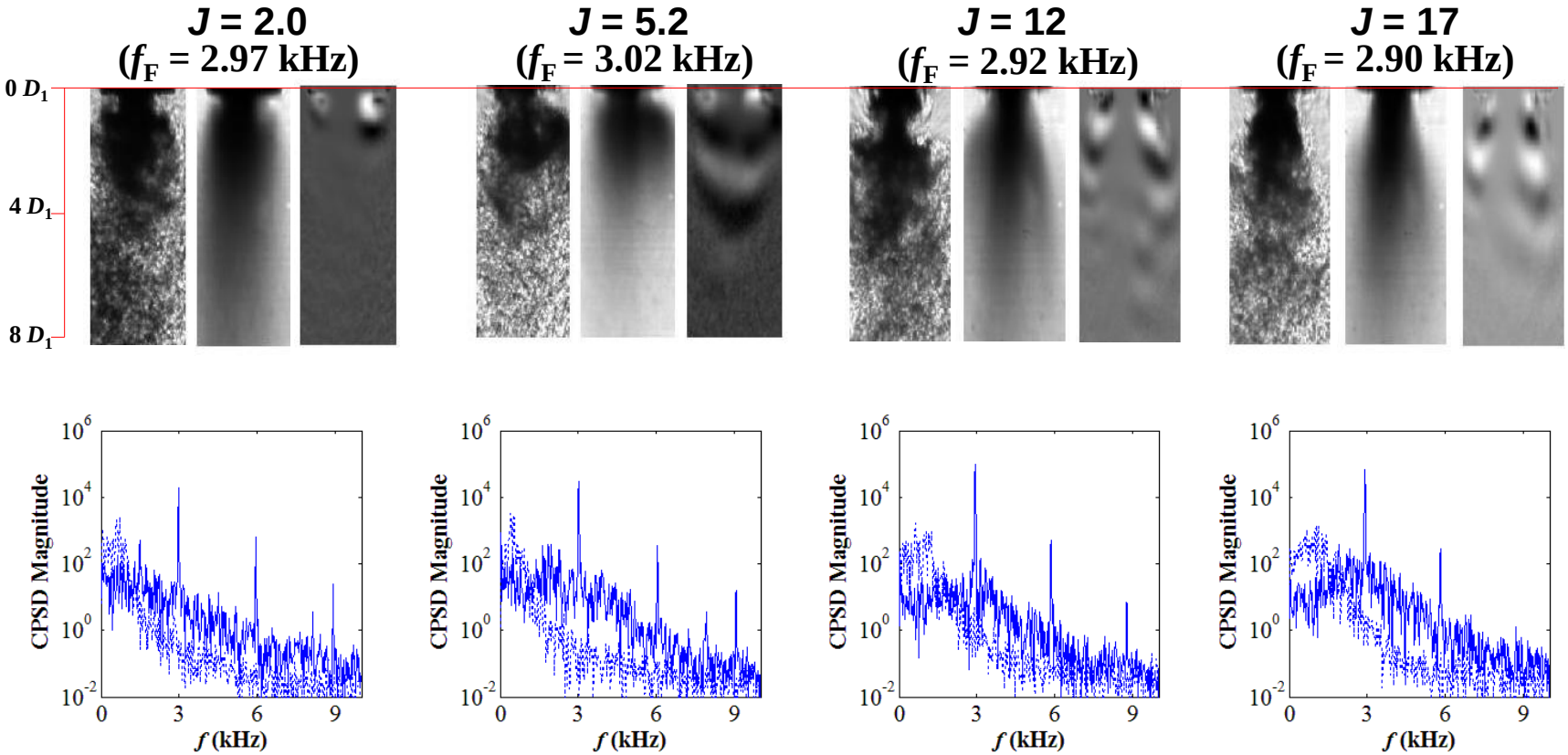

Results – SAR-thick – P_r = 0.44 Baseline

- **Well-defined antisymmetric flow structures observed for $J \geq 2$**
- **Unlike the LAR-thin flows, peaks in CPSD magnitude spectra remained at the lower end of the frequency spectrum despite increasing J**

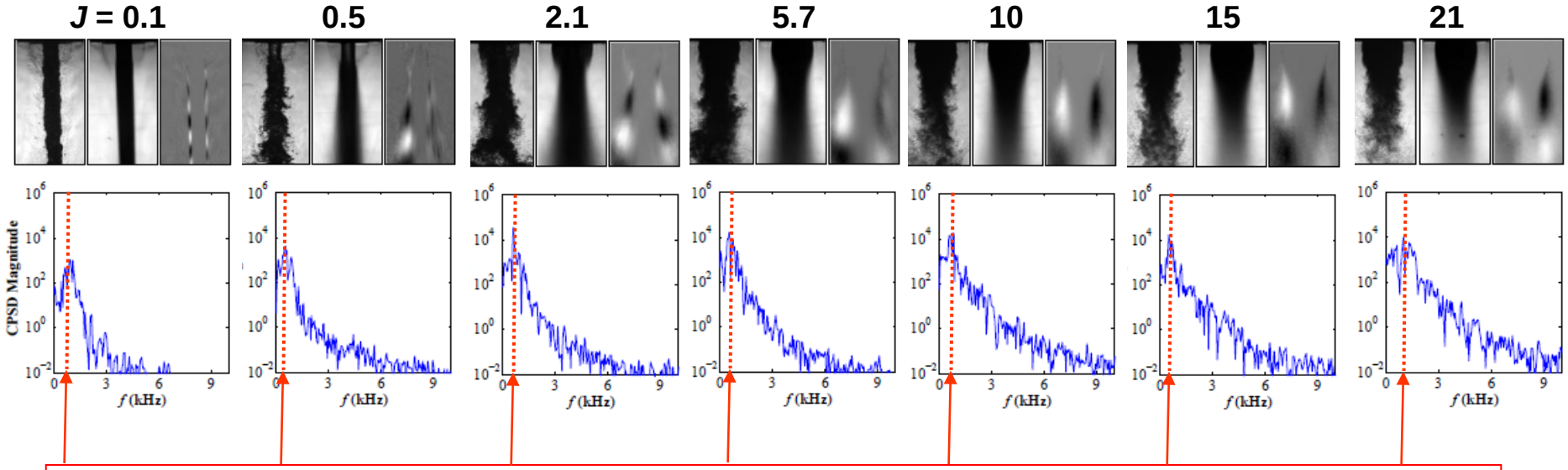

Unlike LAR flows, characteristic peaks showed minimal variation in frequency with increasing J

Results – SAR-thick – P_r = 0.44, PAN

J = 0.5
f_F = 3.04 kHz

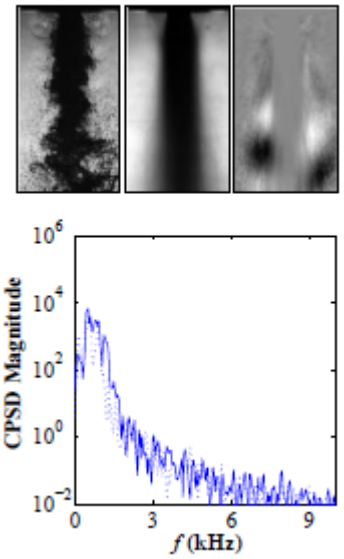

J = 2.1
f_F = 3.07 kHz

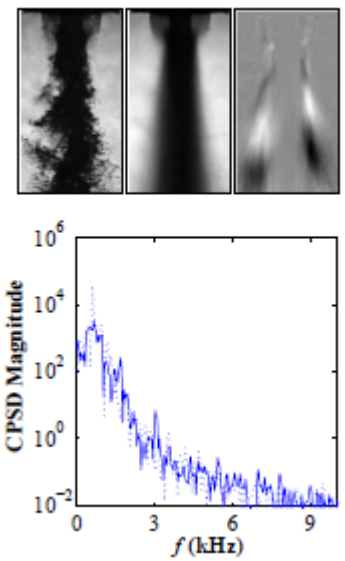

J = 5.7
f_F = 3.11 kHz

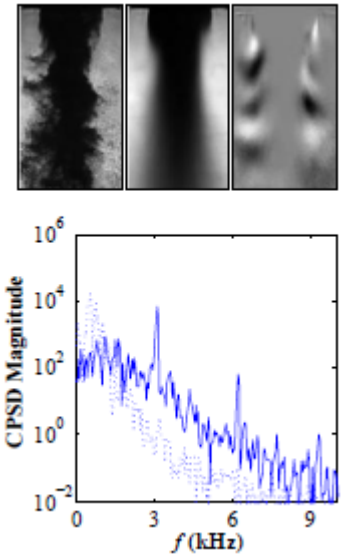

J = 10
f_F = 3.11 kHz

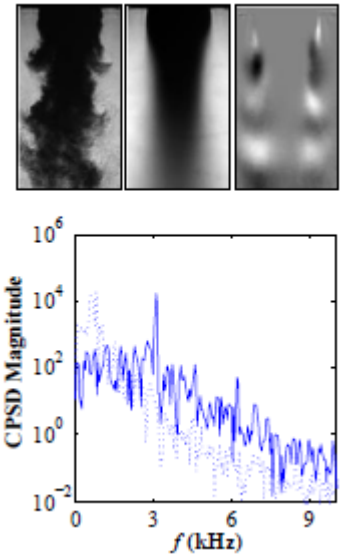

J = 21
f_F = 3.11 kHz

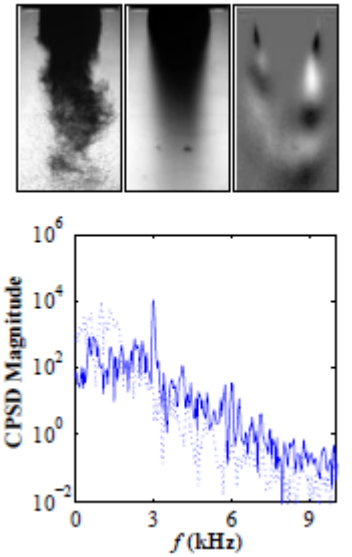

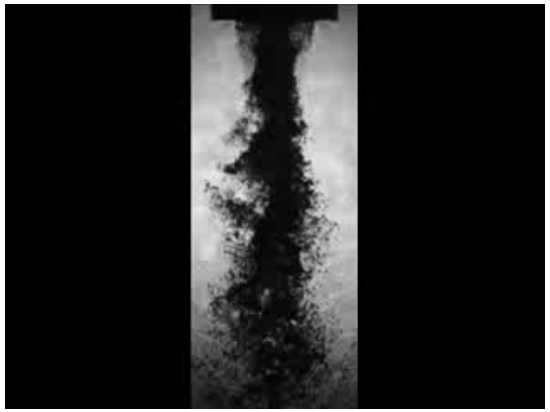

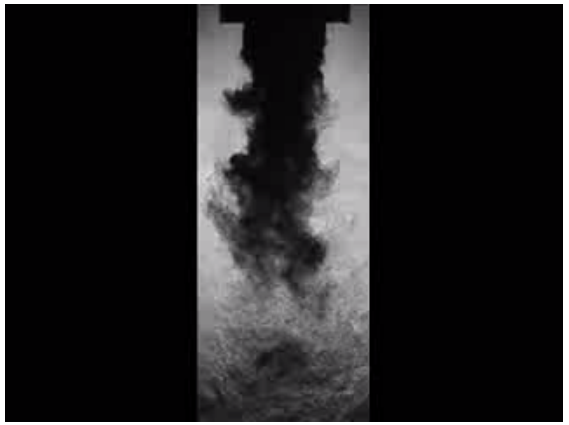

Collaboration with ECP: Thomas Schmitt, Juan Rodriguez (AFRL post-doc), Sebastien Candel, Ivett Leyva

Velocity Fields for Different J values

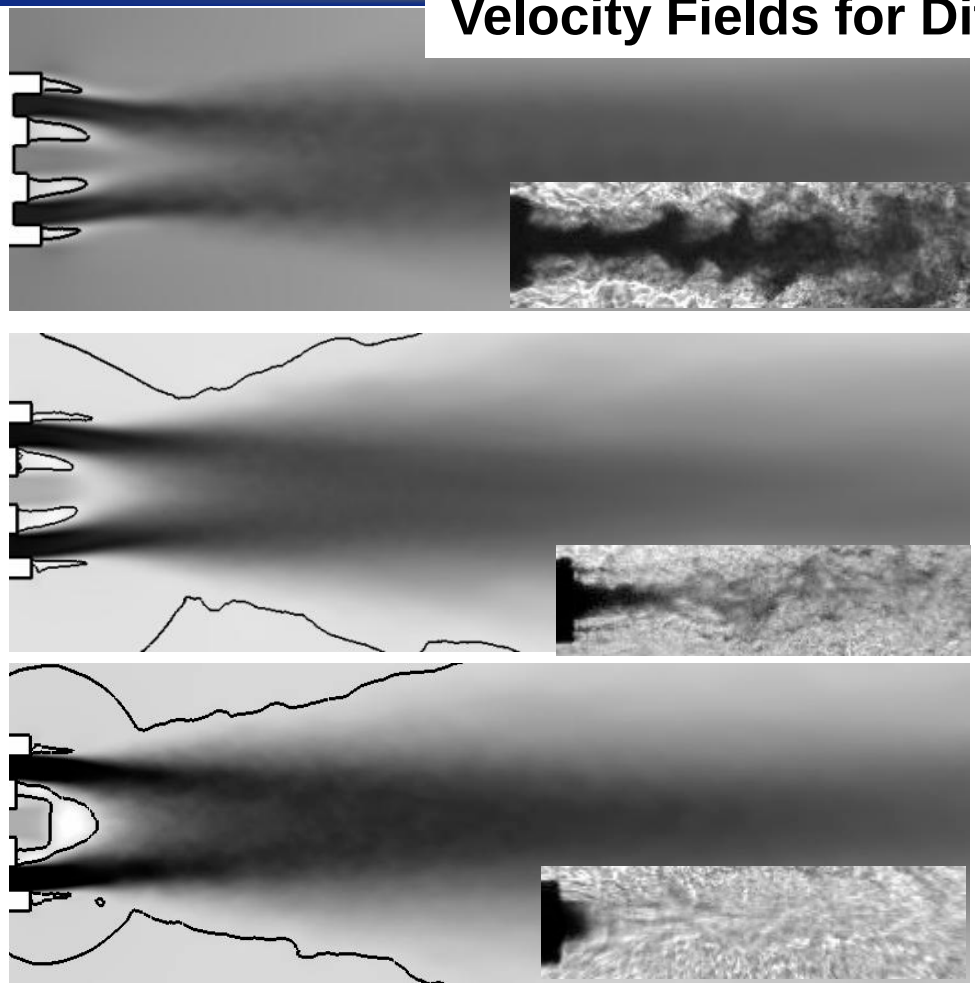

Longitudinal slice of axial velocity. White: minimum; black: maximum. Dark line indicates iso-contour of zero axial velocity. Top: J = 1.1; middle: J = 3.0; bottom: J = 9.3.

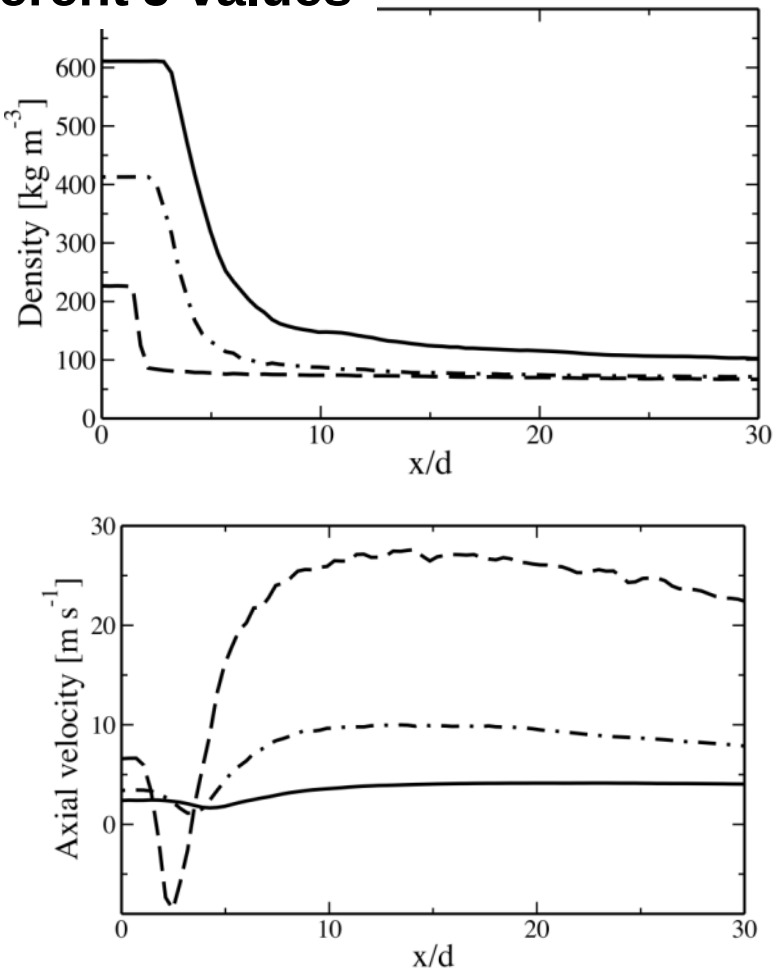

Top: centerline profile of density; bottom: centerline profile of velocity. Dark line: J = 1.1; dash point line: J = 3.0; dashed line: J = 9.3.

Fundamental frequencies for baseline conditions

Case "N6" (*J=3.05*) *Density distribution (white: 60 kg/m³; black: 410 kg /m³; logarithmic scale).*

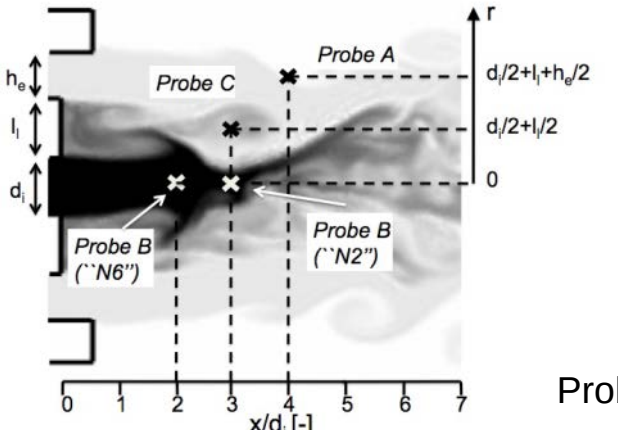

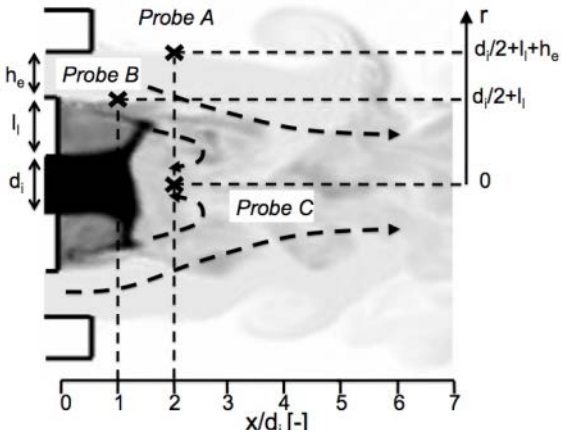

Probe A

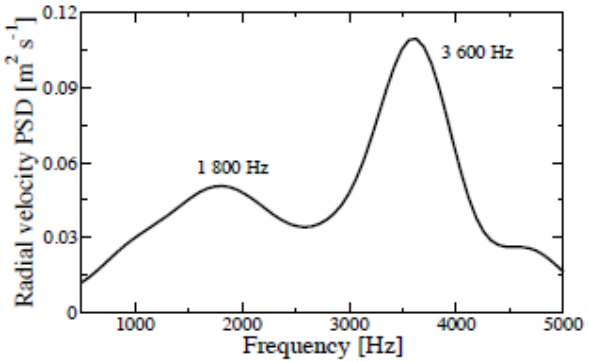

(b)

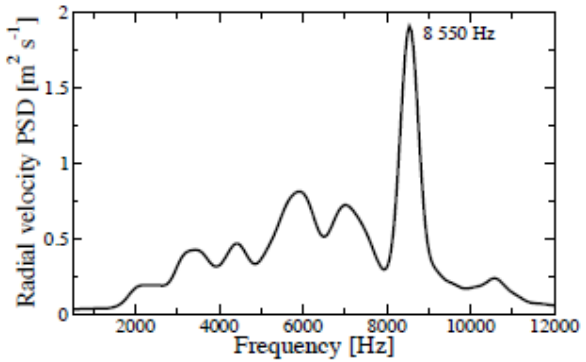

Case "N8" (*J = 9.3*) *Density distribution (white: 60 kg/ m³; black: maximum ; logarithmic scale).*

OUTER JET J=1.05 R=2.48

OUTER JET J=3.05 R=4.18

Case	$St^e = h_e f/U_{oj}$ (probe A)	$St^i = d_i f/U_{ij}$ (probe B)	$St^l = l_l f/U_{oj}$ (probe C)
N2	0.25	0.34	0.15
N6	0.25	0.26	0.14

Found relevant St numbers for our configurations

AFOSR/NASA Combustion Stability Workshop, July 8-11 2008

- **The single largest unknown in combustion instability is the “combustion response” (how combustion responds to acoustic waves)**

- **Within the combustion response, flame holding in the near injector field is a key mechanism**

- **GA Tech was selected to lead an effort on a closed-loop study.**

EC-4H – Combustion Instability Lab

- Concentrate on near injector field
- Measure p’ and q’ simultaneously to evaluate the Rayleigh criteria for combustion instability
- Start with shear coaxial jets – cold flow heritage
- Lab designed for 2000 psi – about double the pressure from other labs in the world
- Start with current design for acoustic drivers pressure nodes and antinodes

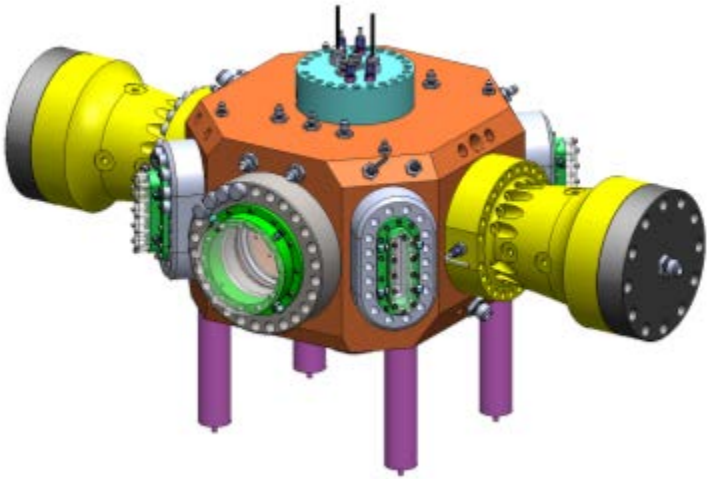

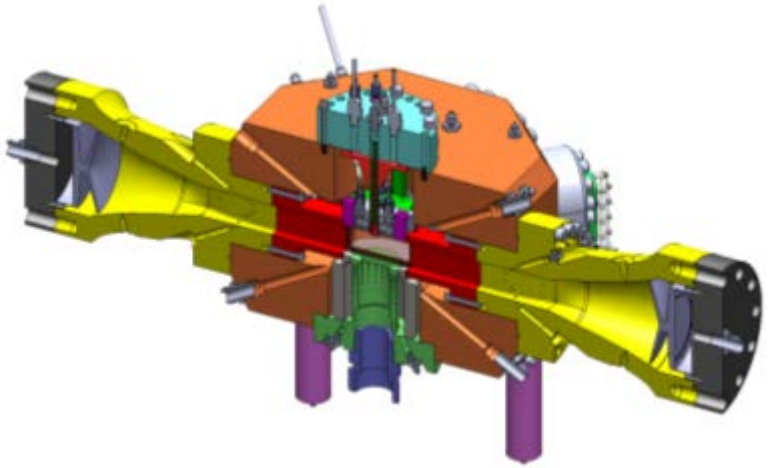

Status

- 1500 g LN2 tank installed Sept 28, 2011
- Installed Class I Div 2 outlets (115V, 208V, 240V) – stripped floor for O2 compatibility, painted cell
- First chamber pieces arrived week of March 5, 2012
- Fluid systems in full construction
- Data acquisition components starting to arrive

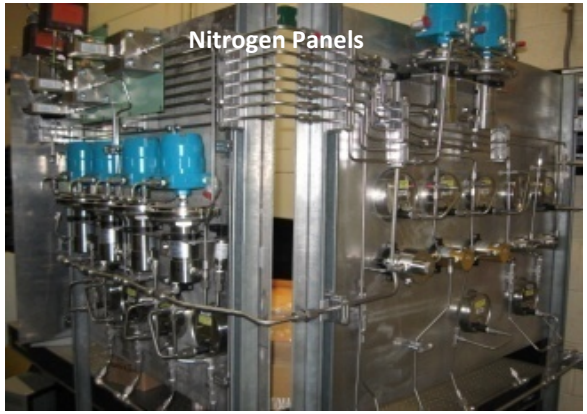

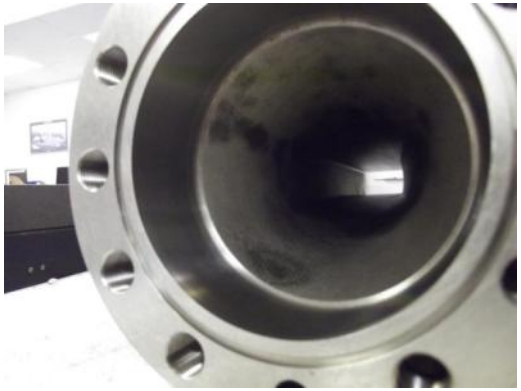

Construction/integration to be finished by 3Q 2012

Conclusions

- **J is not the only parameter to characterize mixing in shear coaxial jets - Area ratio, Inner jet post thickness, and reduced densities matter!**
  - Found functional correlations for dark core lengths
- **Based on four geometries, mixing is enhanced with increasing J and t/D1 but less efficient with increasing Ao/Ai**
- **Through LES found relevant St numbers for one geometry for different J**
- **Helical instabilities were observed for LAR-thin and SAR-thick, SAR-thin geometries at large J for baseline conditions**
- **Geometry plays a role for the response of the jet to acoustics, at PAN:**
  - LAR-thin: The flow became less sensitive to applied PAN forcing with increasing J
  - SAR-thick: Recirculation zone dampens the effect of PAN forcing at lower J, but at higher J (>10) measurable effect
  - SAR-thin: Flow responds to forcing acoustic frequency at all J

BACKUP MATERIAL

Conclusions

- **Mixing for shear coaxial jets has other major variables other than momentum flux ratio (J)**
  - Ratio of inner jet temperatures is another important variable
  - Geometry – Area ratio and lip thickness also affect mixing
- **For LARthick**
  - Found bending mode with largest effect at velocity antinodes
  - The reduction on the dark core length was greatest for a medium J range
  - For near critical pressures, the collaboration with ECP determined relevant St for our injector configuration and was able to capture qualitative behavior of natural and excited jets
- **For SARthin**
  - Did not see bending mode for conditions studied
  - Saw vortex roll-up and puffing occurring over entire J range (0.09-21) tested –
  - PAN forcing produced symmetric flow structures regardless of *J*
  - Spectral plots showed strong response to PAN forcing at low and high *J*
- **For LARthin**
  - Sees both bending and vortex roll-up modes depending on the acoustic frequency
  - PAN forcing at low *J* produced symmetric flow structures, while at higher *J*, influence of forcing subsided
  - Spectral magnitude plots showed decreasing influence of PAN forcing with increasing *J*

New Combustion Chamber

AFRL – Edwards was tasked to develop an experiment and to lead a joint experimental / modeling team to study coupled flame holding mechanisms.

LEVERAGE EXPERIENCE GAINED WITH COLD FLOW EXPERIMENTS

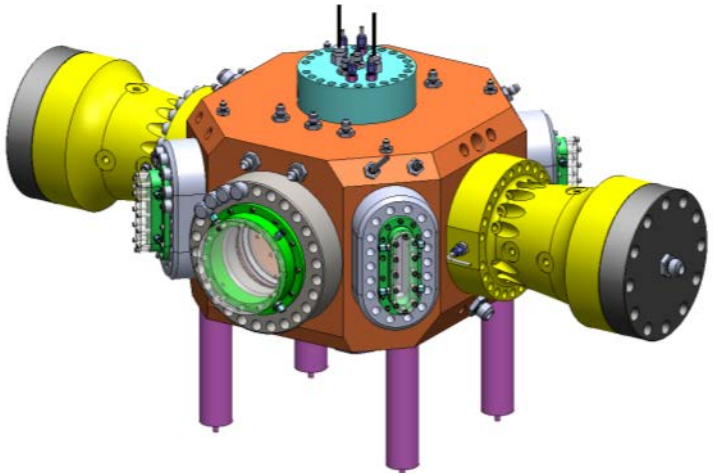

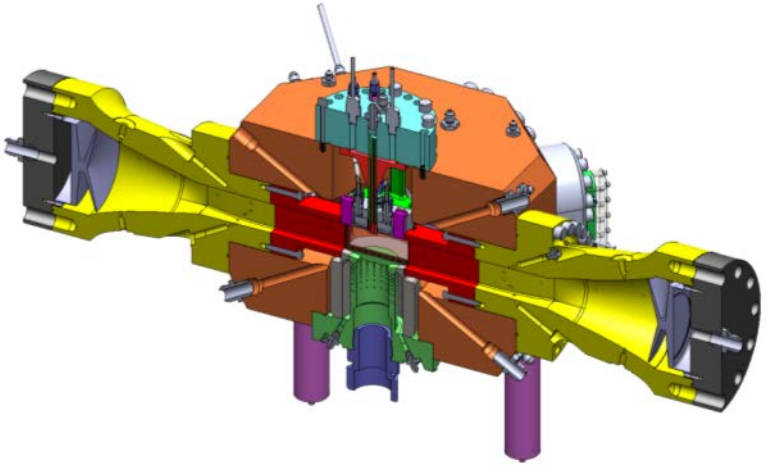

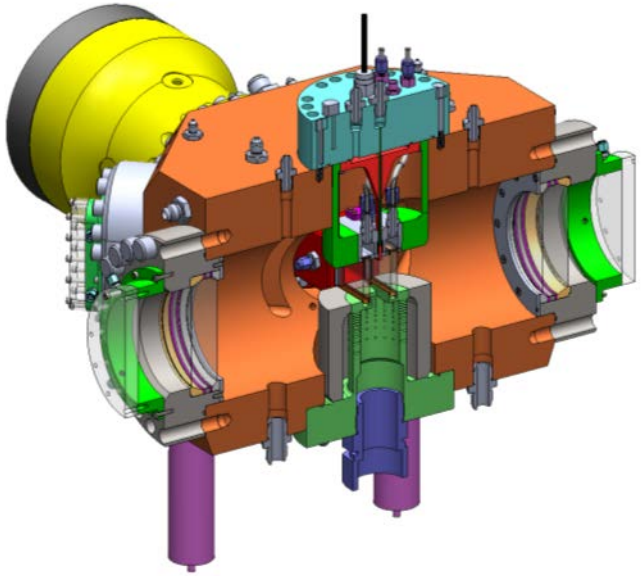

Construction and Organization of Data Set

- First, form a row vector consisting of all pixel intensity values of each snapshot image (with resolution of *n* rows by *m* columns) in order of increasing columns, then increasing rows

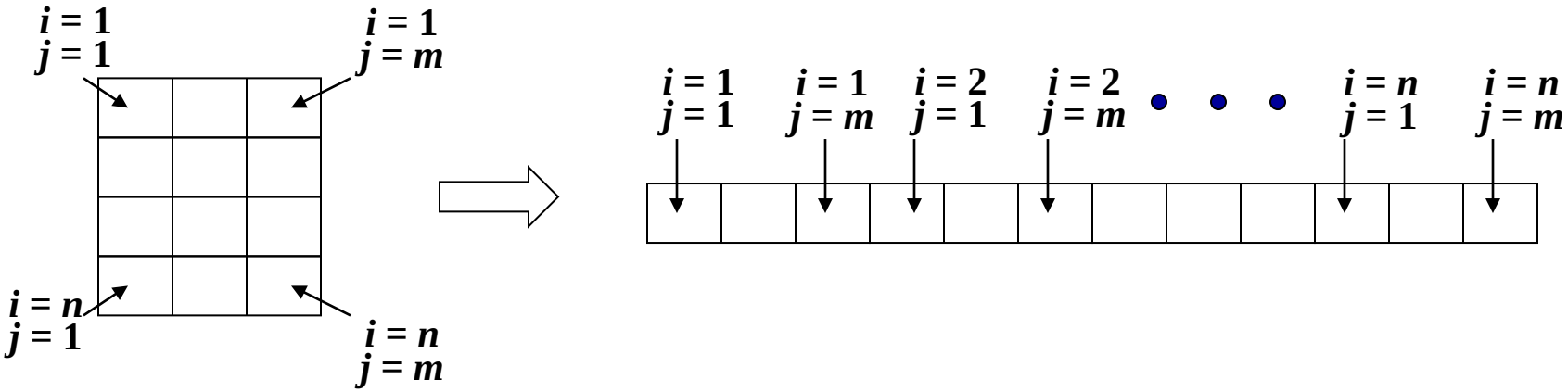

- Then, combine all such row vectors for *N* sequences of image frames resulting in a matrix A consisting of *N* rows by (*M* = *n* x *m*) columns of intensity values.

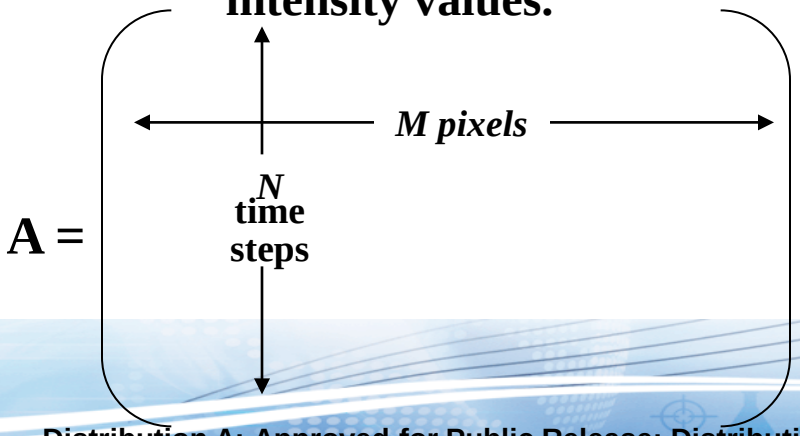

Matrix Decomposition

- **Eigenvalue decomposition or singular value decomposition (SVD) can be used**
- **SVD Subroutine readily available in MATLAB®**
- **Prior to matrix decomposition, the temporal mean of A was subtracted resulting in a matrix of intensity fluctuations Ã, i.e.,**

$$\tilde{A}_{ij} = A_{ij} - \frac{1}{N}\sum_{i} A_{ij} \qquad \text{for } i = 1\ldots N,\ j = 1\ldots M$$

- **Application of SVD on Ã gives two orthogonal matrices U (NxN) and V (MxM), and a diagonal matrix S (NxM) of singular values in increasing order of magnitude**

$$\tilde{A} = USV^{T} = QV^{T}$$

- **Thus, a time-resolved set of images intensity fluctuations Ã(*x*,*t*) can be represented as a linear combination of orthonormal basis functions ϕ_k such that**

$$\tilde{A}(x,t) = \sum_{k=1}^{M} a_k(t)\phi_k(x)$$

where $a_k(t)$ are time dependent orthonormal amplitude coefficients and $\phi_k(x)$ are the proper orthogonal modes of Ã.

- **Equivlance: columns of Q ~ $a_k(t)$, columns of V ~ $\phi_k(x)$**

Acoustic Analysis for Injectors

In collaboration with Jeff Muss and Rory Davis, Sierra Engineering

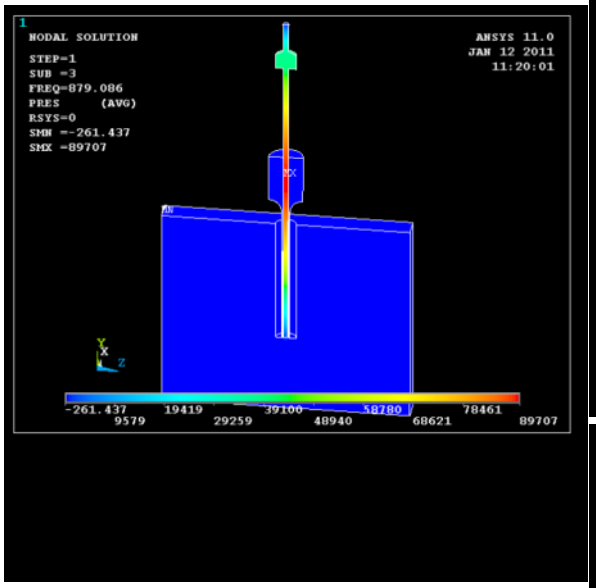

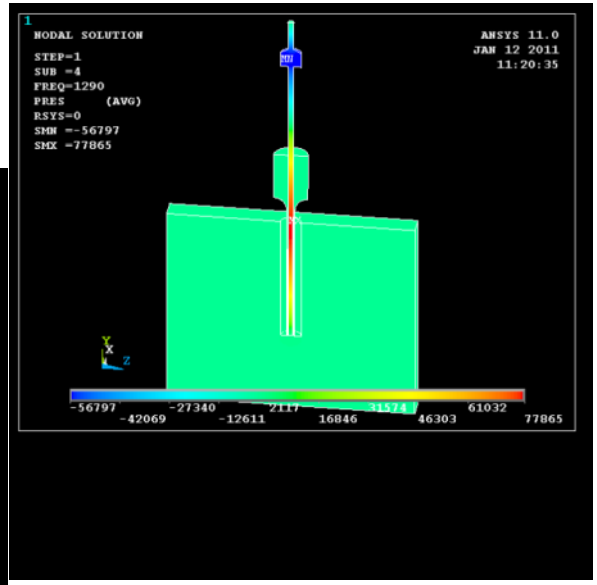

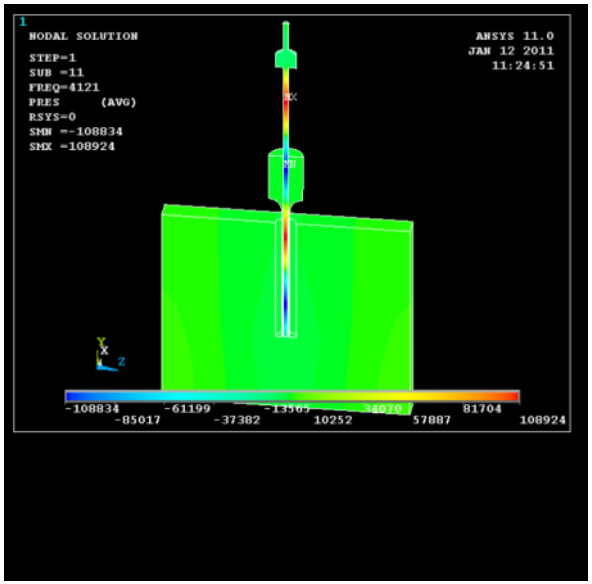

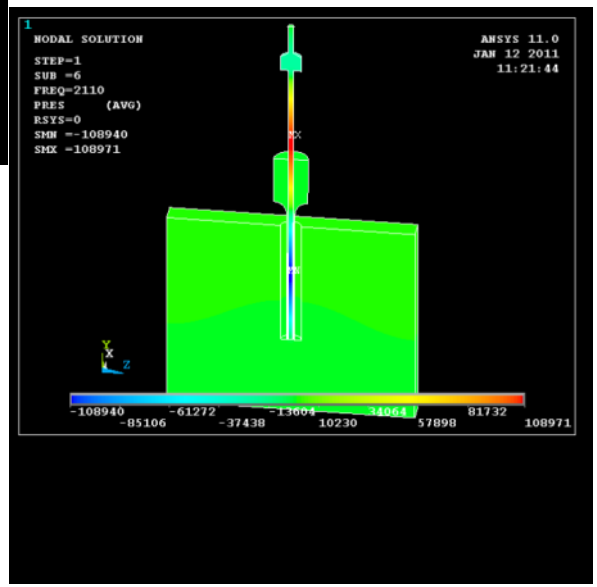

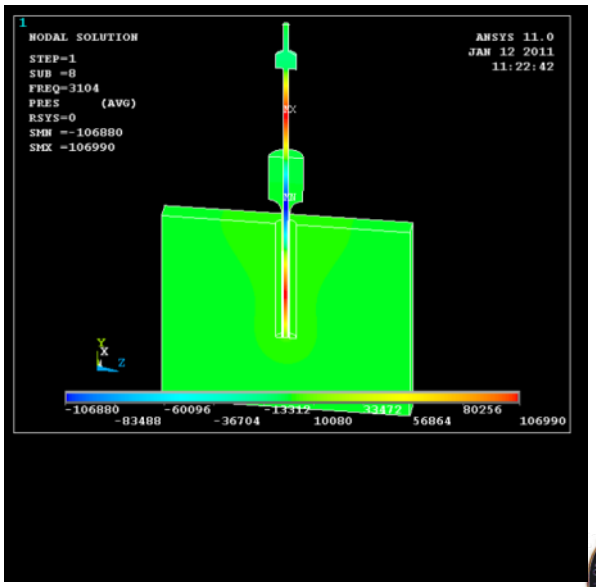

Have more accurately computed the acoustic modes for the inner and outer jets for constant and linearly varying temperatures for subcritical and supercritical pressures

Acoustic Analysis for Injectors

In collaboration with Jeff Muss and Rory Davis, Sierra Engineering

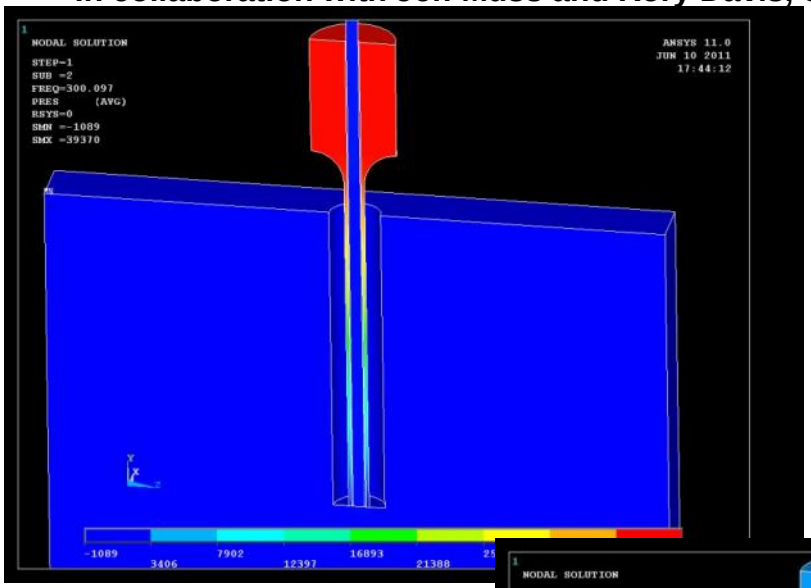

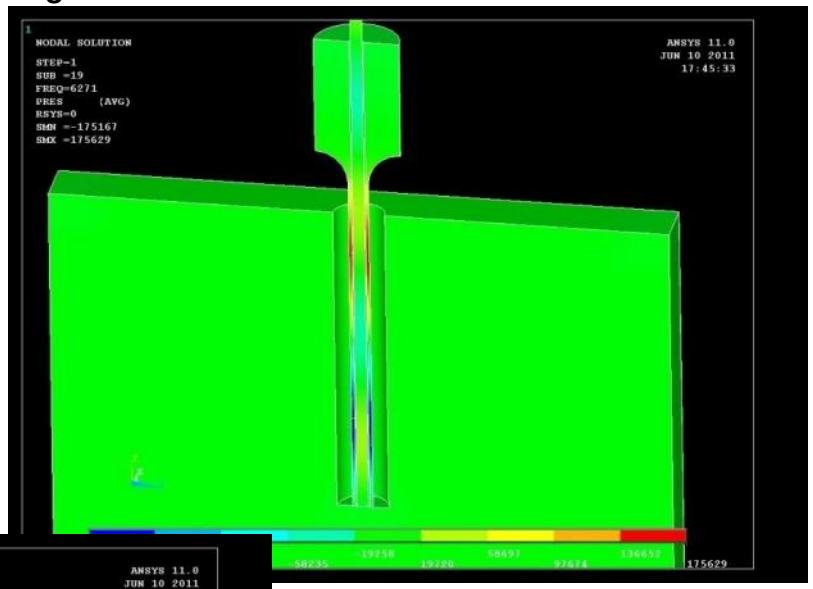

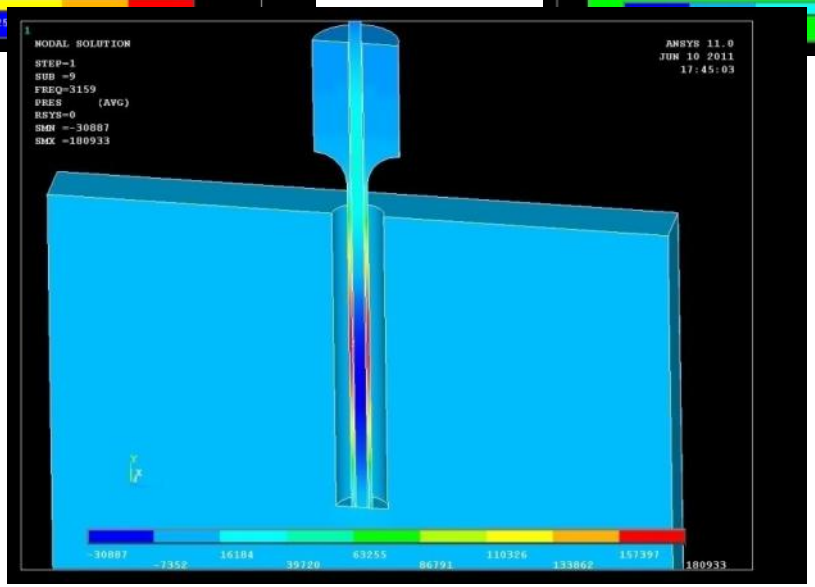

Have more accurately computed the acoustic modes for the inner and outer jets for constant and linearly varying temperatures for subcritical and supercritical pressures

Effect of R on L/D for a given J

Injector IV: **Constant** J , Varying R

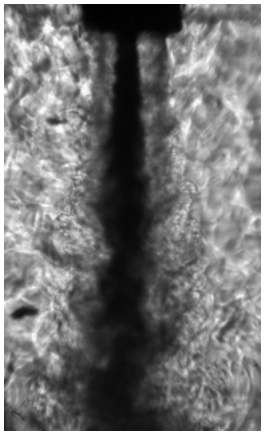

J = 2.0
R = 3.0
L/D_1 = 17.9

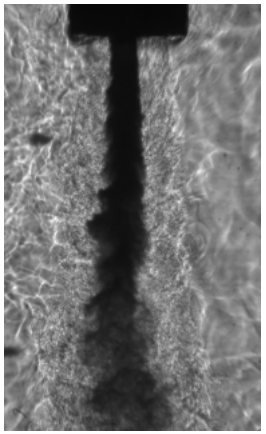

J = 2.0
R = 3.5
L/D_1 = 12.1

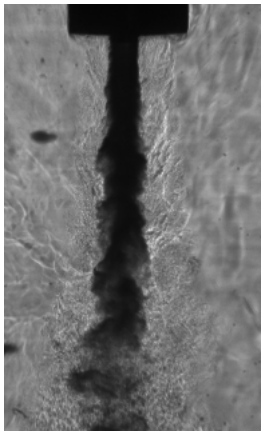

J = 2.0
R = 4.0
L/D_1 = 11.6

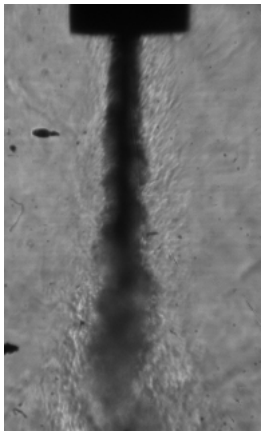

J = 2.1
R = 4.3
L/D_1 = 10.1

Collaboration with ECP: Grid and Mesh

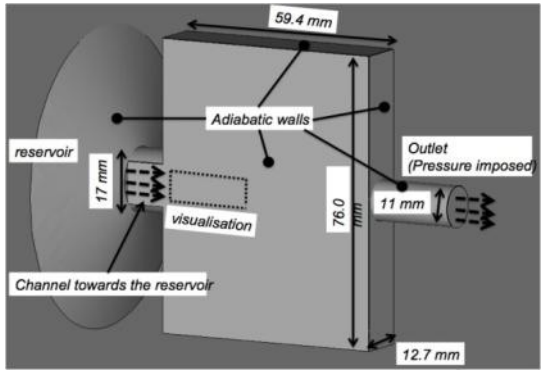

3D visualization of reservoir

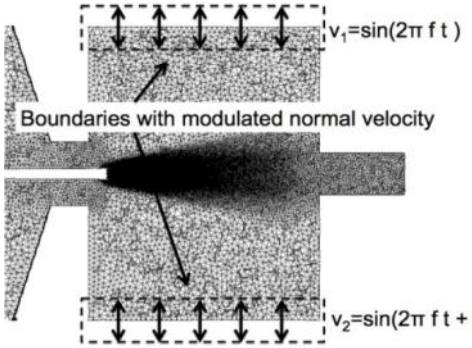

Longitudinal cut of domain with the BC's

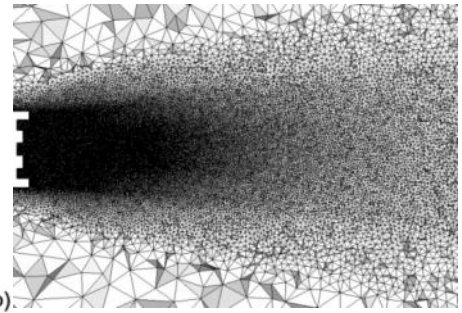

Mesh detail near the injector

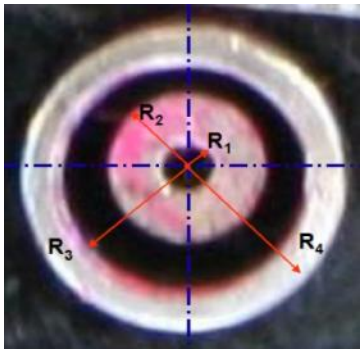

Experimental Injector

- **Solver: AVBP – state of the art LES code**
  - **With real fluid properties to tackle supercritical fluids**
- **Mesh: 2 100 000 nodes/10 000 000 tetrahedra**
  - **Highly refined near the injector (0.032 mm on a distance of 10 inner jet diameters)**
- **CPU hours on Europe SuperComputer Center: 100,000**

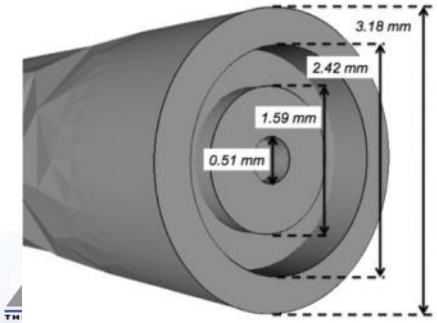

CFD Injector

Effect of Temperature on L/D for a given J

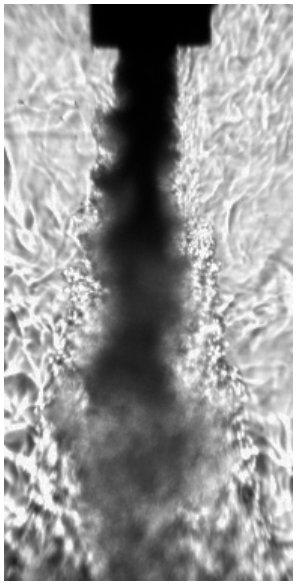

J = 9.4 R=9.9

109K/203K

Ui=0.93/9.2m/s

SAR_thinLip

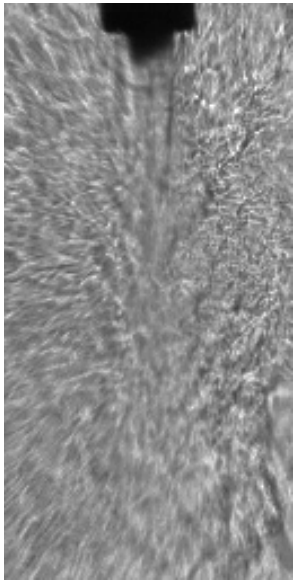

J = 9.4 R=9.9

128K/192K

Ui=6.6 /36.2m/s

LAR_thickLip

Flow Structure Comparison

	Date & Case	F_f (kHz)		P_c (MPa)	T_{outer} (K)	T_{inner} (K)	u_{outer} (m/s)	u_{inner} (m/s)	density ratio	VR	J	oj mode match	P'_{center}/P_c (%)	P'_{inner}/P'_{center} (%)	P'_{outer}/P'_{center} (%)	Structure Type
Graham Recess = 0																
SbC1	04May09 c1	3.04		1.49	207	106	1.4	0.87	0.036	1.5	0.09	Y up	0.68	13.47	187.21	large ij vortex roll up (puffs), intermitent penetration of ij
SbC2	04May09 c2	2.96		1.5	187	110	2.7	0.97	0.045	2.8	0.35	Y dwn	0.64	10.16	198.53	med ij vortex roll up at ~3000 Hz, no penetration of ij
SbC3	23April09 c2	2.96		1.5	150	106	5.6	0.94	0.057	5.8	2.02	Y up	1.06	21.24	60.55	large ij vortex roll up at ~2857 Hz
SbC7	22April09 c1	3.04		1.49	188	110	14	0.98	0.045	14.2	9.00	Y up/down	0.81	3.75	61.47	large ij vortex roll up @~2857 Hz
SbC8	23April09 c1	3.04		1.5	170	109	15	0.94	0.050	16.0	12.55	N?	1.13	3.37	55.84	large ij vortex roll up @~2857 Hz, oj flips ij vortices
SbC9	22April09 c2	2.96		1.5	187	110	17.4	0.99	0.045	17.5	13.80	Y up	1.31	1.90	49.22	large ij vortex roll up downstream, large oj roll up at exit
SbC10	23April09 c3	3.06		1.5	178	110	21.51	0.99	0.048	21.2	21.03	N?	0.56	13.32	5.15	med ij vortex roll up downstream
NC1	05May09 c2	3.09		3.57	176	120	3.7	1.0	0.140	3.6	1.92	Y up	0.85	4.96	72.69	large ij vortex roll up, pinched off
NC2	05May09 c3	3.06		3.57	186	122	5.7	1.2	0.136	5.2	3.07	Y up/down	0.66	2.36	64.30	large ij vortex roll up
NC3	30Apr09 c1	3.02		3.58	209	112	6.1	1.0	0.097	6.9	3.92	N	0.20	14.63	30.67	minimal ij disturbance
NC4	27Apr09 c2	2.98		3.57	181	112	9	0.98	0.118	9.2	9.92	Y up/down	0.33	5.29	96.91	large ij vortex roll up
NC5	27Apr09 c3	3.05		3.57	183	113	13	0.98	0.118	13.0	20.69	Y up	0.31	13.95	51.82	large ij vortex roll up downstream
Rodriguez Recess = $0.5D_1$																
SbC1	06Nov08 c1	3.01		1.48	199	105	1.4	0.9	0.040	1.5	0.09	Y dwn	0.38	3.29	326.90	large ij vortex roll up (puffs), intact core flow
SbC2	07Nov08 c1	2.96		1.49	197	106	3	0.9	0.039	3.3	0.43	Y dwn	0.62	4.70	155.04	large ij vortex roll up (puffs), no intact core
SbC3	10Nov08 c1	2.97		1.49	195	109	6.6	1.0	0.042	6.9	2.00	Y up/down	0.58	3.77	117.85	large ij vortex roll up
SbC4	10Nov08 c2	3.04		1.49	189	110	8.5	0.97	0.045	8.7	3.40	Y up/down	0.85	1.40	65.43	large ij vortex roll up, pinched off
SbC5	10Nov08 c3	3.02		1.49	184	110	10	0.97	0.043	11.0	5.20	Y up/down	1.18	2.01	49.59	large ij vortex roll up
SbC6	12Nov08 c1	2.96		1.49	193	108	13.0	0.9	0.040	14.0	7.80	Y dwn	0.61	1.18	113.90	large ij vortex roll up
SbC7	12Nov08 c2	2.92		1.49	194	108	16	0.9	0.042	17.0	12.00	Y dwn	0.59	1.09	107.52	large ij vortex roll up
SbC8	12Nov08 c3	2.9		1.48	201	109	20	1.0	0.041	21.0	18.00	N	0.51	4.89	102.90	large ij vortex roll up downstream
NC1	18Nov08 c1	2.98		3.56	213	109	2.2	0.93	0.095	2.3	0.50	N	0.75	21.49	72.45	minimal ij disturbance (small pulsing)
NC2	18Nov08 c2	3.06		3.56	209	109	3	0.93	0.095	3.2	0.97	Y up	0.35	10.69	55.31	minimal ij disturbance (small pulsing)
NC3	30Dec08 c1	3		3.58	198	108	4.3	0.92	0.100	4.7	2.20	Y dwn	0.23	9.83	96.60	small ij shedding
NC4	30Dec08 c3	3.11		3.58	199	109	6.3	0.93	0.102	6.7	4.60	Y up/down	0.35	5.57	105.82	med ij vortex roll up, no vortex growth
NC5	30Dec08 c4	3.07		3.58	203	109	9.2	0.93	0.096	9.9	9.40	Y up/down	0.41	3.13	87.66	large ij vortex roll up downstream
NC6	30Dec08 c5	3.09		3.56	207	111	13	0.95	0.097	14.0	19.00	Y dwn	0.42	2.83	88.32	med ij vortex roll up
SpC1	30Dec08 c2	3.11		4.95	212	111	4.1	0.93	0.134	4.4	2.60	Y up	0.40	17.18	53.55	small ij vortex roll up
Teshome Recess = D_1																
NC	23-Mar-10 c1	3.10		3.51	160	121	3.33	1.09	0.164	3.1	1.53	N	0.77	5.54	20.15	small ij vortex roll up
NC	18-Feb-10	3.00		3.49	165	118	6.25	1.06	0.146	5.9	5.07	N	0.19	17.34	149.82	med ij vortex roll up, ij anihilation
NC	26-Mar-10	3.05		3.52	184	129	32.97	8.50	0.389	3.9	5.86	Y up/dwn	0.69	19.31	43.52	laterally undulating jet, ejection of mass, ij vortex roll up downstream
Teshome Recess = $.05D_1$																
NC	03Aug10 c1	3.09	4	3.56	158	126	2.5	2.23	0.207	1.1	0.26	N	0.60	7.93	18.18	small structures shed from the IJ at exit plane
NC	22July10 c1	3.1		3.52	148	123	3.39	1.93	0.203	1.8	0.63	N	0.31	37.60	14.59	not so organized structures shed from ij exit plane
NC	30June10 c1	3.02		3.49	161	117	21.3	3.56	0.150	6.0	5.36	N	0.38	4.44	9.80	minimal ij disturbance
NC	21June10 c1	3.08		3.52	191	130	4.74	1.26	0.393	3.8	5.56	Y up/dwn	0.24	42.63	35.50	large ij vortex roll up
NC	05May10 c1	3.13		3.60	193	130	34.51	8.59	0.375	4.0	6.05	Y dwn				laterallyundulating ij disturbance

Dark-Core Length

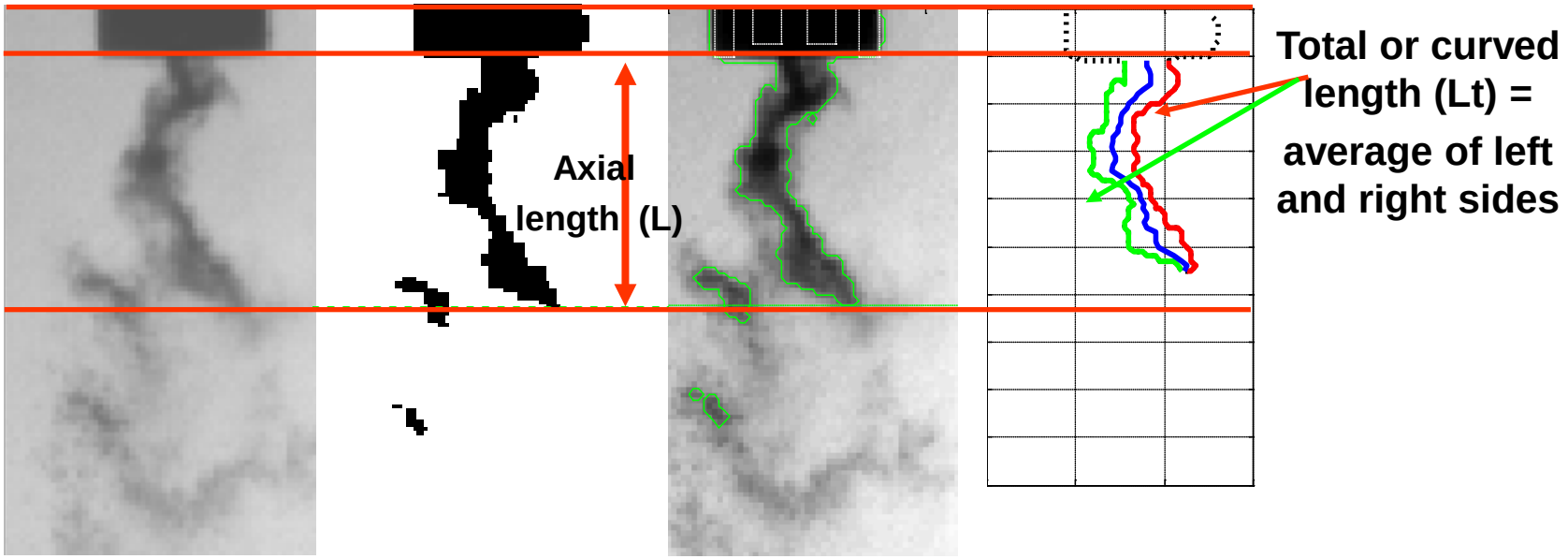

P = 1.50 MPa ; P_r = 0.44; VR = 7.50; J = 2.64; acoustic field on

- **Threshold Images based on Otsu's method** (N. Otsu, "A Threshold Selection Method from Gray-Level Histograms," IEEE Transactions on Systems, Man, and Cybernetics, vol. 9, no. 1, pp. 62-66, 1979.)
- **Accounts for variability from image to image (including d1 the parameter by which the jet is normalized)**

Acoustic Forcing Results

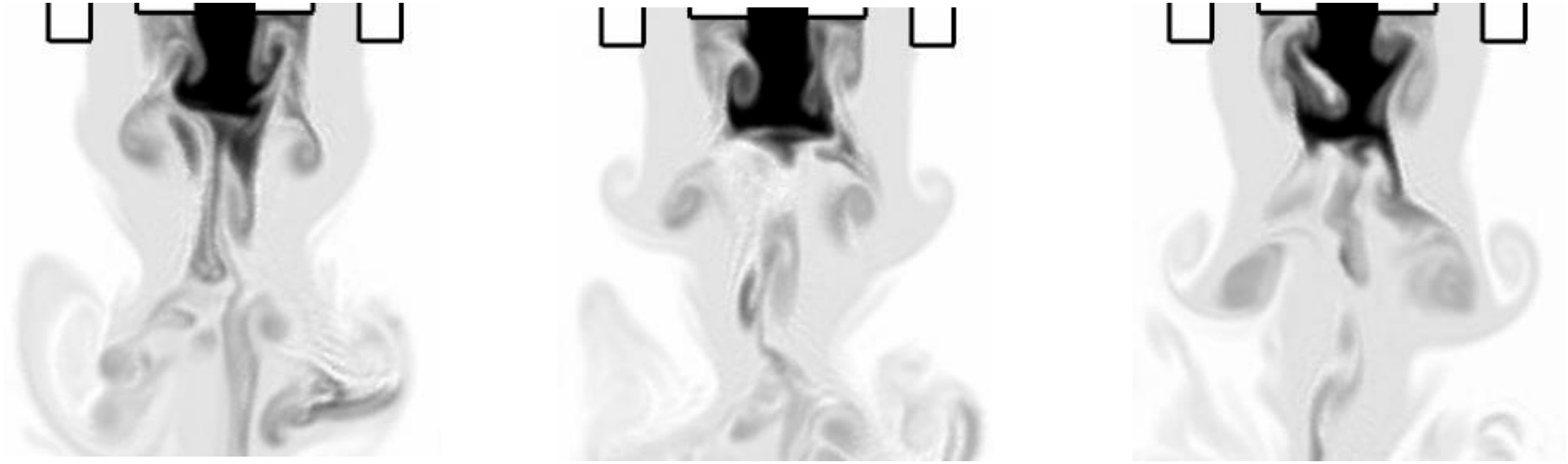

Instantaneous images of the simulation of an acoustic case with the injector at a pressure antinode for a J = 3.0

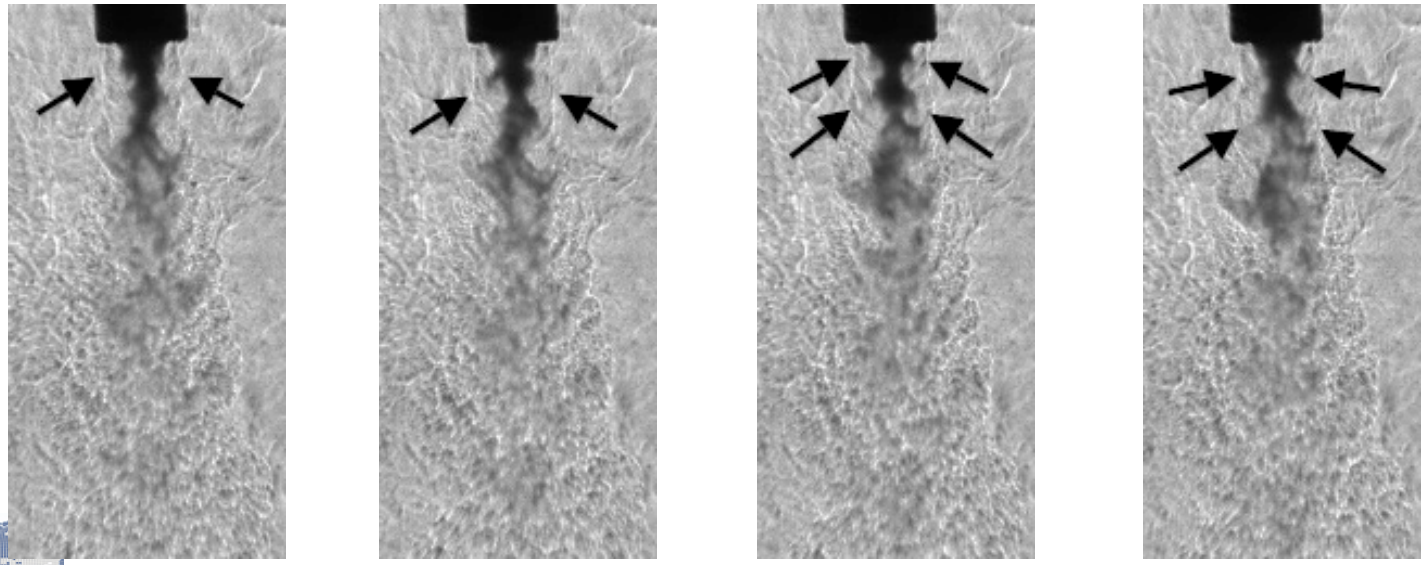

Instantaneous images of an experimental acoustic case with the injector at a pressure antinode for a J = 2.9

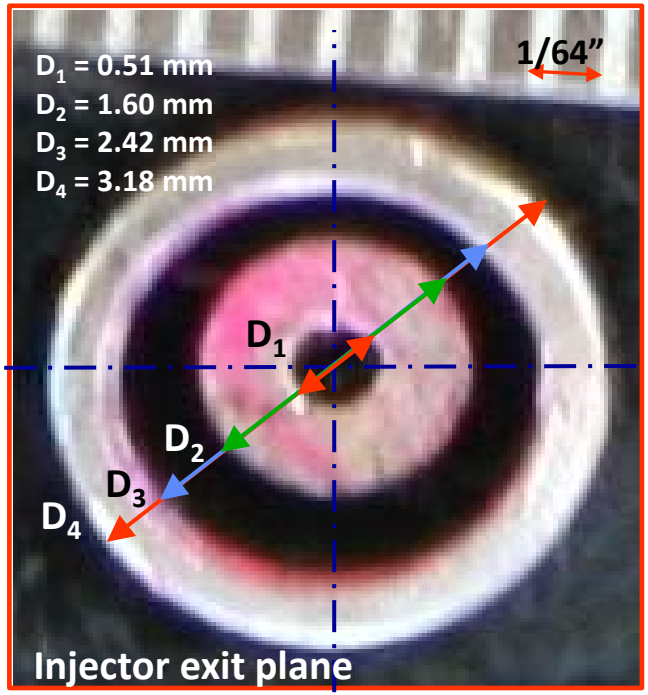
D1 = 0.51 mm
D2 = 1.60 mm
D3 = 2.42 mm
D4 = 3.18 mm
1/64”
D1
D2
D3
D4
Injector exit plane

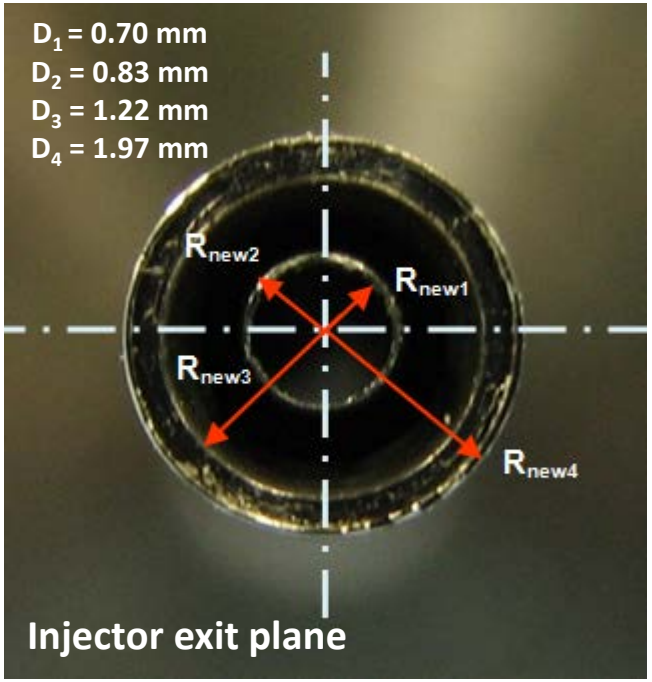
D1 = 0.70 mm
D2 = 0.83 mm
D3 = 1.22 mm
D4 = 1.97 mm
Rnew2
Rnew1
Rnew3
Rnew4
Injector exit plane

Synchronized p' and images: Pr=1.03, J=5.1, VR=5.9

Center

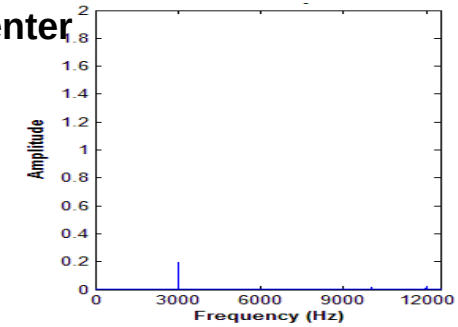

Outer

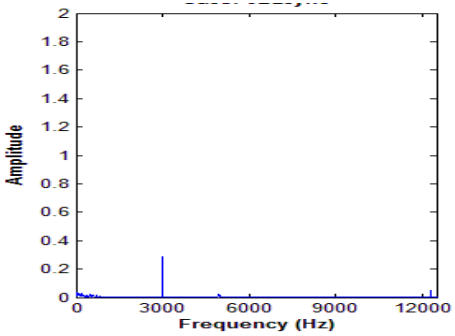

Inner

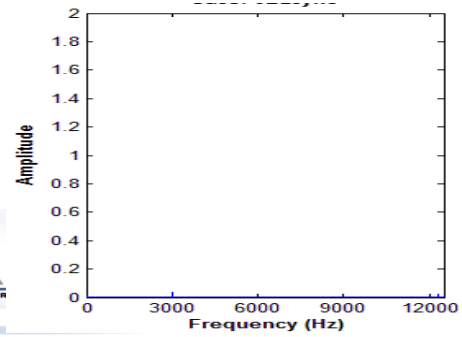

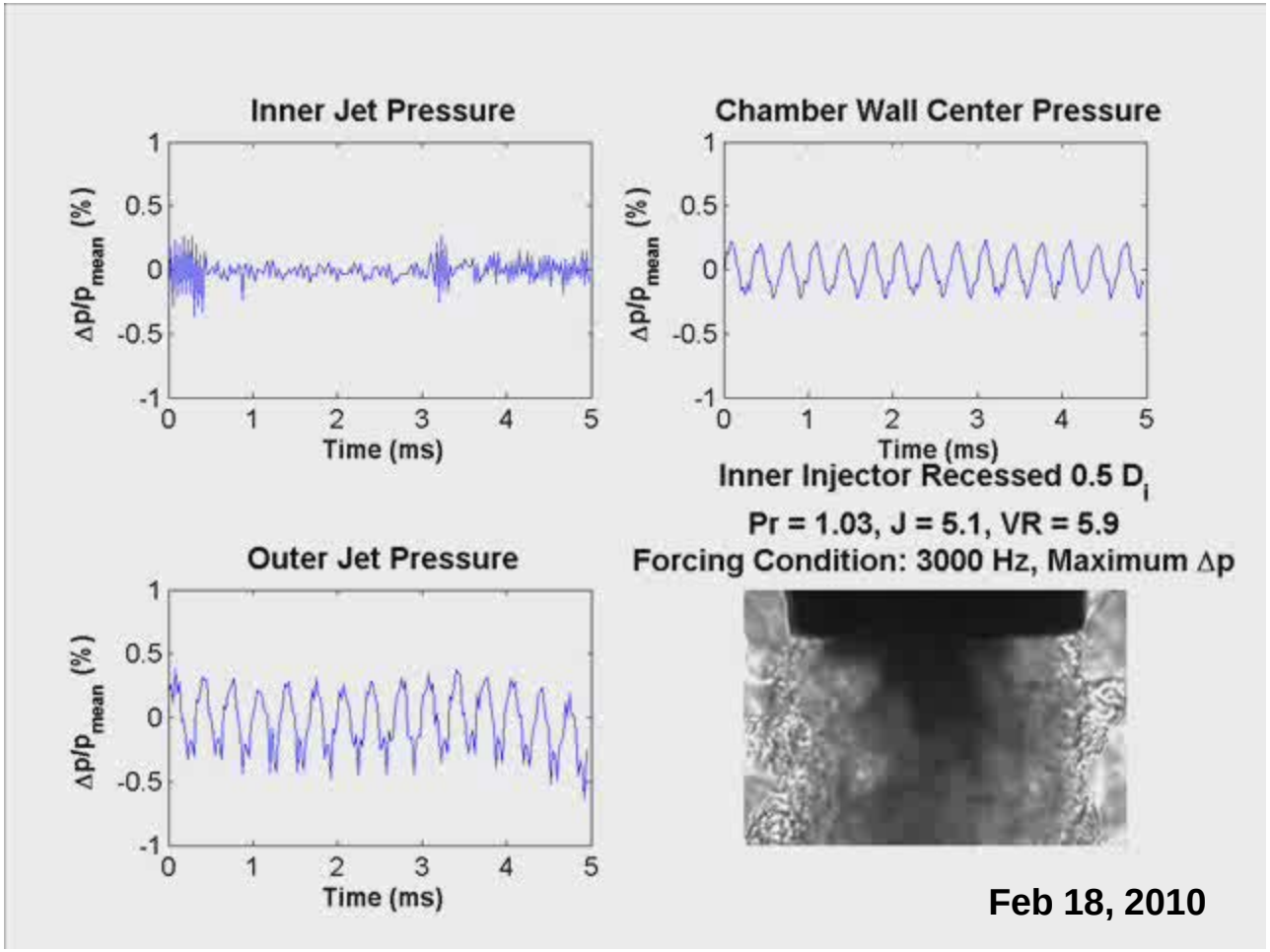

Uo=6. 25 m/s, Ui=1.06 m/s, To=165K , Ti=118 K

MOVIE

Synchronized p' and images: Pr=1.03, J=5.4, VR=6.0

Center

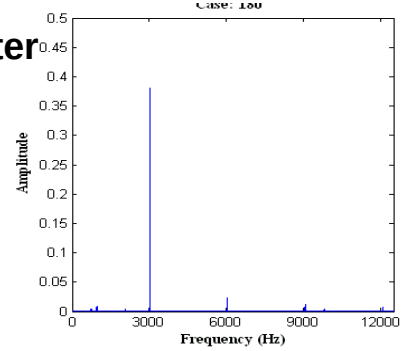

Outer

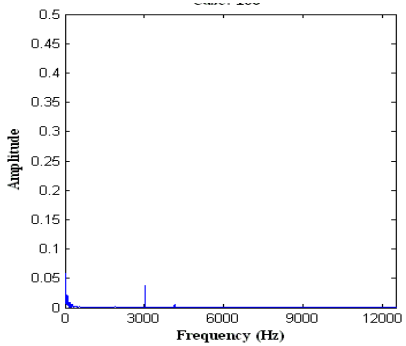

Inner

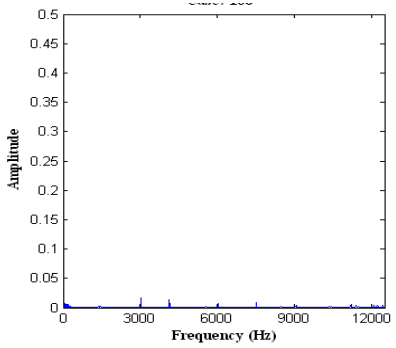

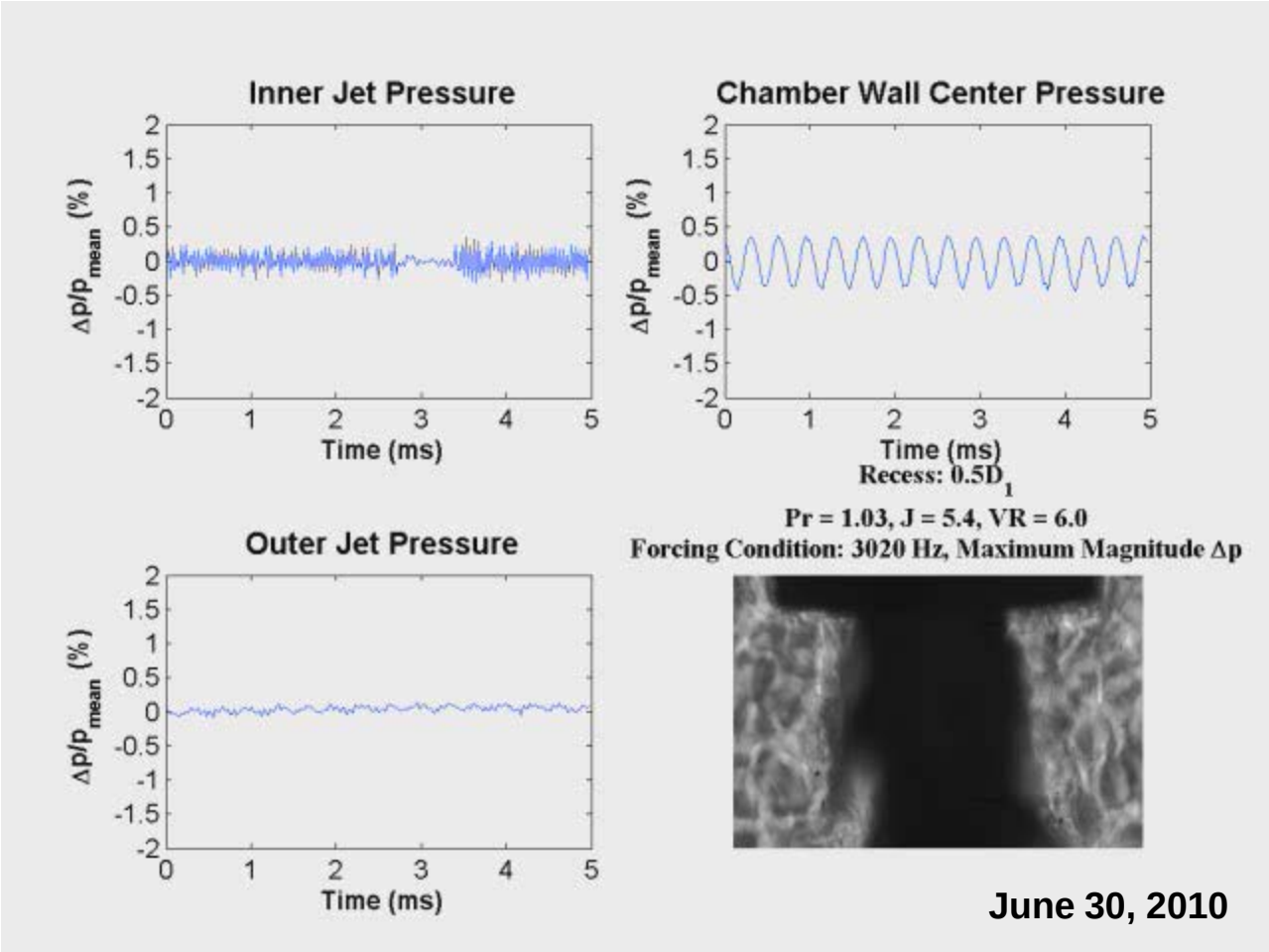

Uo=21.3 m/s, Ui=3.56 m/s, To=161K , Ti=117 K

MOVIE

Synchronized p' and images: Pr=1.03, J=5.4, VR=6.0

Center

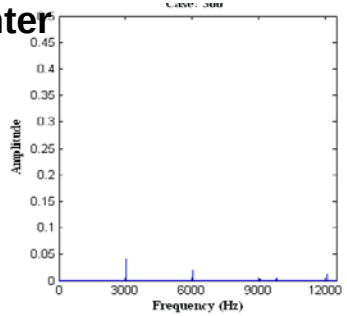

Outer

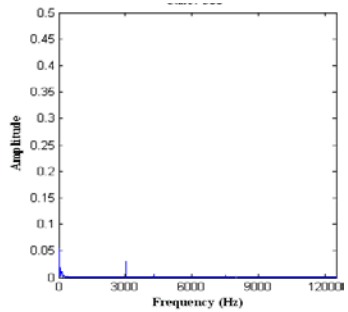

Inner

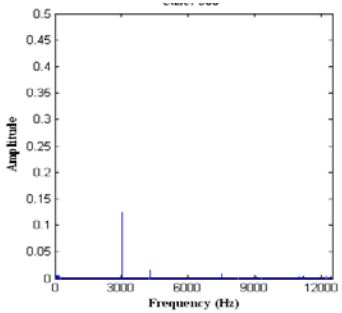

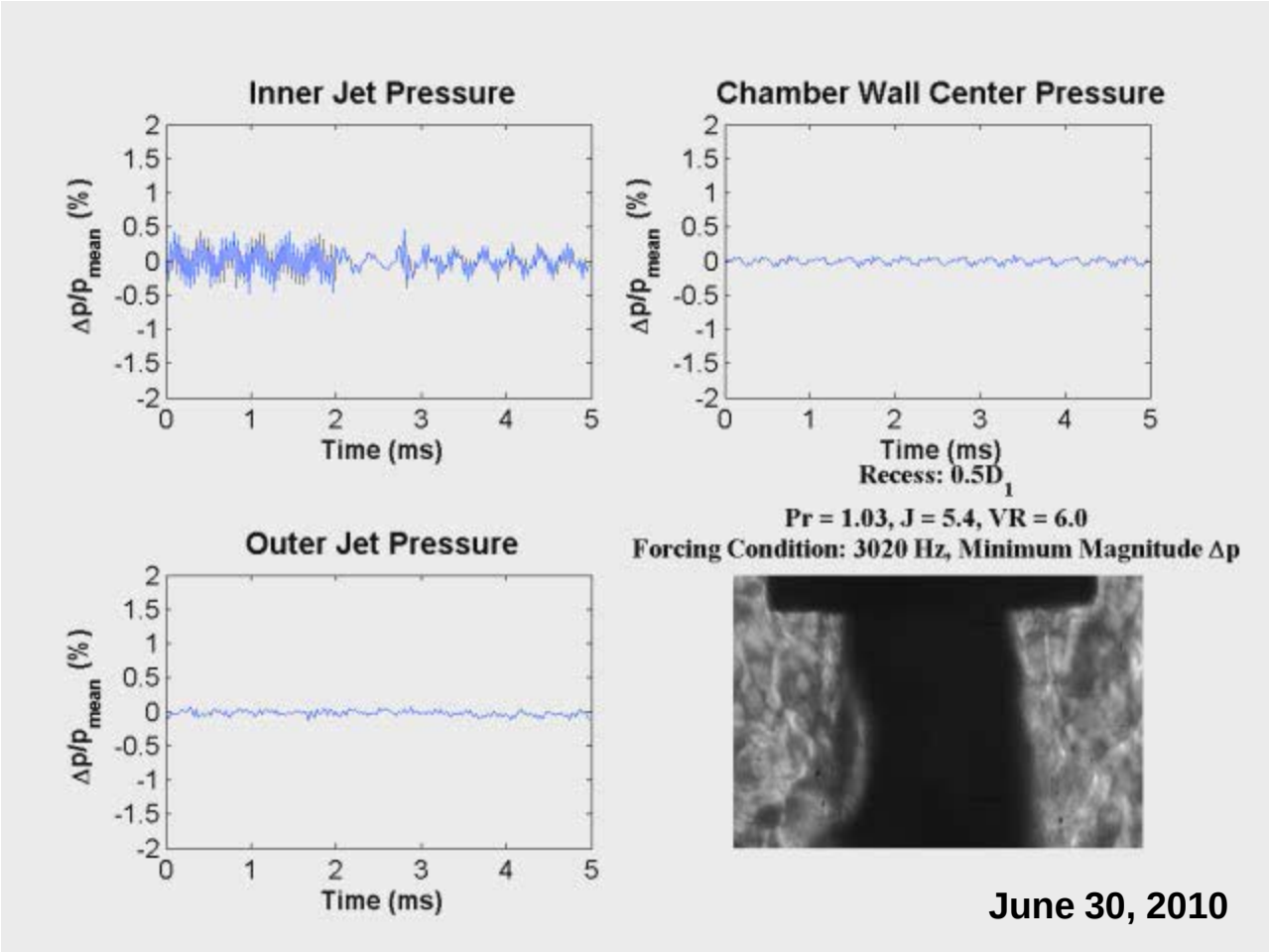

Uo=21.3 m/s, Ui=3.56 m/s, To=161K , Ti=117 K

MOVIE

Synchronized p' and images: Pr=1.03, J=5.9, VR=3.9

Center

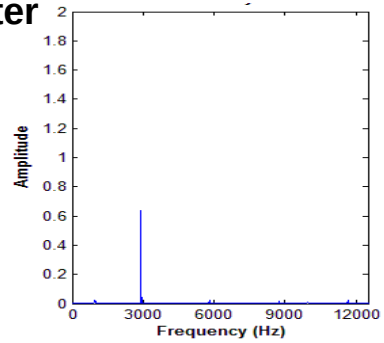

Outer

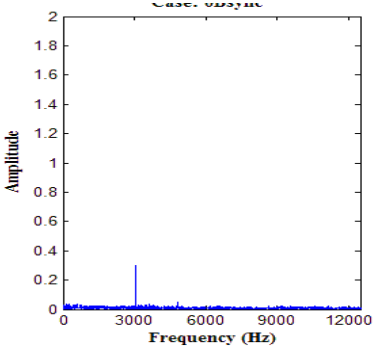

Inner

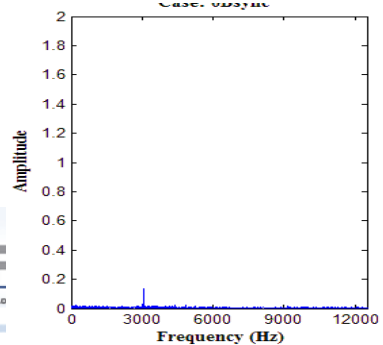

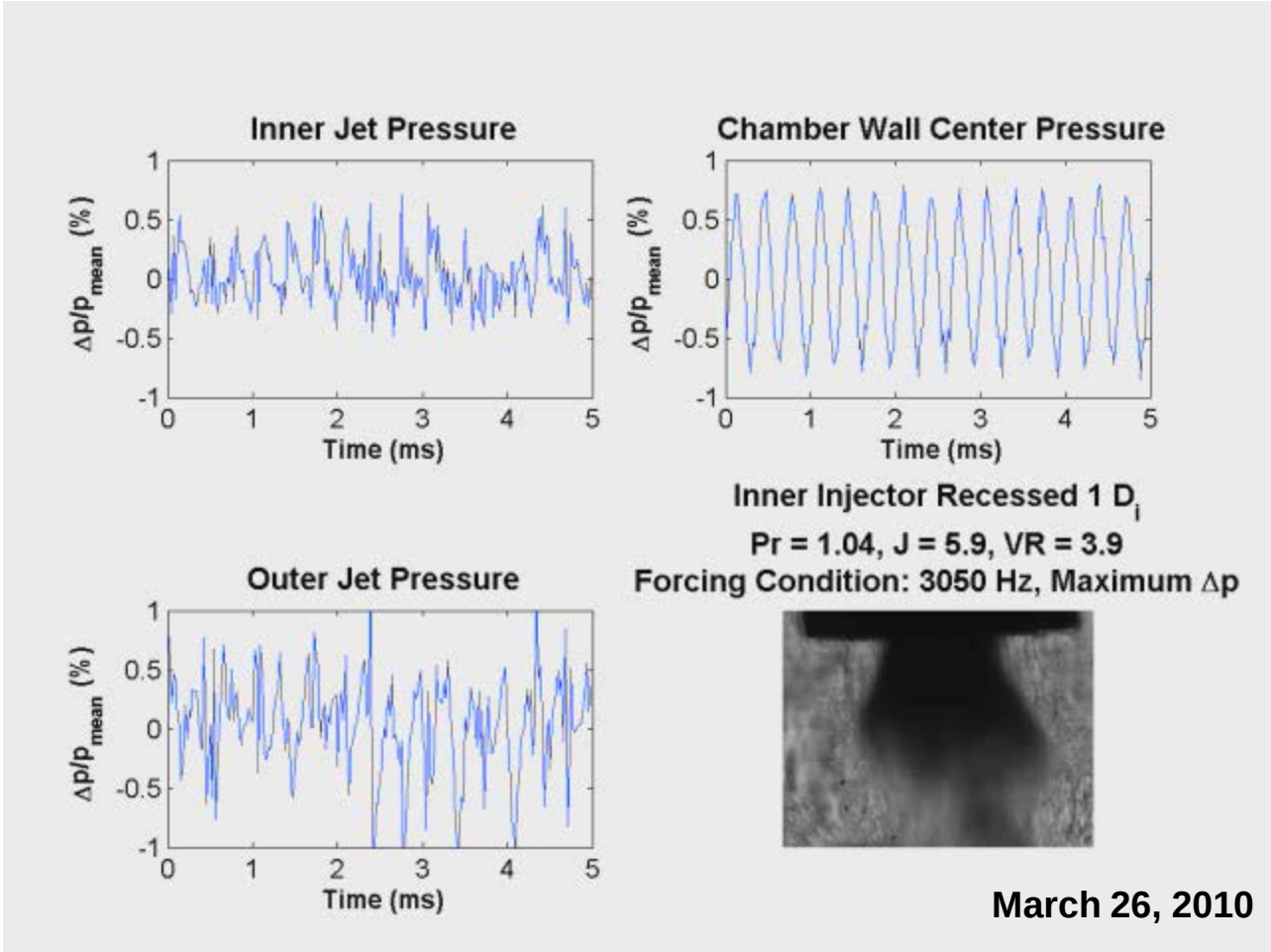

Uo=33.0 m/s, Ui=8.50 m/s, To=184K , Ti=129 K

MOVIE

Synchronized p' and images: Pr=1.03, J=5.9, VR=3.9

Center

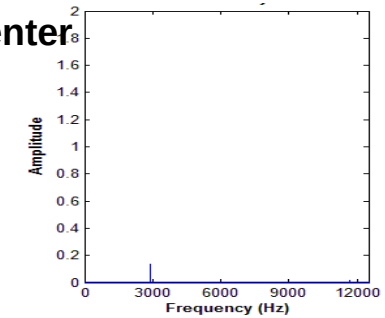

Outer

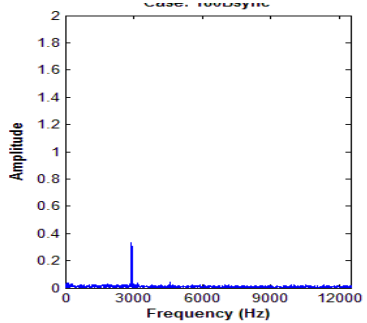

Inner

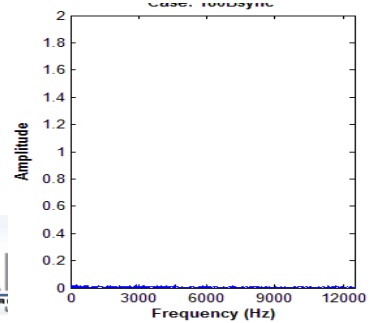

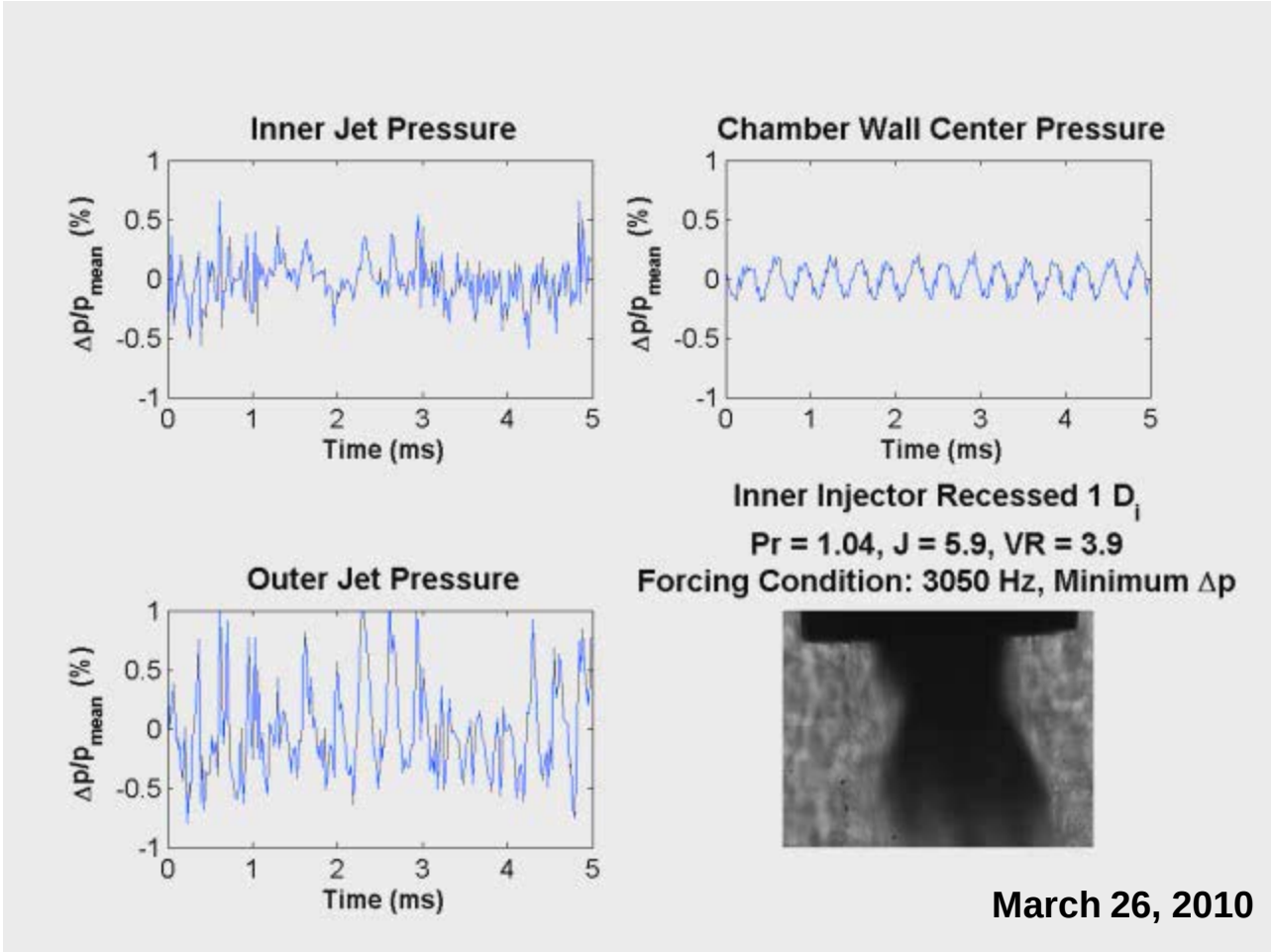

Uo=33.0 m/s, Ui=8.50 m/s, To=184K , Ti=129 K

MOVIE

Synchronized p' and images: Pr=1.02, J=5.7, VR=3.8

Center

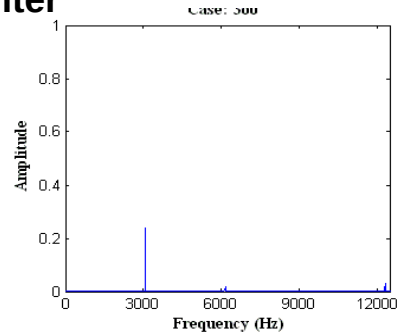

Outer

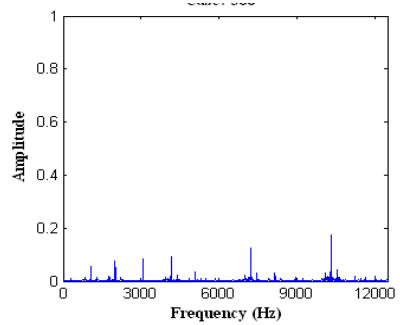

Inner

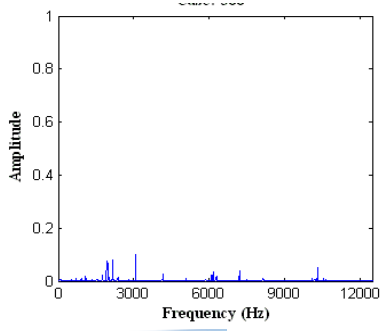

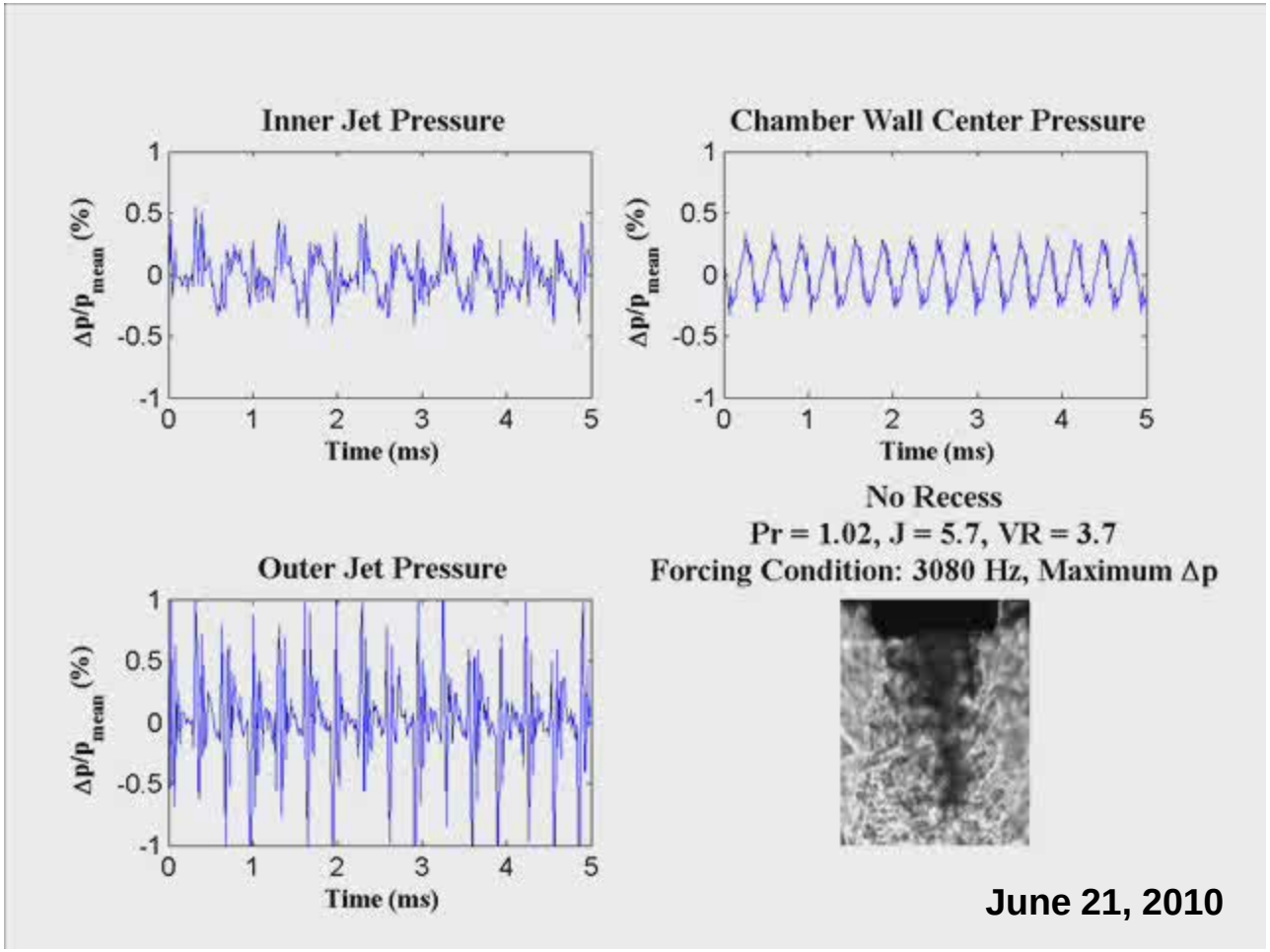

Uo=4.74 m/s, Ui=1.26 m/s, To=191K , Ti=130 K

MOVIE

Synchronized p' and images: Pr=1.02, J=5.7, VR=3.8

Center

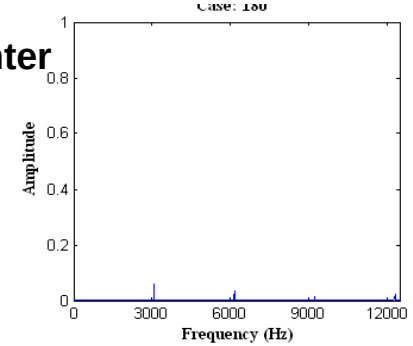

Outer

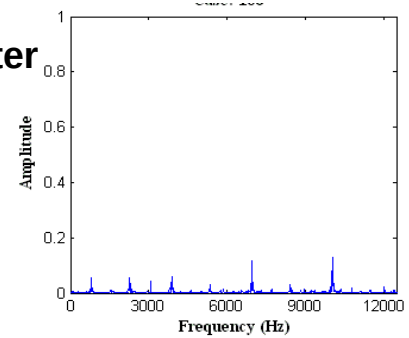

Inner

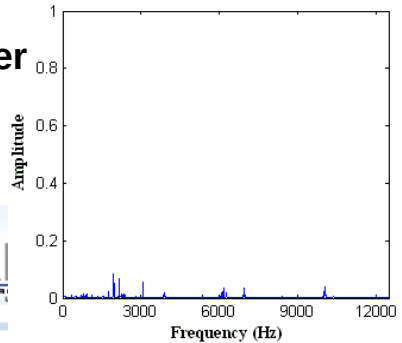

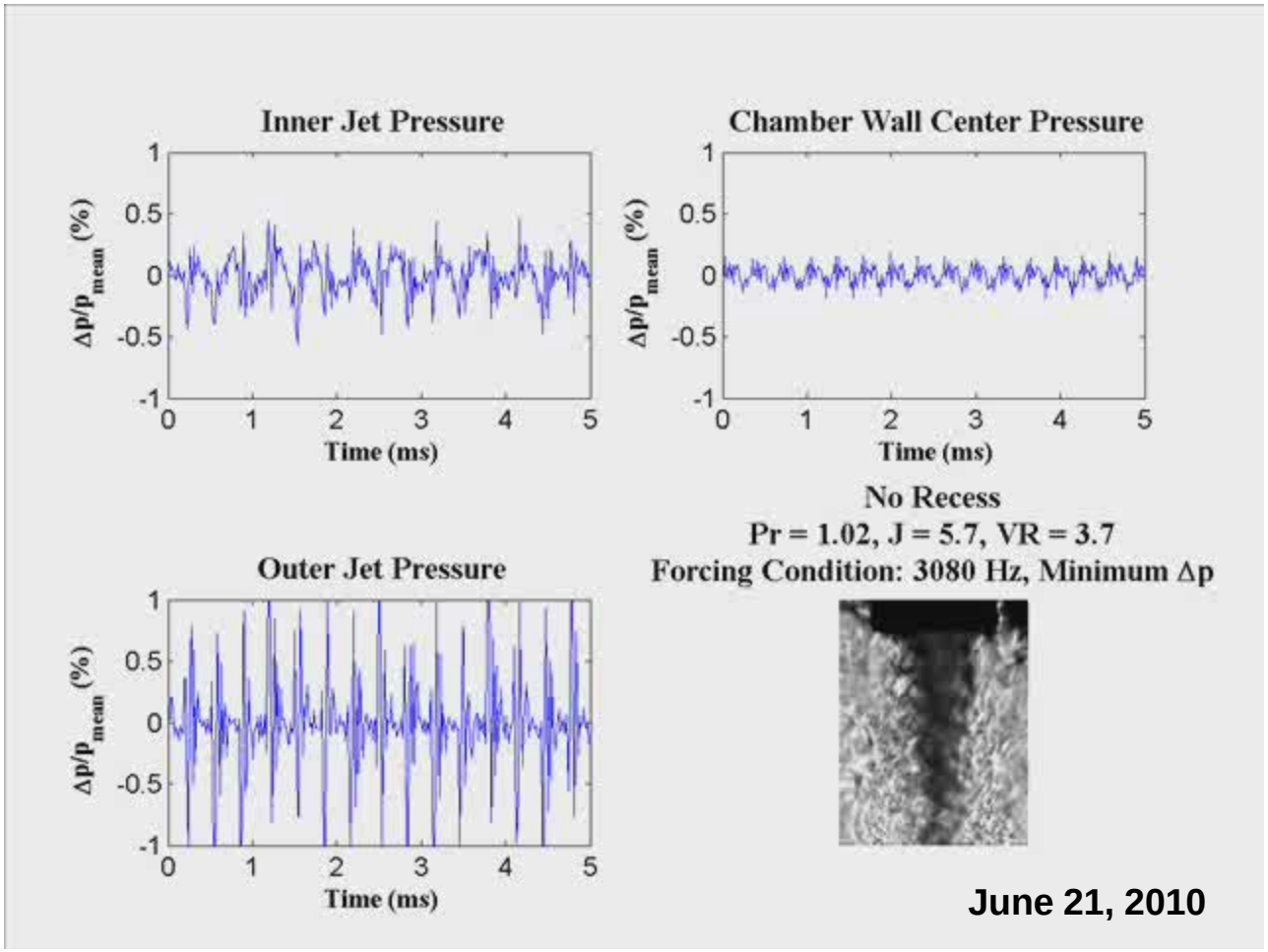

Uo=4.74 m/s, Ui=1.26 m/s, To=191K , Ti=130 K

MOVIE

Typical FFT of Dark Core Length

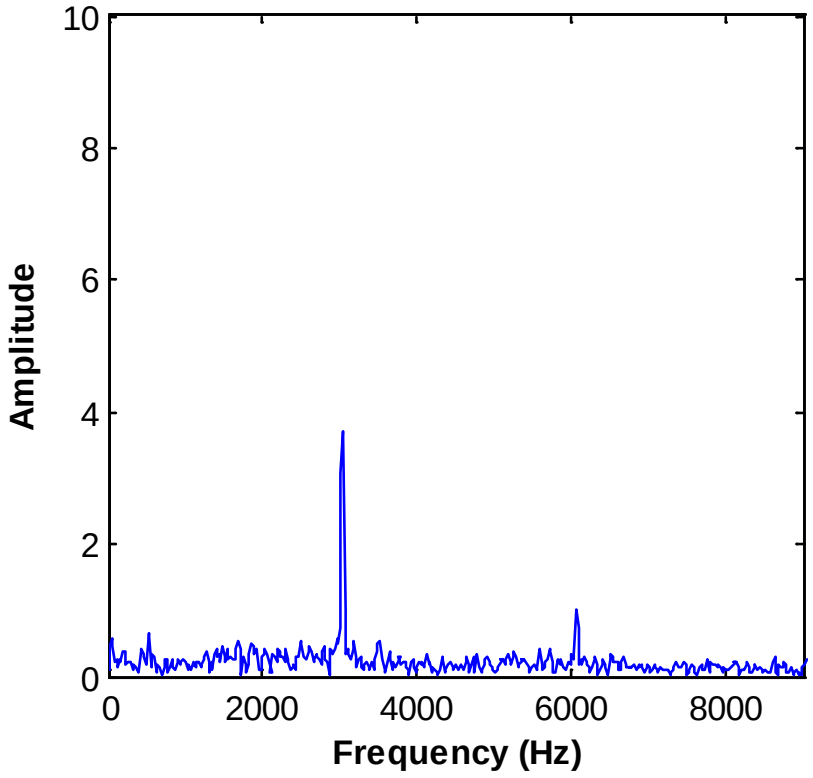

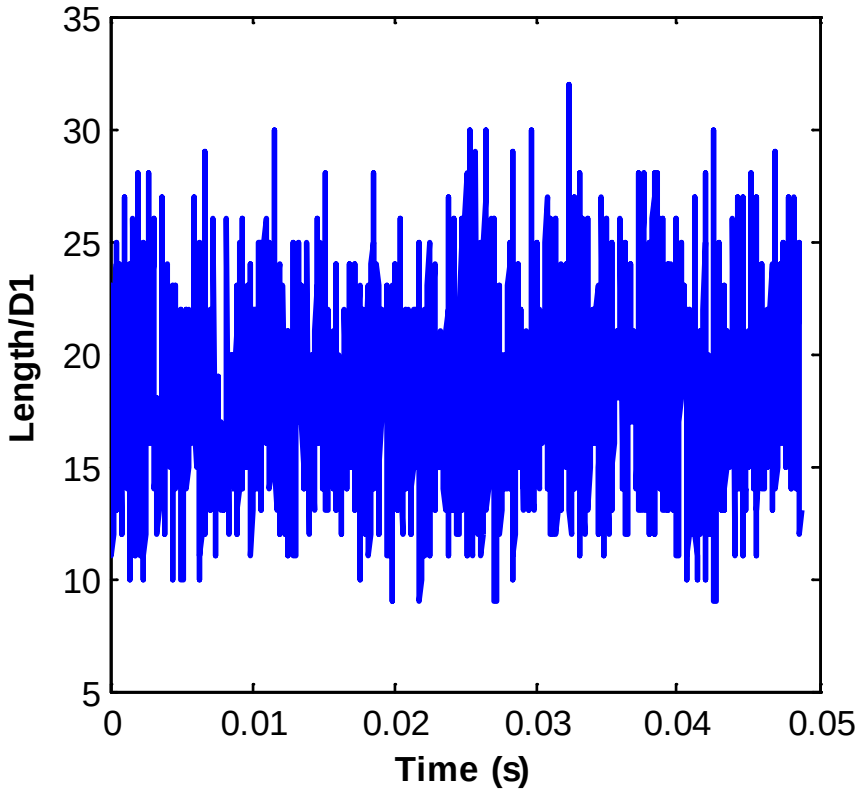

Sampling Frequency=41kHz, Driving frequency=3.05kHz, Pch=3.5MPa; Pr=1.03; VR=2.68, MR=2.27,

Subcritical Low J

$P_{chamber}$ = 1.5 MPa (Pr = 0.44)

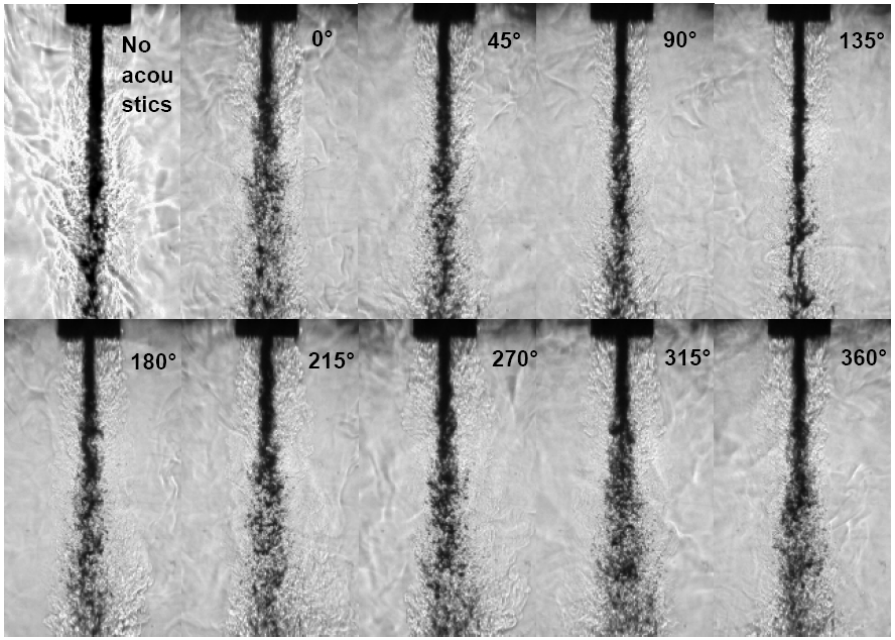

J = 0.17

VR =

$\Delta p_{peak\text{-}to\text{-}peak} / p_{chamber}$ =

$\dot{m}_{outer} / \dot{m}_{inner}$ =

thick inner post injector

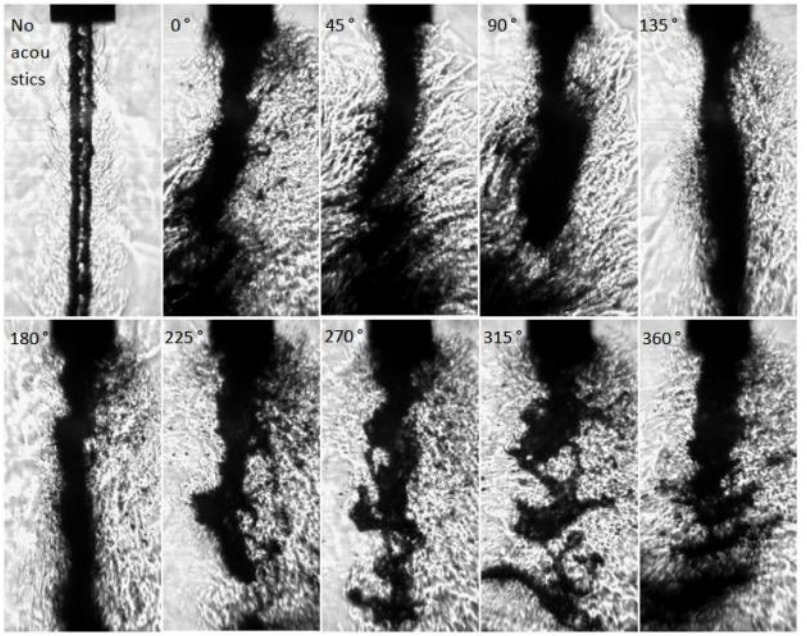

J = 0.089 with thin inner post injector

Negligible effect vs. violent destruction of the jet

Subcritical Moderate J

$P_{chamber}$ = 1.5 MPa (Pr = 0.44)

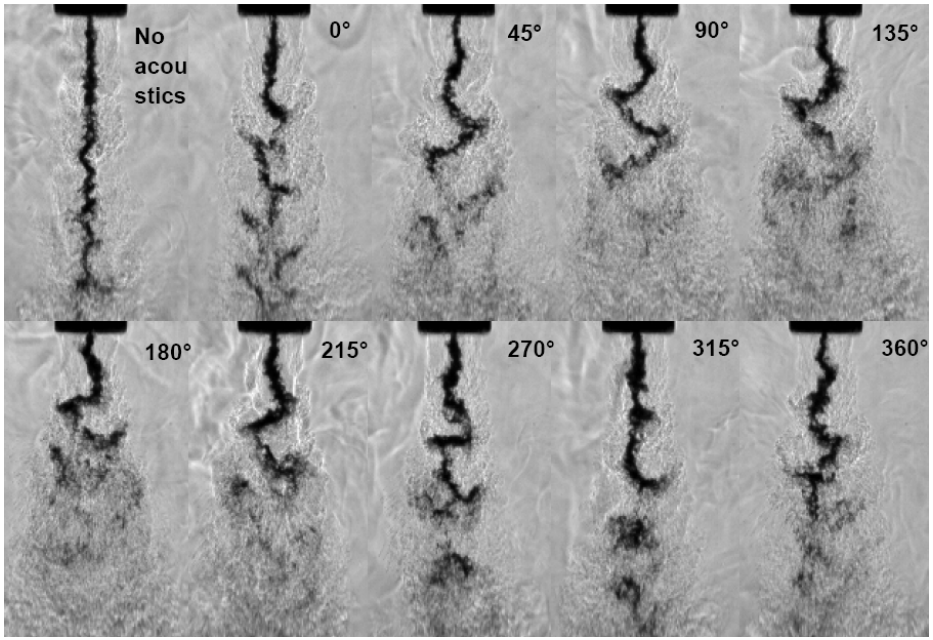

J = 2.6 with thick inner post injector

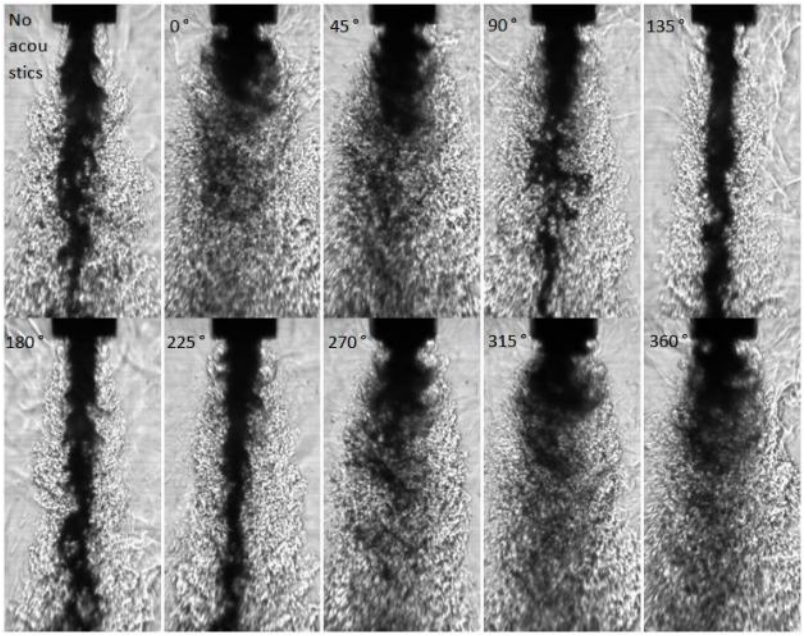

J = 2.0 with thin inner post injector

Bending vs. vortical structures with fine atomization

Subcritical Large J

$P_{chamber}$ = 1.5 MPa (Pr = 0.44)

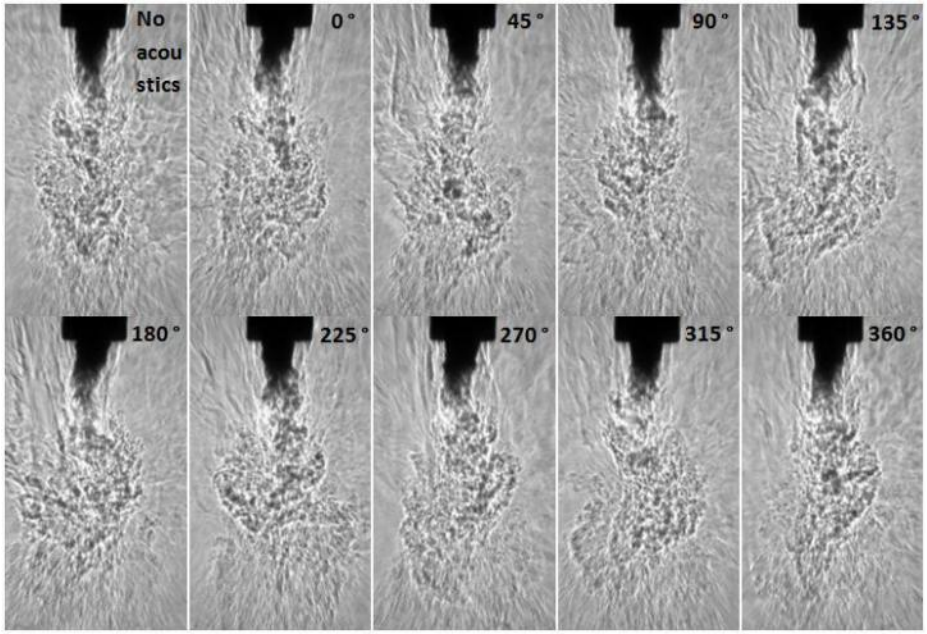

J = 23 with thick inner post injector

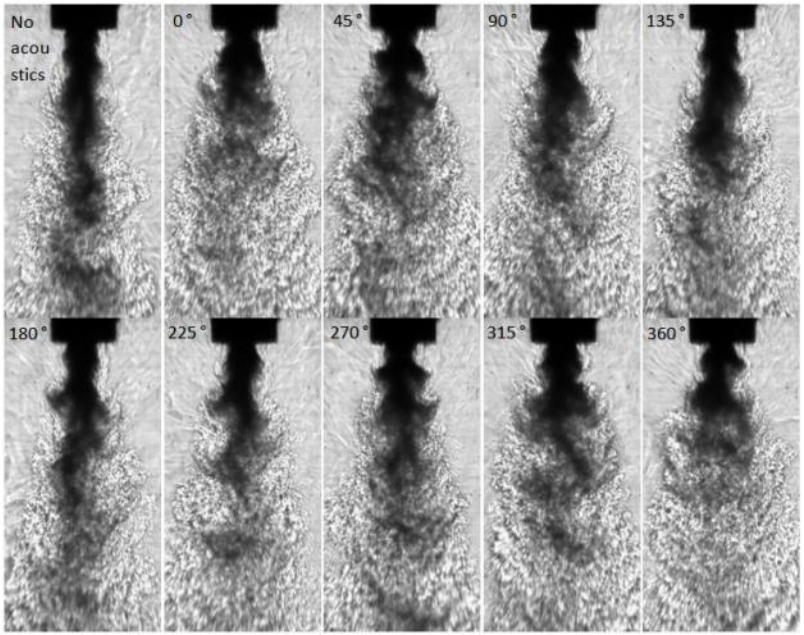

J = 18 with thin inner post injector

Two different mixing mechanisms for similar large J values

Nearcritical Large J

$P_{chamber}$ = 3.6 MPa (Pr = 1.1)

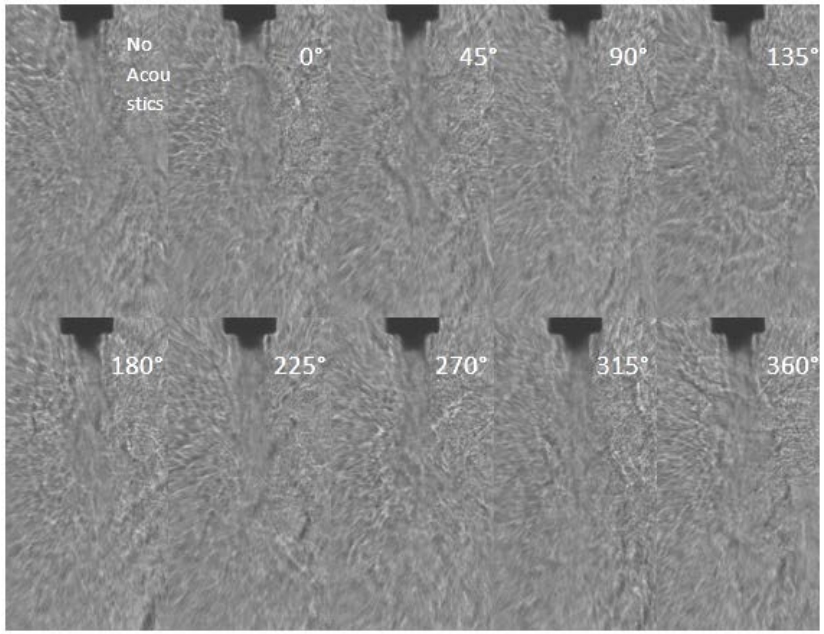

J = 9.3 with thick inner post injector

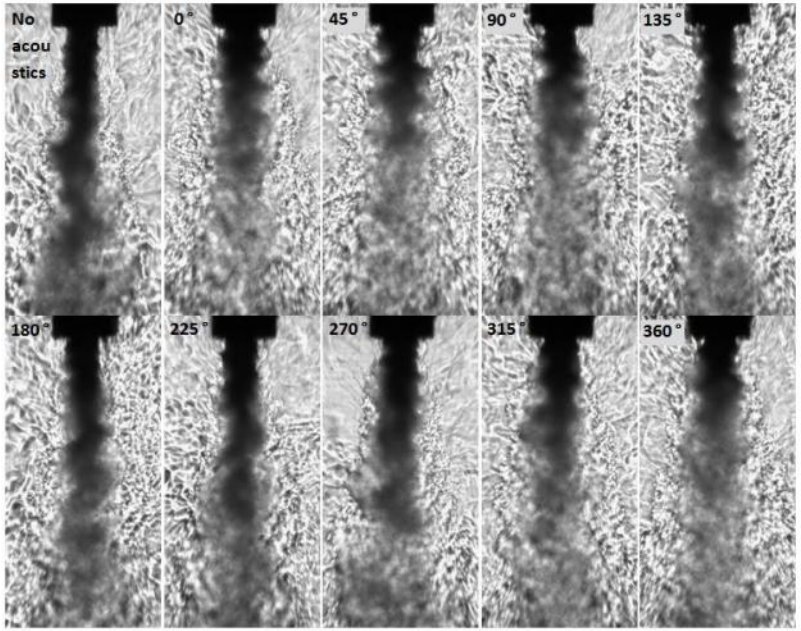

J = 9.4 with thin inner post injector

Longer dark core lengths and hence visible effect of acoustics for thin inner post geometry

Supercritical Moderate J

$P_{chamber}$ = 5.0 MPa (Pr = 1.5)

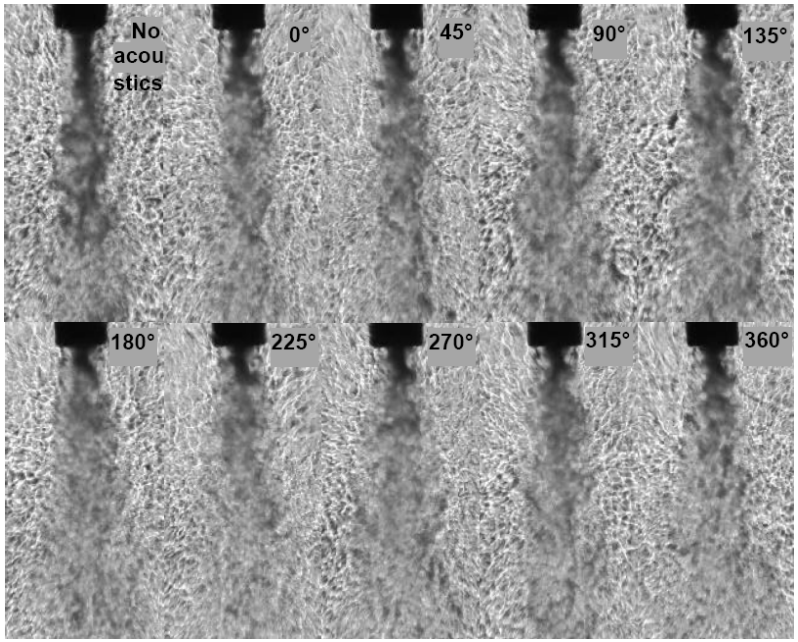

J = 2.4 with thick inner post injector

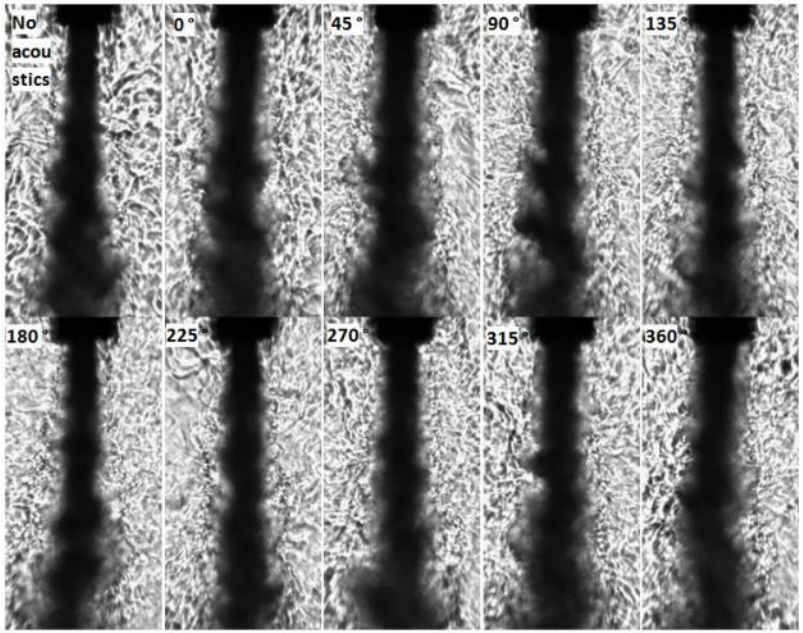

J = 2.6 with thin inner post injector

Large dark core lengths for the thin post geometry prevent us from observing acoustic effects, if any

thick inner post injector

	$T_{chamber}$ (K)	$\rho_{chamber}$ (kg/m^3)	$P_{chamber}$ (MPa)	T_{outer} (K)	$\dot{m}_{outer}$ (mg/s)	ρ_{outer} (kg/m^3)	u_{outer} (m/s)	Re_{outer} (10^4)	T_{inner} (K)	$\dot{m}_{inner}$ (mg/s)	ρ_{inner} (kg/m^3)	u_{inner} (m/s)	Re_{inner} (10^4)	L/D_1 (baseline)	Freq. (kHz)	$P'_{RMS\ max}$ (kPa)	VR	J
SUB																		
sub1	233	22.0	1.50	191	310	27.6	4.30	0.768	109	279	630	2.2	1.2	26.2	2.98	21.5	2.0	0.17
sub2	231	22.2	1.50	183	790	28.8	11.0	2.02	109	283	630	2.2	1.2	17.1	3.06	20.1	4.8	1.0
sub3	226	21.9	1.45	183	1230	27.8	16.9	3.16	109	284	630	2.2	1.2	16.6	3.06	17.8	7.6	2.6
sub4	226	22.9	1.51	185	1560	28.7	20.9	3.96	109	279	630	2.2	1.2	15.2	2.96	15.7	9.5	4.2
sub5	210	24.9	1.50	182	2400	29.3	31.3	6.18	109	279	630	2.2	1.2	8.40	3.01	16.9	14	9.6
sub6	216	24.1	1.50	191	3640	27.7	50.3	9.02	109	279	630	2.2	1.2	5.63	3.02	16.3	23	23
NEAR																		
near1	223	56.6	3.58	180	1060	75.4	5.38	2.58	123	290	520	2.8	2.0	24.4	3.08	9.04	2.0	0.55
near2	207	62.0	3.57	152	1570	101	5.95	4.16	117	289	590	2.4	1.5	15.5	3.04	10.8	2.5	1.0
near3	228	55.1	3.58	185	1590	72.4	8.40	3.80	126	293	440	3.3	2.5	14.6	3.00	11.8	2.6	1.1
near4	223	56.1	3.55	184	2170	72.3	11.5	5.21	127	294	360	4.0	3.4	12.1	3.01	11.4	2.8	1.6
near5	230	54.2	3.56	199	2120	65.1	12.5	4.84	126	292	440	3.3	2.5	12.9	3.03	12.1	3.8	2.1
near6	229	54.5	3.56	183	2690	73.1	14.1	6.48	126	292	420	3.4	2.5	5.98	3.05	11.1	4.1	2.9
near7	219	57.6	3.56	194	3080	67.4	17.5	7.15	125	289	480	3.0	2.2	5.56	3.06	11.8	5.9	4.9
near8	213	59.6	3.56	192	6460	68.3	36.2	15.1	128	295	220	6.6	5.2	2.45	2.93	9.73	5.5	9.3
SUPER																		
super1	231	76.1	4.96	198	292	93.9	1.19	0.642	136	291	300	4.8	3.9	37.7	3.05	8.01	0.25	0.019
super2	231	76.1	4.96	193	997	97.7	3.90	2.22	130	292	460	3.1	2.4	26.7	3.01	10.2	1.2	0.33
super3	221	80.4	4.95	180	2050	109	7.19	4.72	128	291	490	2.9	2.1	19.2	3.01	10.7	2.5	1.3
super4	222	80.1	4.96	182	3110	107	11.1	7.13	134	288	360	3.9	3.3	10.2	3.05	10.1	2.8	2.4
super5	222	80.3	4.97	191	2820	99.5	10.8	6.32	131	293	440	3.3	2.6	9.02	3.09	12.5	3.3	2.5
super6	211	85.8	4.96	187	5820	103	21.6	13.2	132	286	410	3.4	2.7	3.04	3.05	10.7	6.3	9.9

New Injector

	$T_{chamber}$ (K)	$\rho_{chamber}$ (kg/m^3)	$P_{chamber}$ (MPa)	T_{outer} (K)	$\dot{m}_{outer}$ (mg/s)	ρ_{outer} (kg/m^3)	u_{outer} (m/s)	Re_{outer} (10^4)	T_{inner} (K)	$\dot{m}_{inner}$ (mg/s)	ρ_{inner} (kg/m^3)	u_{inner} (m/s)	Re_{inner} (10^4)	L/D_1 (baseline)	Freq. (kHz)	$P'_{RMS\ max}$ (kPa)	VR	J
SUB																		
subnew1	235	22	1.48	199	90	26	1.4	0.21	105	920	660	0.91	1.3	13+	3.01	8.86	1.5	0.089
subnew2	237	22	1.49	197	200	26	3.0	0.47	106	925	655	0.92	1.3	13+	2.96	14.0	3.3	0.43
subnew3	246	21	1.49	195	450	27	6.6	1.1	109	925	630	0.96	1.5	11+	2.97	12.1	6.9	2.0
subnew4	224	23	1.49	189	600	28	8.5	1.5	110	925	620	0.97	1.5	10.4	3.04	10.2	8.7	3.4
subnew5	217	24	1.49	184	750	29	10	1.9	110	925	620	0.97	1.5	9.29	3.02	11.5	11	5.2
subnew6	228	22	1.49	193	880	27	13	2.1	108	925	640	0.94	1.4	8.08	2.96	12.7	14	7.8
subnew7	222	23	1.49	194	1100	27	16	2.6	108	925	640	0.94	1.4	7.63	2.92	11.2	17	12
subnew8	217	24	1.48	201	1300	26	20	3.0	109	925	630	0.96	1.5	7.26	2.90	9.16	21	18
NEAR																		
nearnew1	228	55	3.56	213	330	60	2.2	0.70	109	925	650	0.93	1.3	14+	2.98	10.8	2.3	0.50
nearnew2	226	55	3.56	209	460	61	3.0	1.0	109	925	650	0.93	1.3	14+	3.06	9.17	3.2	0.97
nearnew3	230	54	3.58	198	730	66	4.3	1.6	108	925	655	0.92	1.3	13+	3.00	9.12	4.7	2.2
nearnew4	216	59	3.58	199	1030	65	6.3	2.3	109	925	650	0.93	1.3	13+	3.11	16.0	6.7	4.6
nearnew5	214	59	3.58	203	1460	63	9.2	3.2	109	925	650	0.93	1.3	7.01	3.07	15.0	9.9	9.4
nearnew6	215	59	3.56	207	2060	62	13	4.5	111	925	635	0.95	1.4	3.55	3.09	18.3	14	19
SUPER																		
supernew1	219	81	4.95	212	890	85	4.1	1.8	111	925	650	0.93	1.4	13+	3.11	17.0	4.4	2.6

Highlights from previous work 1/2

- Crow and Champagne, 1971
  - Single jet preferred mode, St=fd/U~0.3
- Ko et al,1976-1989
  - Some of earliest detailed description of near field mixing for coaxial jets
- Boldman et al, 1975
  - Experimental and theoretical analysis for mixing of two streams with different velocities – points out different vortex interactions
- Gutmark and Ho, 1983
  - Collects previous results on jet preferred mode, St has a range from ~0.24-0.64
- Dahm et al, 1992
  - Points out importance of layer thickness and velocity defect on shear layers seminal pictures of different instabilities
- Villermeaux 1998
  - Inner jet core length expression, $L/D_1=6/J^{0.5}$
- Richecoeur et al (Candel's group), 2006
  - Forced transverse acoustic excitation of flames

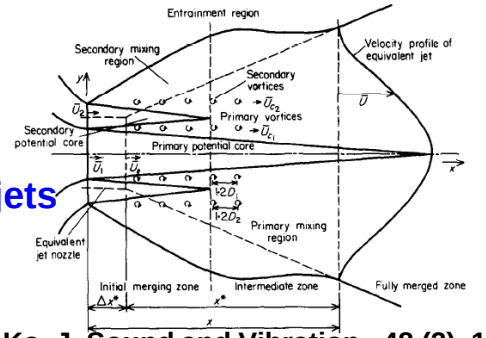

Kwan and Ko, J. Sound and Vibration, 48 (2), 19

Dahm et al, JFM (241) 1992

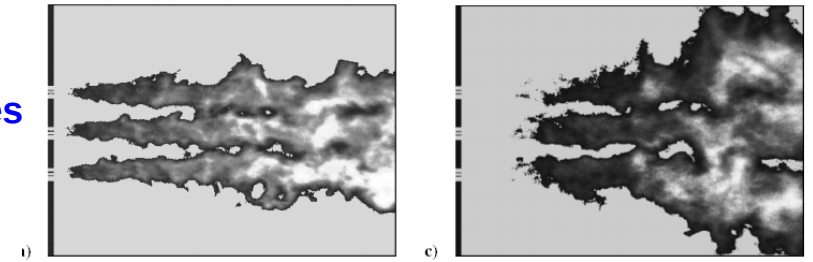

Richecoeur et al, JPP (22) No 4, 2006

Short Thick post behavior families

Base-line

Max Δp

Min Δp

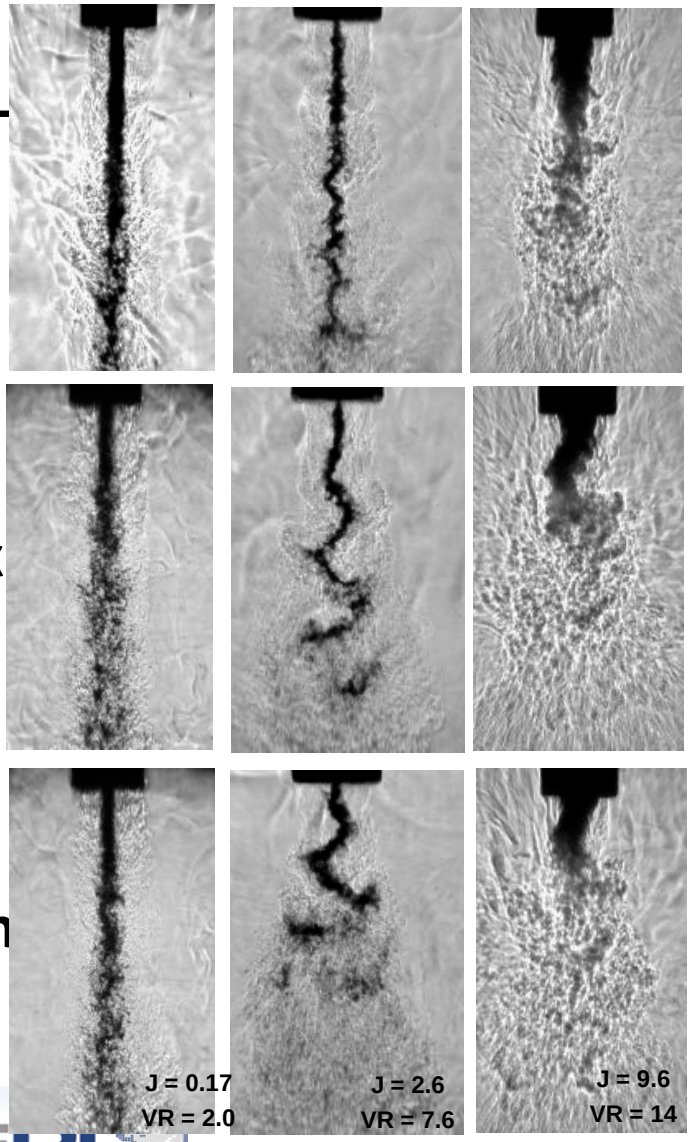

Subcritical conditions

- Acoustics undulate inner jet like in Heidmann's experiments consistent with being driven by an imposed velocity field
- Reductions of core of more than 20% for 0.2 < J <10

Near and supercritical conditions

- Less undulation on inner jet but same mode
- Not a clear effect of phase on the reduction of the dark core length
- Max reduction of inner jet occurred at 1<J<5

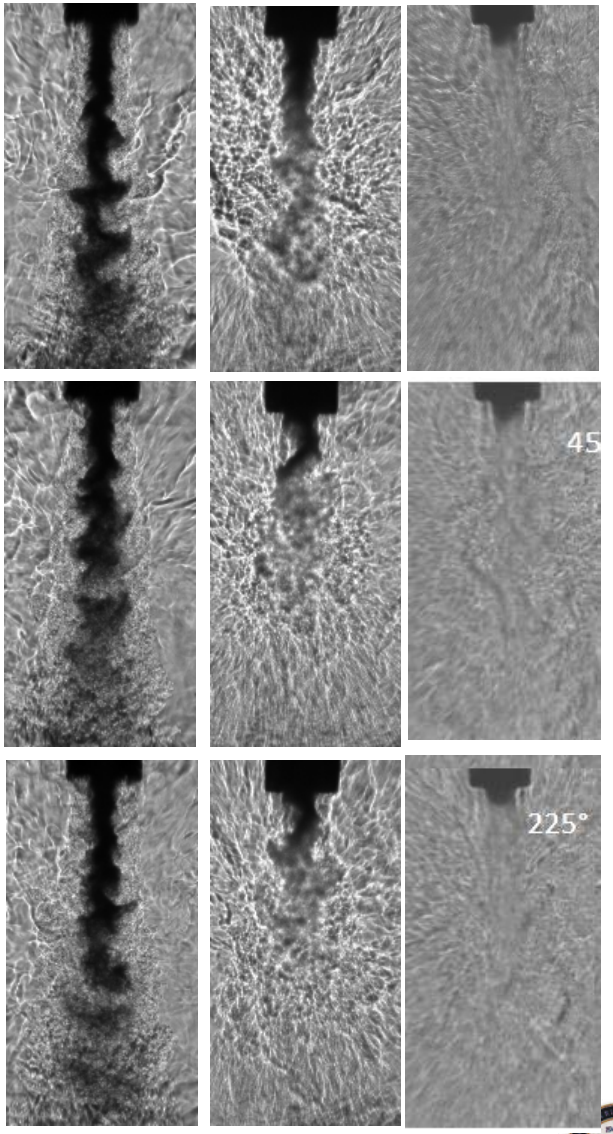

Conditions of Interest

Run Date	$T_{chamber}$ (K)	$\rho_{chamber}$ (kg/m^3)	$P_{chamber}$ (MPa)	T_{outer} (K)	M_{outer} (mg/s)	ρ_{outer} kg/m^3	u_{outer} (m/s)	Re_{outer} (10^4)	T_{inner} (K)	M_{inner} (mg/s)	ρ_{inner} (kg/m^3)	u_{inner} (m/s)	Re_{inner} (10^4)	Freq. (kHz)	VR	J	Recess
2010_02_18	233	52	3.49	165	1330	84	6.25	3.3	118	938	576	1.06	1.8	3.00	5.9	5.1	D1
2010_03_26	201	63	3.52	184	5976	72	32.97	17	129	2408	185	8.50	14	3.05	3.9	5.9	D1
2010_06_21 case1	234	53	3.54	191	814	68	4.74	1.9	130	333	175	1.26	2.4	3.08	3.8	5.5	0.5D1
2010_06_30 case1	174	78	3.51	161	4732	88	21.3	12	117	3199	586	3.56	6.0	3.02	6.0	5.4	0.5D1

Synchronized p' and images: Pr=1.03, J=5.1, VR=5.9

Center

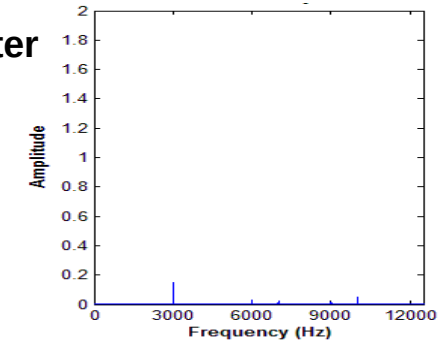

Outer

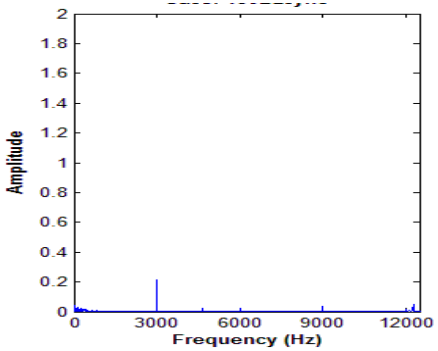

Inner

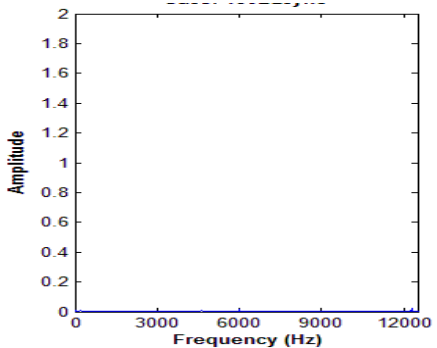

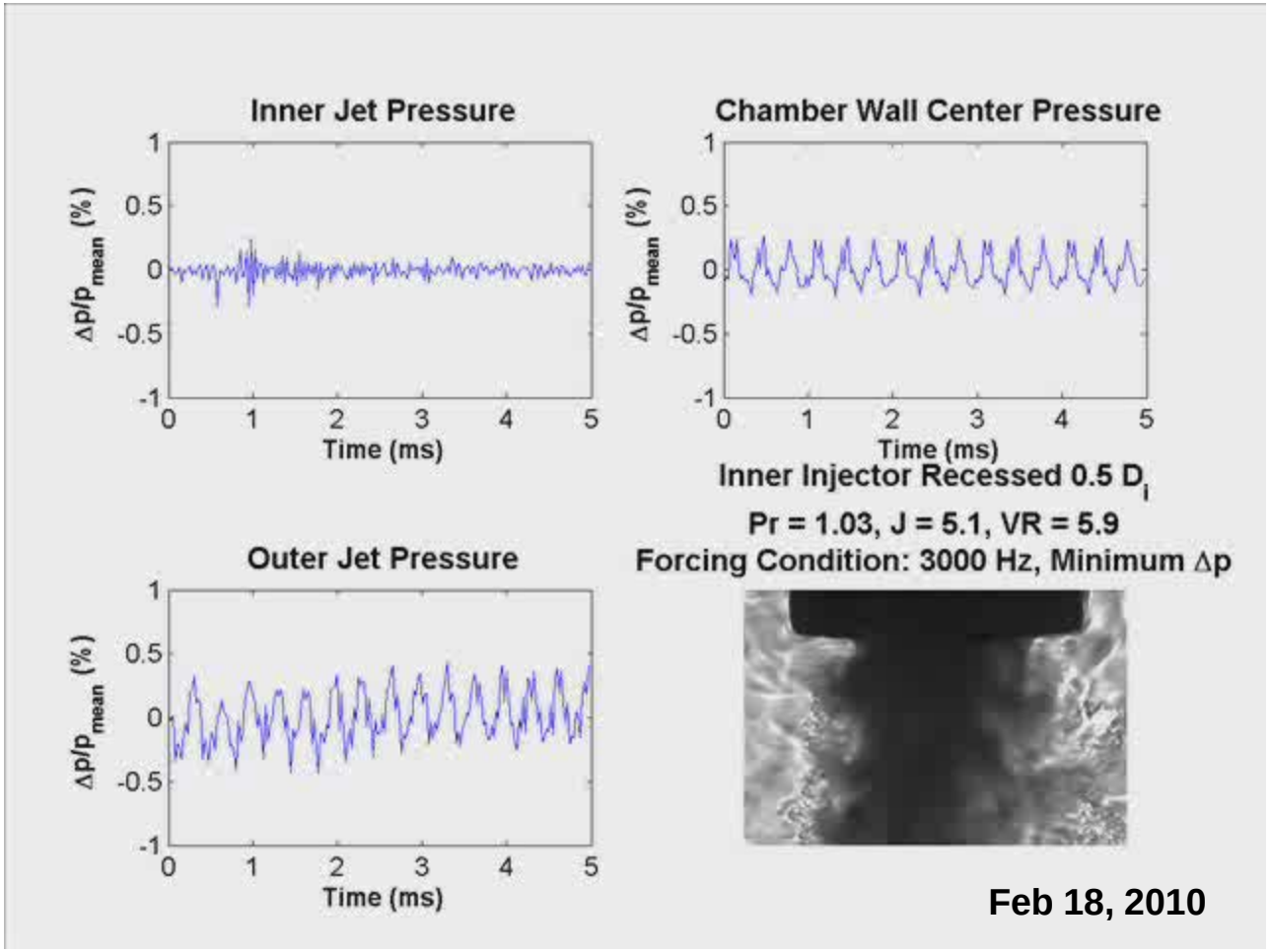

Uo=6. 25 m/s, Ui=1.06 m/s, To=165K , Ti=118 K

MOVIE

Jet Temperature Profiles

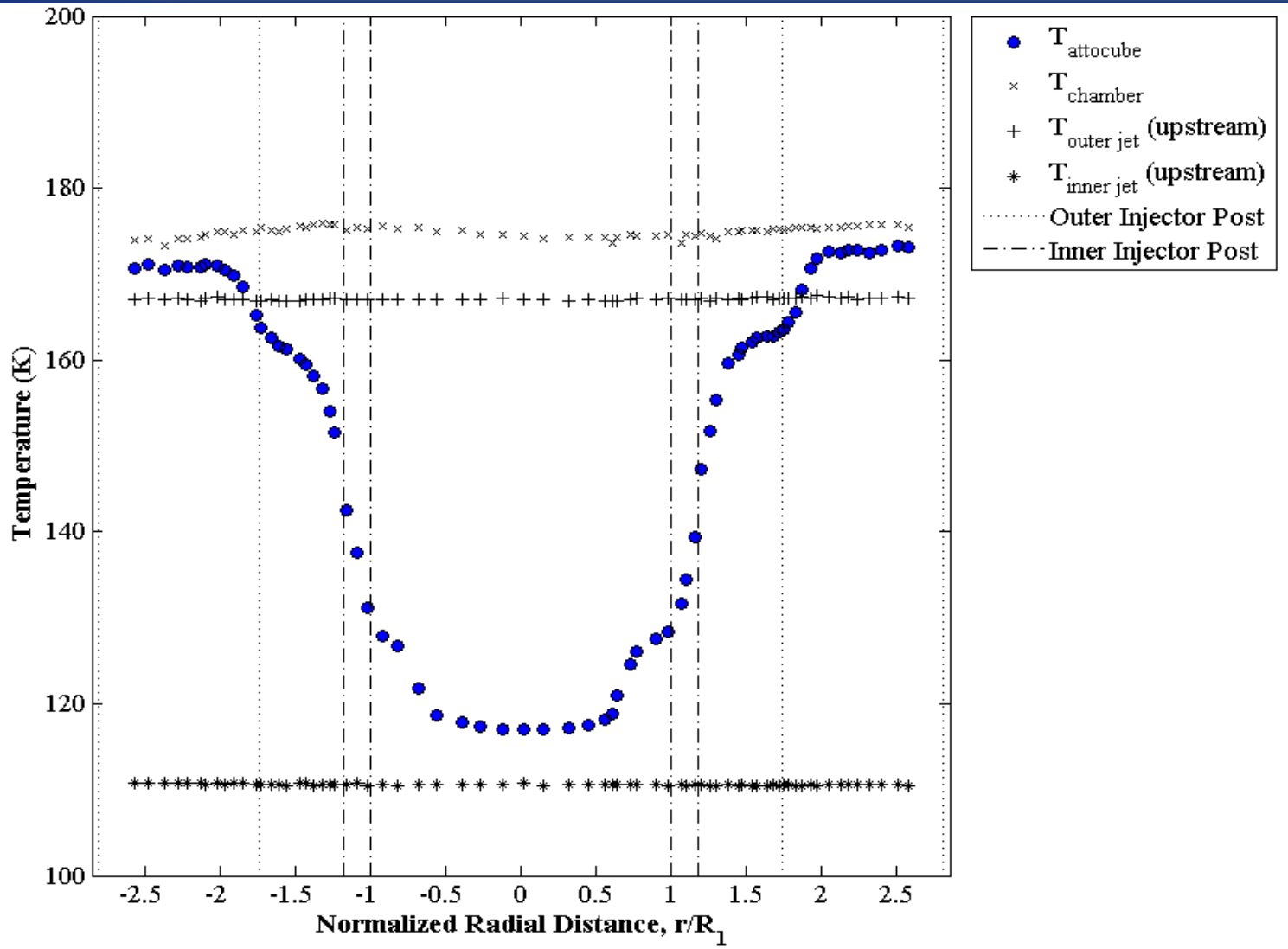

Effect of Recess: SAR_ThinLip; Pr=0.45, J~0.09

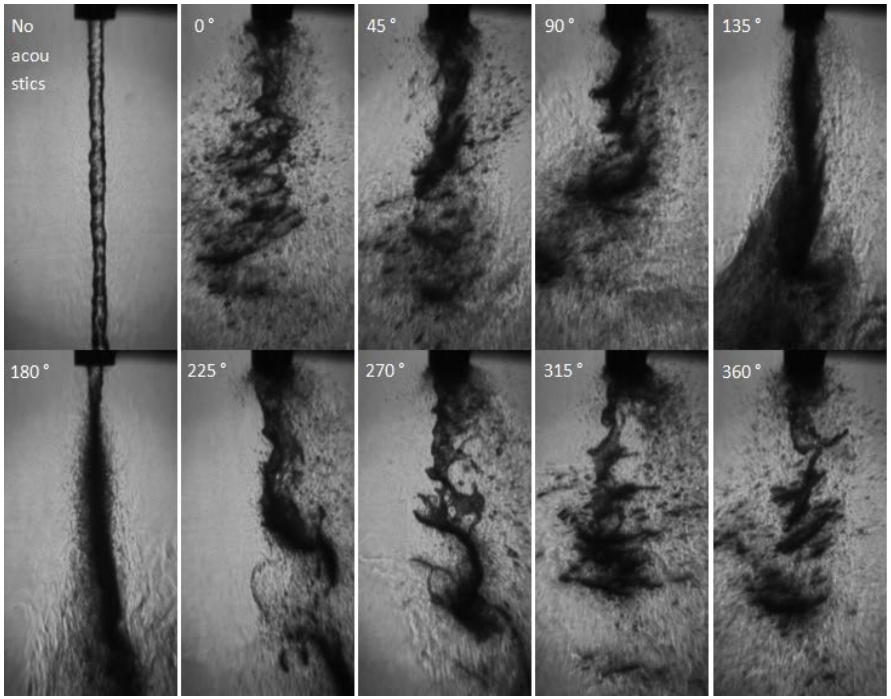

Flush inner post, J=0.09, p´/p=0.45%

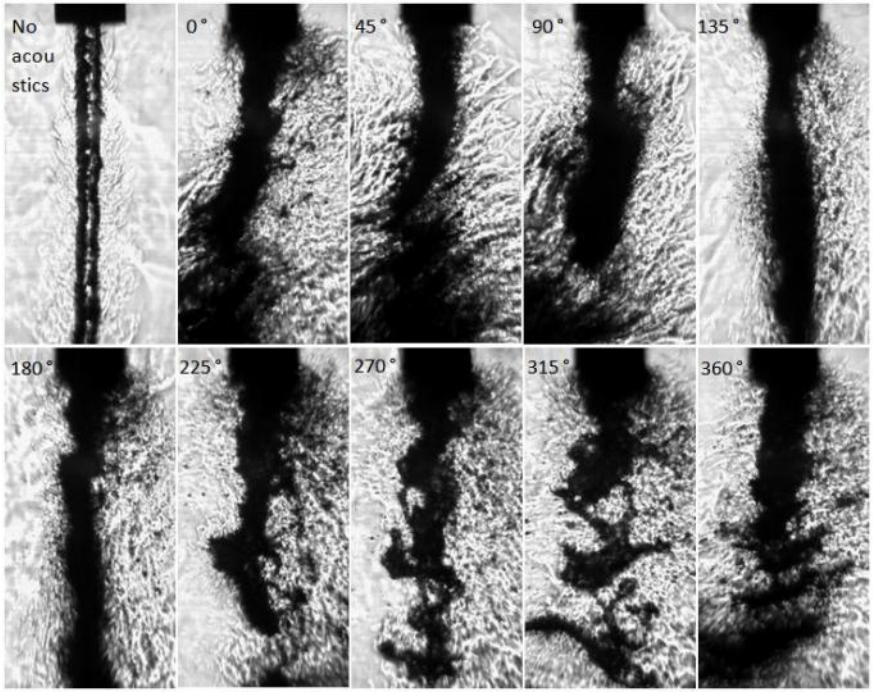

Recessed inner post, J=0.089, p´/p=0.60%

Qualitatively similar at very low J values

Case I: Baseline Flow

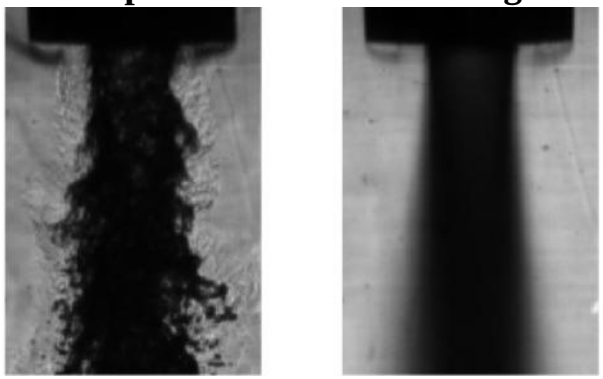

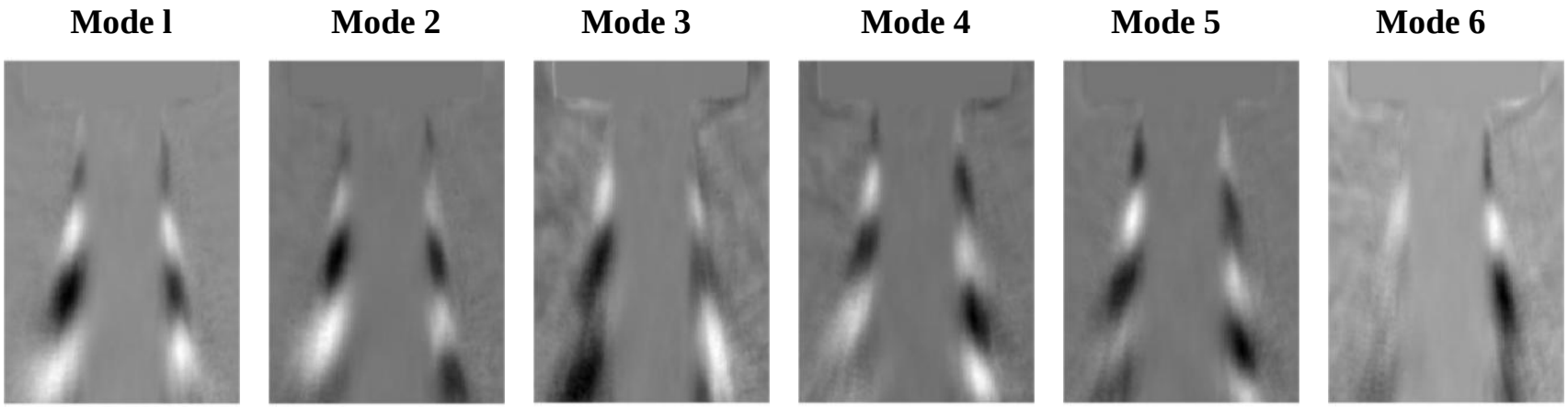

Case	P_R	$T_{R,OJ}$	$T_{R,IJ}$	R	J
I	0.44	1.19	0.84	5.8	2.0

Case I: Acoustically Forced Flow

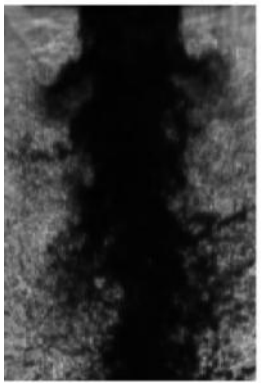

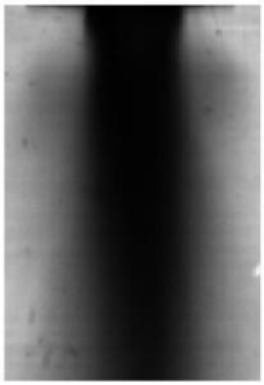

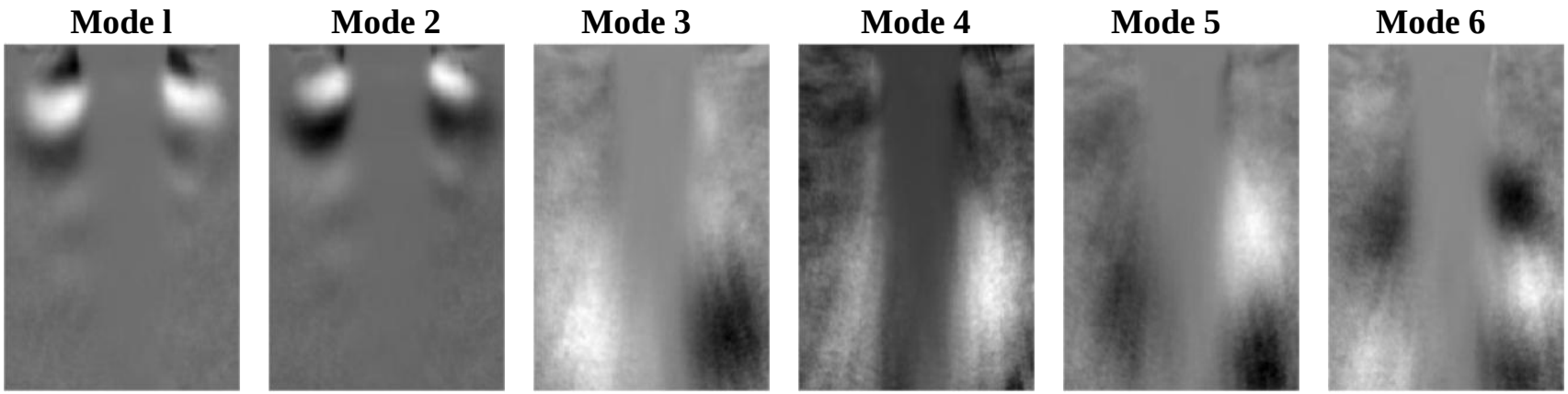

Case	P_R	$T_{R,OJ}$	$T_{R,IJ}$	R	J	f (kHz)
I	0.44	1.19	0.84	5.8	2.0	2.96

Geometric Rationale

LAR_ThinLip

LAR_ThickLip

SAR_ThinLip

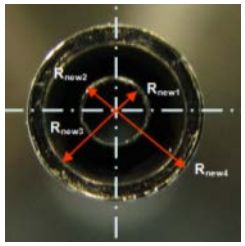

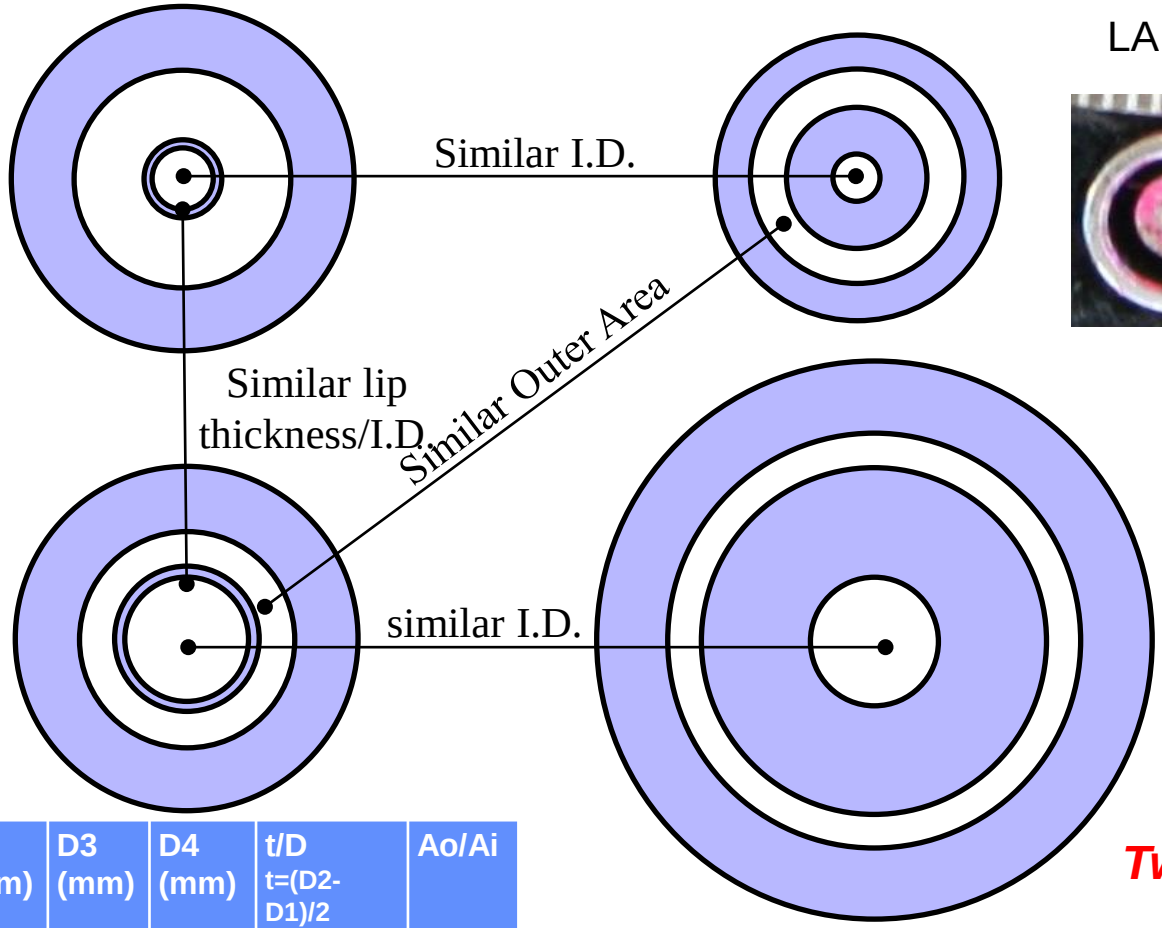

SAR_ThickLip

	D1 (mm)	D2 (mm)	D3 (mm)	D4 (mm)	t/D t=(D2-D1)/2	Ao/Ai
LAR_thickLip	0.51	1.59	2.42	3.18	1.05	12.9
SAR_thinLip	1.40	1.65	2.44	3.94	0.09	1.6
SAR_thickLip	1.47	3.96	4.70	6.35	0.84	2.9
LAR_thinLip	0.70	0.89	2.44	3.94	0.13	10.6

Two recesses

SAR, LAR -> Small, Large Area Ratio

ThickLip, ThinLip -> Post lip thickness

Chronological progression (only coaxial results are summarized in what follows)

- Single jets, no coaxial flow
  - Davis et. al. (Ph.D. thesis) – single jets, no coaxial flow
- Coaxial jets
  - Davis et al. (Ph.D. thesis) – LAR thick
  - Leyva et.al. – LAR_thick
  - Rodriguez et. al. (Ph.D. thesis) – LAR_thick, SAR_thin
  - Graham et. al. – SAR_thin, two recesses
  - Teshome et. al. (Ph.D. thesis, expected April 2012) – complete all four geometries
    - Also complete modal analysis of earlier geometries
- Future: Combusting coaxial jets
  - Wegener et. al. (Ph.D. thesis) (in process)
  - Article 219 facility funds

Baseline Dark-Core Lengths

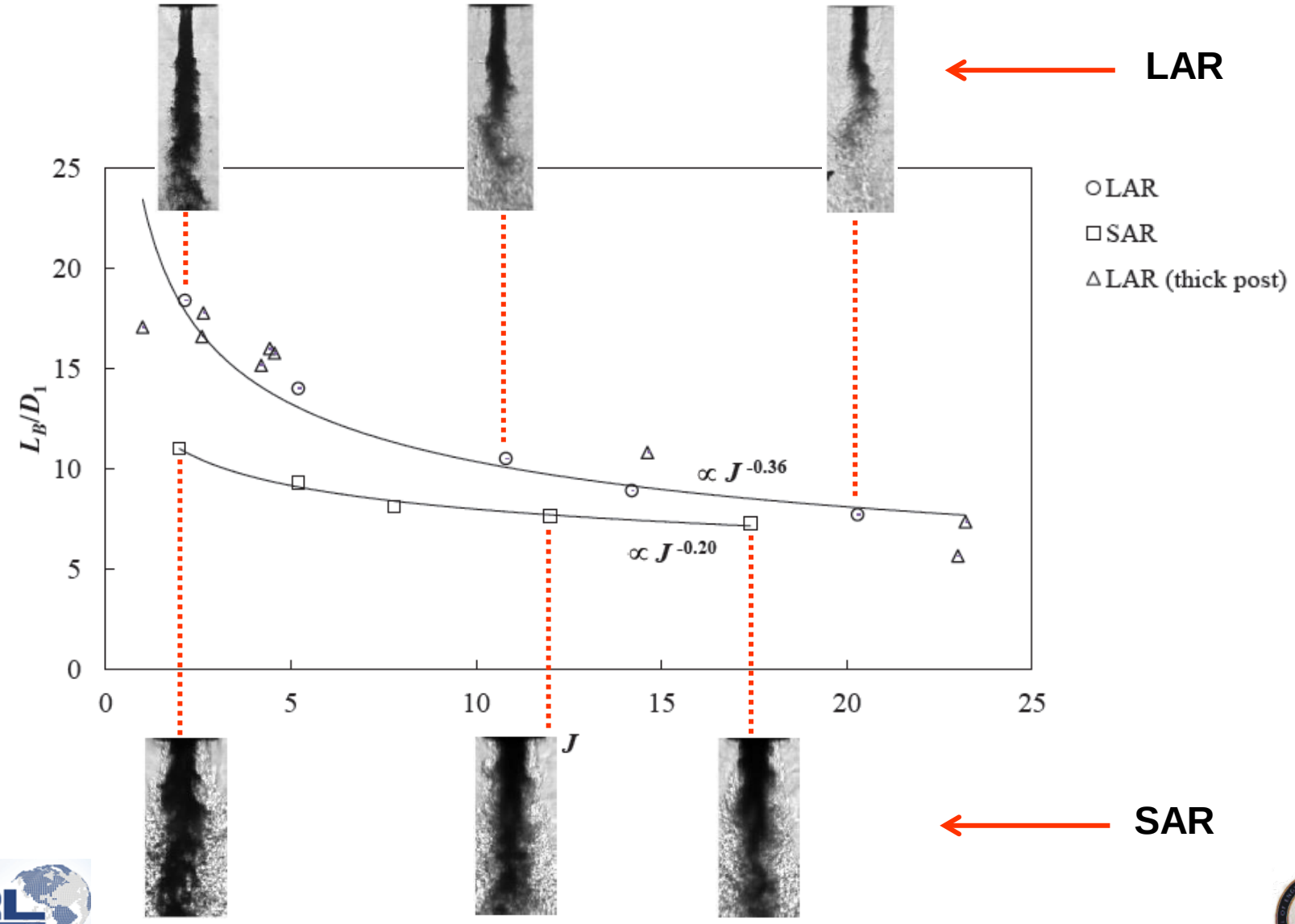

Image interpretation key

pressure = fixed

J ($\rho_o u_o^2/\rho_i u_i^2$) = fixed

Acoustics on
0^o
PAN, VN
"Pressure coupled"

Subsequent images:
acoustics on;
Phase increases by 45^o

Baseline:
Acoustics
off

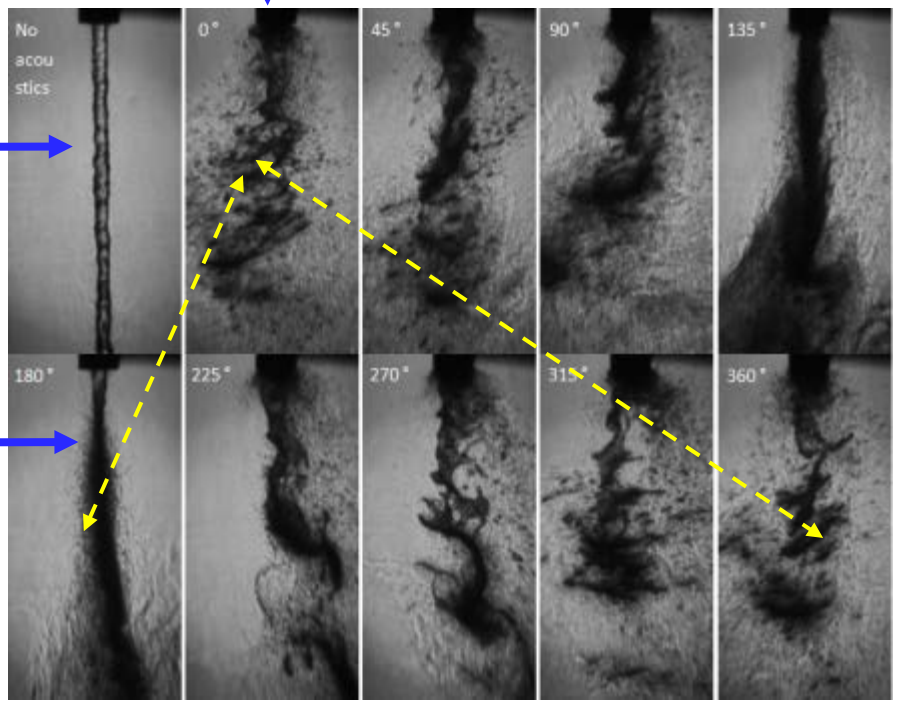

PN – pressure node - Min
PAN – pressure antinode - Max
VN – velocity node
VAN – velocity antinode

180^o
PN, VAN
Largest difference
expected from 0^o
"Velocity coupled"

360^o
should look
similar to 0^o

Acoustic Analysis for Injectors

In collaboration with Jeff Muss and Rory Davis, Sierra Engineering

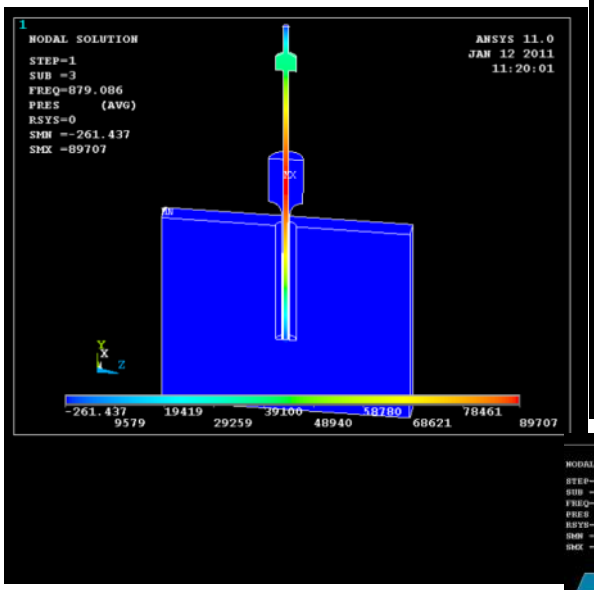

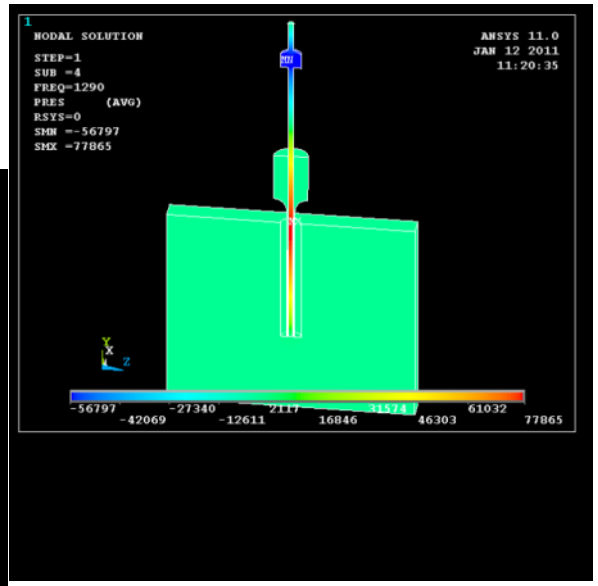

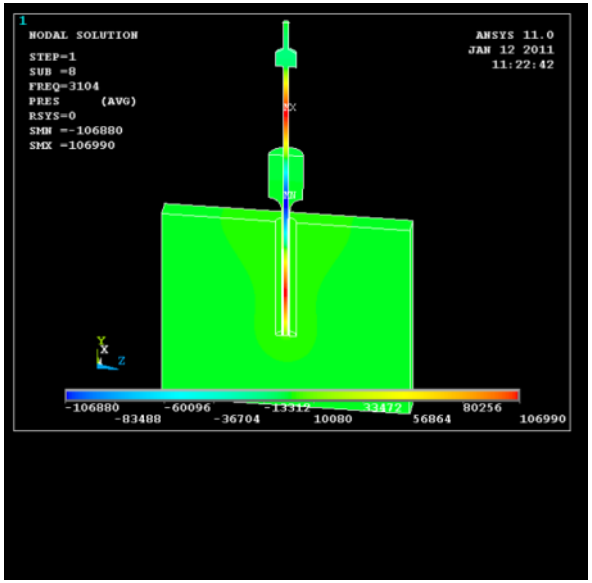

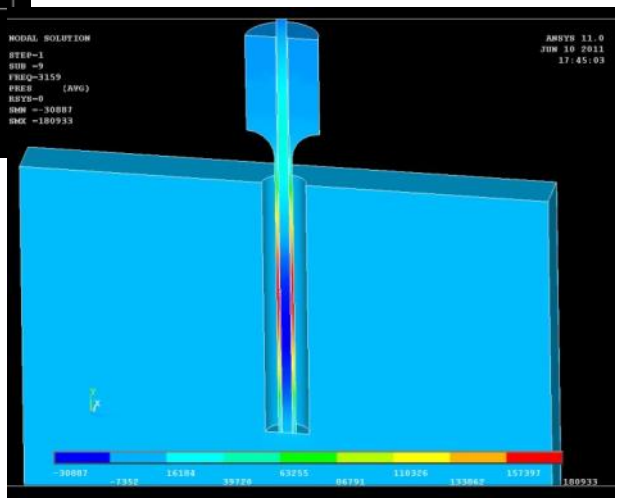

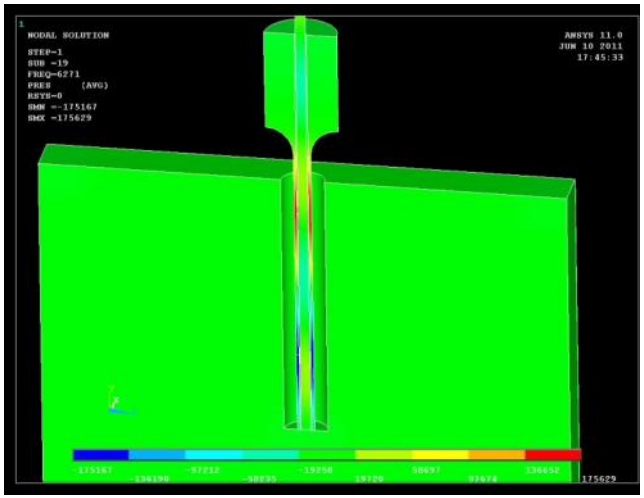

Have more accurately computed the acoustic modes for the inner and outer jets for constant and linearly varying temperatures for subcritical and supercritical pressures